Isolation and functional characterization of the osteoblast specific gene, Tmem16f

Inaugural-Dissertation

zur

Erlangung des Doktorgrades

Dr. rer. nat

des Fachbereichs

Biologie und Geografie

an der

Universität Duisburg-Essen

vorgelegt von

Milana Chinenkova

aus Moskau

Februar 2010

Die der vorliegenden Arbeit zugrunde liegenden Experimente wurden am Max-Planck-Institut für molekulare Genetik (Otto-Warburg Laboratories, AG Vortkamp) und in der Abteilung Entwicklungsbiologie II der Universität Duisburg-Essen durchgeführt.

1. Gutachter: Prof. Dr. A. Vortkamp
2. Gutachter: Prof. Dr. M. Ehrmann

Vorsitzender des Prüfungsausschussess: Prof. Dr. P. Bayer

Tag der mündlichen Prüfung: 30. August 2010

Contents

Contents

Contents

Contents

1. Introduction

1.1 Skeleton general

The skeleton of vertebrates is composed of approximately 200 elements. All these elements have their own shape, size and location. The skeleton is a complex organ made of two distinct tissues, cartilage and bone. Its main functions are to provide mechanical support (ribs), to allow locomotion (long bones), to provide protection (scull bones, ribs) and to act as a metabolic reservoir (Karsenty, 2003; Stevens and Lowe, 2005, Karsenty and Wagner, 2002). The skeleton is divided into three parts: the craniofacial skeleton, the axial skeleton (vertebrae, pelvis and ribs) and the appendicular (limb) skeleton (bones of forelimbs and hindlimbs). These structures are formed by cells of different origin: the craniofacial skeleton is formed by cranial neural crest cells, the axial skeleton is derived from somites (paraxial mesoderm) and the limbs are products of the lateral plate mesoderm (Olsen, et al., 2000).

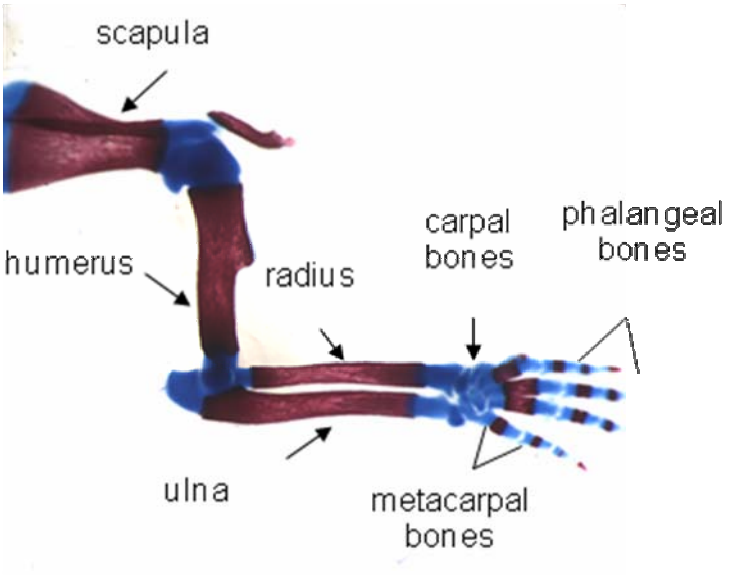

Figure 1: The anatomy of the forelimb.

E18.5 mouse embryo. From proximal to distal (from left to right, respectively): scapula, humerus, ulna and radius (lower and upper bones, respectively), carpal, metacarpal bones and phalangeal bones.

To decipher the mechanism of bone development two model systems are used widely- chick and mouse embryos. A number of the experiments are done on the long bones of the skeleton, particularly on the fore- and/or hindlimbs. The forelimb

consists of scapula, humerus, ulna and radius, carpal, metacarpal and phalangeal bones (Fig.1, direction from proximal to distal) (Kaufmann, 1992).

Histologically skeleton is made out of two tissues: cartilage and bone. Cartilage is avascular and consists of chondrocytes. Cartliage matrix is reach of collagen type II and can be mineralized, but to a lesser extent than the bone matrix (Cormack, 1987). Cartilage can grow both by internal expansion and by apposition. Bone is a highly vascular tissue which is heavily mineralized. Two types of cells are present in the bone: osteoblasts and osteoclasts. Osteoblasts produce a bone matrix whereas osteoclasts resorb this matrix. The osteoblasts, embedded in the bone matrix are called osteocytes. The bone matrix is reach in collagen type I and hydroxiappatite crystalls ($Ca_{10}(PO_4)_6(OH)_2$). Bone can grow only by apposition, i.e. by laying down of additional matrix and cells on the free surface of existing bone (Cormack, 1987; Alberts et al., 2002). Interestingly, condrocytes and osteoblasts are of mesenchymal origin, whereas osteoclasts derive from the myelomonocytic lineage (Cormack, 1987; Erlebacher et al., 1995; Ducy et al., 1997).

Bone is a dynamic system, which is build and resorbed, i.e., remodeled throughout the embryonic development and adult life.

1.2 Bone formation

Bones develop by two mechanisms: by intramembranous ossification directly in vascularized mesenchyme and by endochondral ossification in the center of cartilaginous models (cartilage anlage) of future bones (Kormack, 1987).

1.2.1 Intramembranous ossification

The cranial and facial flat bones, mandible and clavicles develop directly from mesenchymal cells by a process called intramembranous ossification (Kormack, 1987; Stevens and Lowe, 2005). Mesenchymal cells proliferate and condense, forming compact nodules. Some of these cells change their shape and become osteoblasts. The osteoblasts secrete bone matrix, which is able to bind calcium. Further, bony spicules radiate out from the region where ossification began. Later, the whole region of bone spicules becomes surrounded by the periosteum- a membrane of compact mesenchymal cells which surrounds the bone (Gilbert, 2003). The cells on the inner surface of the periosteum become osteoblasts, which deposit bone matrix parallel to existing spicules providing the growth of the bone. It was

established that during intramembranous bone formation the osteoblasts are differentiating through four distinct stages: early preosteoblast, preosteoblast, chondrocyte-like osteoblast and mature osteoblast stages (Abzhanov et al., 2007).

1.2.2 Endochondral ossification

The bones of the axial and appendicular skeleton are also derivatives of mesenchyme, but they develop indirectly through a cartilage model. Such bones develop and grow as a result of progressive replacement of preexisting cartilage. This complex process is called endochondral ossification (Fig.2). Briefly, clusters of mesenchymal cells adhere and form condensations. The cells in the condensations differentiate into chondrocytes, the primary cell type of cartilage. The cells at the border of condensations form the perichondrium, a sheeth of fibroblast like cells. Chondrocytes in the center of the cartilage model proliferate and synthesize type II collagen, one of the major components of the cartilage matrix. As the cartilage anlagen enlarge in size, the chondrocytes in the center stop proliferating and undergo hypertrophy. These cells change their genetic program and synthesize type X collagen (Col10a1). The hypertrophyc chondrocytes mineralize the surrounding matrix and trigger the invasion of blood vessels. The hypertophic chondrocytes undergo cell death. Perichondrial cells adjacent to the hypertrophic chondrocytes differentiate into osteoblasts, which form the so called bone collar. Some of the osteoblasts of the periosteum invade the hypertrophic region of the cartilage template along with blood vessels and start the production of bone matrix using the degraded cartilage matrix as a scaffold (de Crombrugghe et al., 2001; Kronenberg, 2007). The blood vessels also bring osteoclasts, which degrade the extracellular matrix produced by hypertrophyc chondrocytes. Postnatally, as bones grow further, the secondary-ossification centers are formed (Fig.2). That occurs when the chondrocytes in epiphyseal cartilage of the long bones stop proliferating, hypertrophy, and attract blood vessels to invade along with osteoblasts and osteoclasts (Kronenberg, 2003). The cartilage between the primary spongiosa and secondary ossification center is called “growth plate”, as it enables the long bone to grow postnatally (Kronenberg, 2003; Gilbert, 2003). Addition of the new bone to the outer surface of long bones is continuously maintained in adult life by intramembranous ossification from the periosteum (Erlebacher et al., 1995; Stevens and Lowe, 2005).

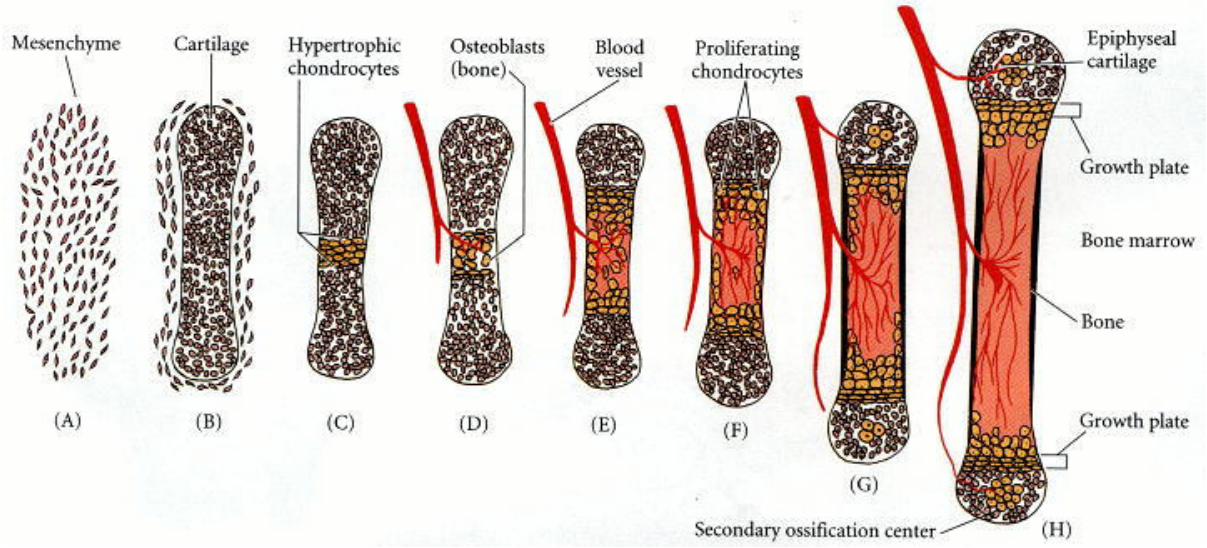

Figure 2: Endochondral ossification

Mesenchymal cells condence, aggregate and differentiate in to chondrocytes to form cartilage anlage of bone (A, B). Chondrocytes proliferate and cells in the center of cartilage model undergo hypertrophy (C). Hypertrophyc chondrocytes change and mineralize their extracellular matrix and undergo cell death, allowing blood vessels to enter (D). Blood vessels bring in osteoclasts, which degrade cartilaginous matrix, and osteoblasts, which deposit bone matrix on the remnants of degraded matrix (E, F). The secondary ossification centers are formed as chondrocytes in new locations stop proliferating undergo hypertrophy and attract blood vessels along with osteoblasts (G). A plate of the cartilaginous cells between the bone of primary spongiosa and secondary ossification center called growth plate (H) (From Gilbert, 2003).

1.2.3 Organization of cartilage

Based on the cellular organization, matrix composition and gene expression profile the cartilage can be subdivided into several zones: periarticular, proliferating, prehypertrophyc, hypertrophyc and terminal hypertrophyc chondrocytes (Fig.3). The periarticular chondrocytes consist of small round cells located close to the epiphyseal end of skeletal element. Proliferating chondrocytes secrete matrix rich in collagen type II. They can be divided morphologically into two types of cells: small round cells, which are located closer to the distal end of the epiphysis and flattened cells which are organized in columns. Prehypertrophic chondrocytes are cells larger in size which synthesize Indian hedgehog (Ihh) (Fig.3, C) (Vortkamp, et al., 1996). The postmitotic hypertrophic chondrocytes sectere a mineralized matrix rich in collagen type X (Olsen, et al., 2000; Kronenberg, 2007). The terminal hypertrophyc chondrocytes complete the differentiation process, undergo cell death and are replaced by bone. These chondrocytes express matrix metalloproteinase 13

(MMP13) and osteopontin (Spp1). The mineralized bone collar or periosteum, which consists of osteoblasts is flanking the hypertrophic cells approximately where the transition between proliferating and hypertrophyc chondrocytes takes place (Fig.3, B; Olsen, 2000).

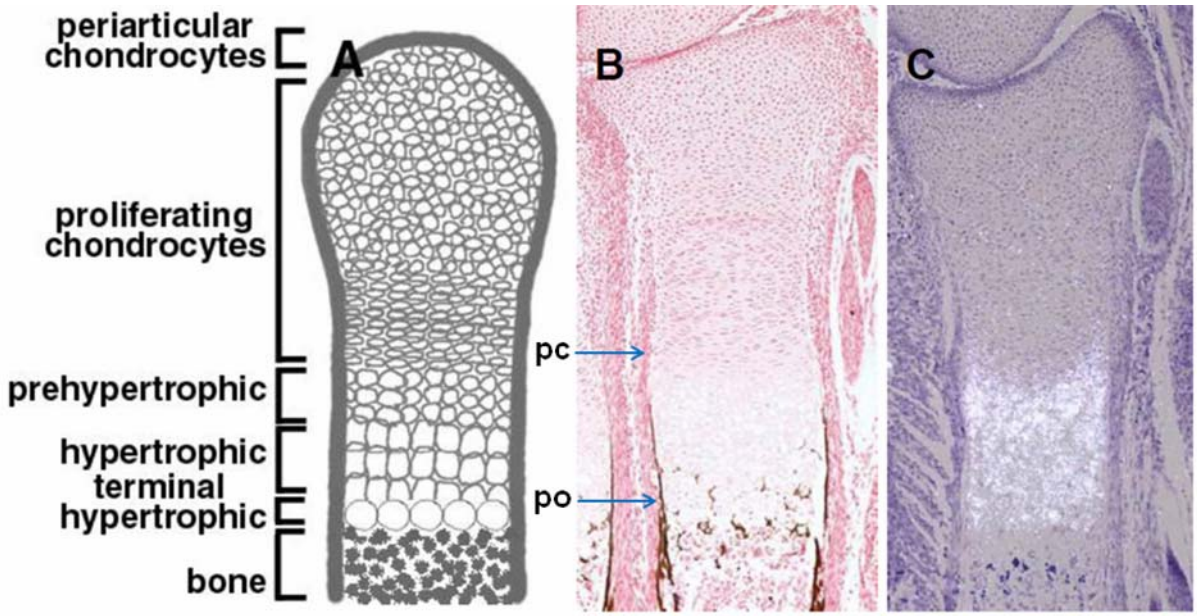

Figure 3: Cellular organization of developing cartilage

The cartilage is divided into zones of periarticular, proliferating, prehypertrophyc, hypertrophyc and terminal hypertrophyc chondrozytes (A). A section of an E 16.5 mouse radius was stained by von Kossa staining and counterstained with Nuclear Fast Red to visualize mineralized matrix (B). A parallel section was hybridized with an antisense riboprobe for Ihh (white) to demarcate the zone of prehypertrophyc chondrocytes. The tissue was counerstained with Toluidin blue (C). pc- perichondrium, po- periosteum

1.3 Relevant mechanisms

1.3.1 Hedgehog signaling

Indian hedgehog is a signaling molecule (secreted factor) that is expressed in the prehypertrophic chondrocytes (Bitgood and McMahon, 1995). No endochondral bone is formed in Ihh-deficient mice indicating that Indian hedgehog is essential for endochondral ossification (St-Jacques et al., 1999).

It was shown that Ihh directly stimulates chondrocyte proliferation and indirectly supresses chondrocyte hypertrophy. Ihh activates PTHrP in the periarticular cells, which in turn acts through its receptor, PPR (PTH/PTHrP receptor), to prevent hypertrophyc differentiation of the chondrocytes (Vortkamp et al., 1996; Lanske et.

al., 1996; Weir et al., 1996; Karp et al., 2000). Thus, the two signals interact in a negative-feedback loop, in which the level of Ihh determines the distance between the periarticular region and the chondrocytes undergoing hypertrophy (Vortkamp et al., 1996). The regulation of chondrocyte proliferation is controlled directly by Ihh signalling, which is most likely mediated through Cyclin D1 (Long et al., 2001, Lai and Mitchell, 2005).

Ihh is also required to direct perichondrial cells to differentiate into osteoblasts which form the periosteum (St-Jacques et al., 1999; Long et al., 2004; Kronenberg, 2007). It was established later, that Ihh signaling is required at the earliest stage of osteoblast development but has no pronounced effect on the subsequent differentiation of osteoblasts (Hu et al., 2005; Rodda and McMahon, 2006). Thus, Ihh acts as a key coordinator of chondrogenesis and osteogenesis in endochondral bones (Chung, et.al., 2001; Kronenberg, 2007).).

1.3.2 Transcription factors Runx2 and Osx regulate bone formation

Runx2, previously also called Cbfa1, is a member of runt family of transcription factors. During mouse embryonic development it was first detected at E 10.5 in lateral plate mesoderm and in all cells of the mesenchymal condensations prefiguring the future skeletal elements. Between E 10.5 and E 12.5 Runx2 is continuously expressed in the osteochondro progenitor cells of the skeletal condensation (Ducy, et al., 1997). After E 12.5, Runx2 expression is steadily decreasing in prehypertrophic and hypertrophic chondrocytes until it becomes undetectable in these cells at birth. At the same time Runx2 expression increases in osteoblast progenitors and later becomes limited to the osteoblast lineage (Inada, et al., 1999; Kim, et al., 1999; Takeda, et al., 2001; Stricker, et al., 2002). Runx2 is also expressed in differentiated osteoblasts postnatally (Ducy, et al., 1999). Runx2 activates osteocalcin expression by binding to the OSE2 site of osteoclacin promoter. Putative Runx2 binding sites were also found in the promoter of type I collagene, bone sialoprotein and osteopontin gene (Ducy, 2000).

Runx2 deficient mice had a cartilaginous skeleton with complete absence of osteoblasts. (Ducy, et al., 1997; Komori et al., 1997; Otto et al., 1997; Harada and Rodan, 2003). Runx2-heterozygous mice had a defect in intramembranous ossification, which resembles cleidocranial displasia in humans, a desease caused by mutation in Runx2 (Mundlos, et al., 1997; Otto, et al., 1997; Zelzer and Olsen, 2003). Analysis of Runx2-null mice on the molecular level revealed that Runx2 is

required for osteoblast differentiation and positively regulates hypertrophic chondrocyte differentiation (Otto, et al., 1997; Komori, et al., 1997; Stricker, et al., 2002). Ectopic expression of Runx2 leads to endochondral ossification in parts of the skeleton that normally never ossify demonstrating that Runx2 is sufficient to induce osteoblast differentiation (Takeda et al., 2001; Ueta et al., 2001). Overexpression of Runx2 under the collagen I promoter in mice leads to osteopenia, demonstrating that Runx2 promotes early differentiation steps and inhibits the later stage of osteoblast maturation (Liu et al., 2001). Transgenic mice expressing a dominant-negative form of Runx2 under the osteocalcin promoter (e. g. in mature osteoblasts), showed decreased bone formation and reduced bone mass. This demonstrates that once osteoblasts differentiation is initiated Runx2 continues to regulate their function, and therefore bone formation, postnatally (Ducy et al., 1999).

Osterix (Osx) is a novel zinc finger-containing transcription factor which is expressed in differentiating chondrocytes and surrounding perichondrium of E 13.5 mouse embryos. At E 15.5 and later Osx is expressed in the osteoblasts and weakly expressed in prehypertrophic chondrocytes. This transcription factor is essential for osteoblast differentiation, acting downstream of Runx2 (Nakashima, et al., 2002).

1.3.3 Mechanism of mineralization

1.3.3.1 Matrix vesicles

Hypertrophic chondrocytes and osteoblasts initiate the mineralization in vivo by releasing matrix vesicles in the extracellular matrix. Matrix vesicles (MVs) are membrane particles about 50-200 nm in diameter. Studies performed by scanning and transmission electron microscopy indicated that MVs are released from the cell surface via polarized budding into the extracellular space (Fig. 4) (Anderson et al., 2005; Xiao et al, 2007). They serve as the initial sites of calcification, since they accumulate Ca^{2+} ions and inorganic phosphate (P_i) which finally leads to hydroxyapatite [$3Ca_3(PO_4)_2 \cdot (OH)_2$]) formation (Anderson, 1995; Anderson et al., 2005; Balcerzak et al, 2008).

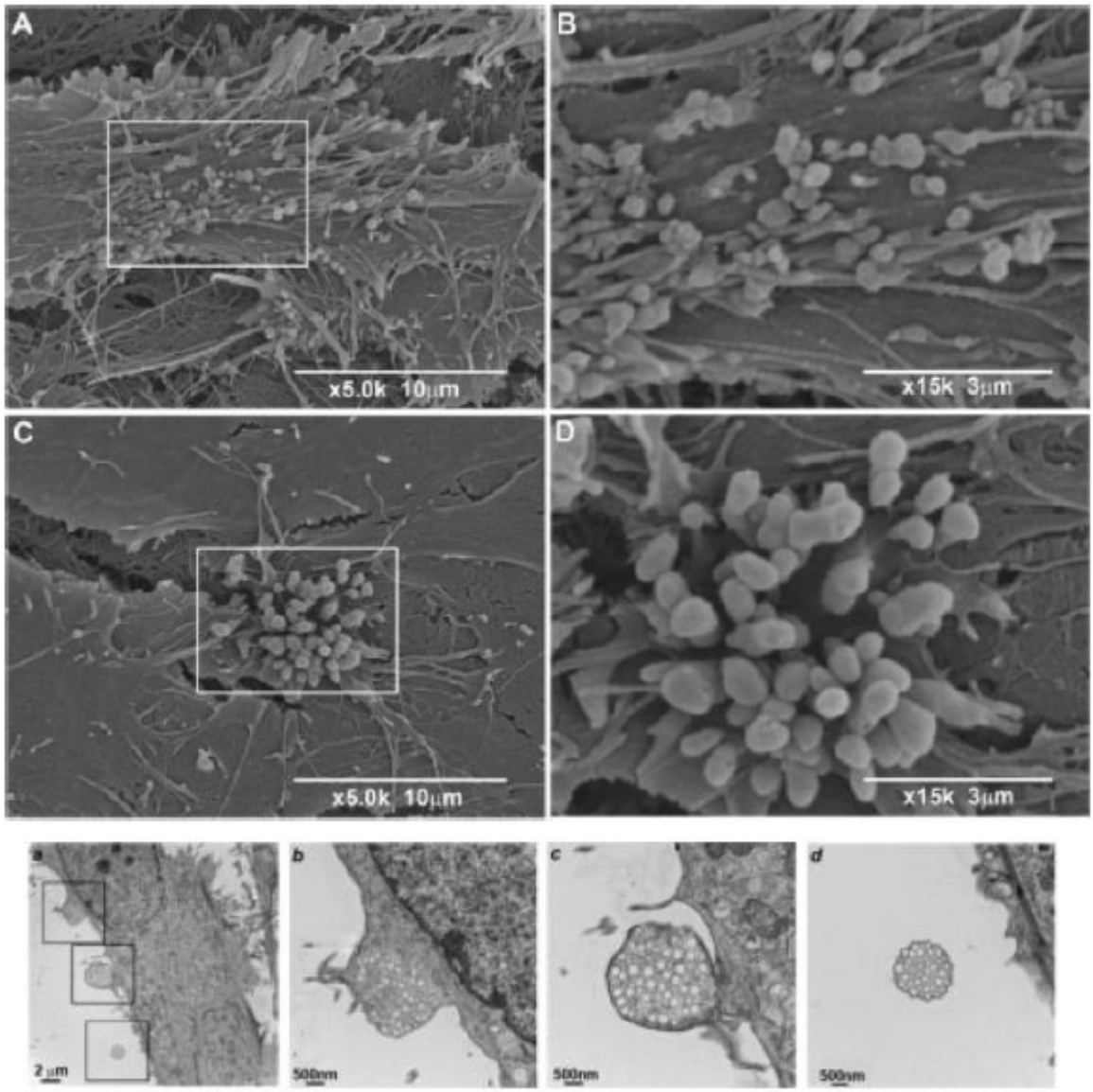

Figure 4: Scanning electron microscopy observation of matrix vesicles on osteoblast cell surface.

Scanning electron microscopy observation of matrix vesicles on osteoblast cell surface (A-D). MVs are either scattered among collagen fibers (A, B) or aggregated on cell surface (C, D). Higher magnification of MVs are shown in (B) and (D), respectively. Transmission electron microscopy observation of the budding MVs in the osteoblast cell culture (a-d). The vesicles first aggregate under, then pinch off from plasma membrane in a sac (b, c, d are higher magnifications of the marked regions from (a). Adopted from Xiao et al., 2007

Deposition of mineral occurs in two phases. During phase 1 the first crystals of hydroxyapatite are formed within MVs. Later, as the crystals become bigger, they penetrate the membrane of MVs, exposing pre-formed mineral to the extracellular fluid (phase 2- mineral propagation, or maturation) (Garimella et al., 2004; Anderson, 1995; Garimella et al., 2006).

MVs are rich of various enzymes, which enable the process of mineralization. Thus, the outer surface of MVs includes enzymes involved in the hydrolysis of organic phosphate esters. These are tissue nonspecific alkaline phosphatase (TNAP), nucleotide triphosphate pyrophosphatase phosphodiesterase (NPP1), ATPase and 5'-AMPase. NPP1 generates pyrophosphate (PPi) from nucleoside triphosphates (Fig. 5). Alkaline phosphatase is one of the most abundant enzymes of MVs. It enables hydrolysis of AMP or pyrophosphate (PPi) to yield phosphate residue (Pi) (Fig. 5). It was shown that a deficiency of the TNAP gene causes the disease hypophosphatasia, which is characterized by weakly mineralized bones. Alkaline phosphatase-deficient mouse model confirmed the previous hypothesis that TNAP stimulates mineralization, since these mice shown skeletal hypomineralization (Anderson at al., 2004) (Fig. 5).

The rate of mineralization is tightly regulated by the activity of these enzymes and the product of their activity. Several research groups confirmed that for example PPi can also regulate the mineralization process in a concentration-dependent manner. Thus, low concentration of PPi (< or = 0.01 mM) promote mineralization, whereas concentrations higher than 1-2 mM inhibit mineralization (Harmey et al., 2004; Garimella et al., 2006).

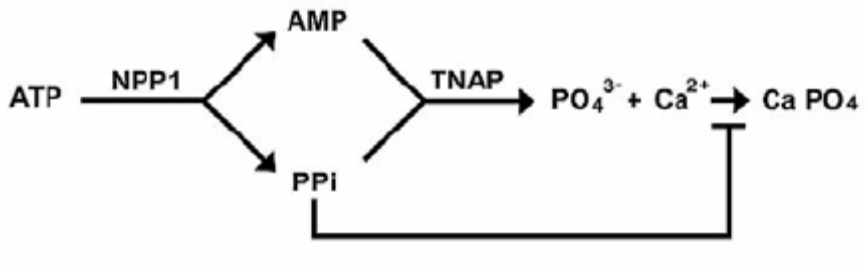

Figure 5: Metabolism of ATP by NPP1 and TNAP.

ATP is hydrolyzed by NPP1 to yield AMP and pyrophosphate (PPi). Both AMP and PPi are further hydrolyzed to orthophosphate (PO_4^{3-}) by TNAP. The orthophosphate molecules are then incorporated into CaPO4 molecules. High concentrations of PPi block the formation of CaPO4. Adopted from Anderson at al., 2004

Matrix metalloproteases (MMPs) such as MMP-2, MMP-9 and MMP13 were also found to be present in the outer surface of matrix vesicles membranes (Balcerzak et al, 2008). MMPs are the proteases, which cleave the protein components of the ECM, and, therefore, are important in tissue remodeling (Stamenkovic, 2003). The inner surface of MVs is rich in Annexins and phosphatidylserine (PS). PS is found in

complexes with Ca2+ and Pi ions (Sauer and Wuthier, 1988; Wu et al., 1993; Genge et al., 2008). Annexin V was shown to promote the inward transport of Ca^{2+} and to enhance the nucleation of the amorphous calcium phosphate in complex with phosphatidylserine (Genge et al., 2007). The binding of Annexin V to type II and type X collagens stimulates its Ca2+ channel activity (Huitema and Vaandrager, 2007).
A novel phosphatase, PHOSPHO1 has been localized in the inner surface of MVs and suggested to act synergistically with TNAP in generating Pi (Stewart et al., 2006; Roberts et al., 2007).

1.3.3.2 Extracellular bone matrix proteins regulating mineralization

Bone sialoprotein (Bsp or Ibsp), osteopontin (Osp or Spp1), osteonectin (On) and osteocalcin (Osc) are non-collagenous bone matrix proteins, which are capable to bind Ca^{2+} ions. It has been shown that Bsp has a high affinity to Ca2+ ions and hydroxyapatite and that Bsp is promoting nucleation of hydrohyappatite crystals, thus, promoting mineralization of the bone (Hunter and Goldberg, 1993; Ganss et al., 1999). In contrast, osteopontin, which shares many of the properties of Bsp, is inhibiting mineralization (Ganss et al., 1999). Osteonectin and Osteocalcin (Osc) have been shown to inhibit mineralization in vivo. Osc-deficient mice show an accelerated rate of bone formation without impairing bone resorption (Ducy et al., 1996; Boskey et al., 1998; Boskey et al., 2003)
Collagens play an important role in nucleating and orienting newly formed apatite crystals during mineralization. Thus collagen of types I and II can promote mineral propagation (Anderson et al., 2005). It has been also shown that type I collagen is essential for retaining BSP at high concentrations, thus enhancing Bsp-mediated matrix mineralization (Xu et al., 2007).

1.4 Tmem16 gene family

The Tmem16 gene family was discovered by two independent groups. In silico analysis of human sequences (chromosome) made by Katoh et al., identified a novel gene family designated Tmem16. It consists of at least eight members in humans (Tmem16A, Tmem16B, Tmem16C, Tmem16D, Tmem16E, Tmem16F, TP53I5 (PIG5), and PCANAP5 (NGEP) (Katoh et al., 2004 (a); Katoh, 2004 (b). These genes encode proteins with homologous eight-transmembrane domains (TM) and a conserved domain referred to as DUF590 (Domain of Unknown Function 590, PFAM

Accession No.: PB175613). Three domains (TM16H1-TM16H3) were identified, as being highly conserved among the TMEM16 family proteins. It was suggested, that the N- and C-terminus of these proteins are facing the cytoplasm. Interestingly, the DUF590 domain was found to be highly conserved among different species, including human, mouse, rats and flies. Phylogenetic analysis revealed TMEM16E and TMEM16F constitute a subfamily among TMEM 16 family proteins (Katoh, 2004 (a).

Another research group has mapped and identified the gene linked to the human disease *Gnathodiaphyseal Dysplasia* GDD1 (Tsutsumi et al., 2003; Kamata, 2004). *Gnathodiaphyseal dysplasia* is a syndrome inherited in autosomal dominant fashion. This rare syndrome exhibit increased bone fragility, sclerosis/bowing of tubular bones and fibro-osseous lesions of the jawbones (Riminucci et al., 2001). It was found, that this disease is caused by the missense mutations (C356R and C356G) of GDD1 (Tsutsumi, 2004). It was established later that GDD1 and TMEM16E represent the same gene which is also found in mouse and other mammals.

1.5 Aim of the study

It has been demonstrated that Ihh, the signaling factor which is expressed by prechypertrophic chondrocytes, is crucially important for endochondral bone development. Ihh signaling regulates chondrocyte proliferation and differentiation and plays a key role in osteoblasts formation (Vortkamp et al., 1996; Lanske et. al., 1996; Weir et al., 1996; Karp et al., 2000; St-Jacques et al., 1999). It was recently shown that Ihh directs perichondrial cells to differentiate into osteoblasts (Long et al., 2004; Kronenberg, 2007). Ihh determines the site of bone collar formation in the adjacent perichondrium and acts as a key coordinator of chondrogenesis and osteogenesis in endochondral bone (Chung et al., 2001; Kronenberg, 2007). In a previous scan for Ihh target genes several genes were identified (Wenzel, 2003). One of them, Tmem16f, was found to be expressed in a newly formed bone and in the periosteum surrounding Ihh domain in E14.5 and E16.5 mice. Additionally, it was shown that Tmem16f expression is upregulated by activation of Ihh signalling (Wenzel, 2003). Thus, we suggested that Tmem16f might be involved in a regulation of bone formation downstream of Ihh.

The aim of the present study was to analyze the function of Tmem16f. First, since only a part of Tmem16f sequence was isolated by the previous study, an assembly of its complete sequence along with the determination of exon-intron structure, start-codon and open reading frame was required. 5'-RACE was carried out to determine the complete 5'-end sequence of Tmem16f. Second, *in silico* methods were essential to predict isoforms of Tmem16f, protein sequence and its structure, transmembrane domains, functional domains and sites of glycosilation. Third, the determination of Tmem16f cell localization could potentially indicate its possible function in the cell. Fourth, to further study the function of Tmem16f it was necessary to develop a strategy to generate Tmem16f-null mice.

Mice lacking Tmem16f were generated by complete deletion of Tmem16f. Additionally, Tmem16f gene trap mouse line which carries a truncated version of Tmem16f protein was generated. This approach allows comparison of the phenotype of two mouse lines which might unravel the function of potential Tmem16f domain(s). To analyze the phenotype on the molecular level in situ hybridization was performed using the chondrocyte- and osteoblast-specific markers. Mineralization of the bone

was analyzed by histological staining for $Ca2^{+}$-ions. Additionally, analysis of alkaline phosphatase as one of the markers of osteoblast activity to mineralize the matrix and analysis of Tartrate Resistant Alkaline Phosphatase as a marker of osteoclasts which resorb the bone was performed to investigate the impaired ossification in mutant mice.

The results of this study help to clarify the regulation of Tmem16f by Ihh, Runx2 and Osx.

2. Materials and methods

2.1. Materials

2.1.1 Chemicals

Acetic anhydride (Sigma)

Agar (Difco or Roth)

Agarose (Gibco BRL)

Ampicilin (Sigma)

BSA (New England Biolabs, USA)

Carbenicillin disodium salt (GERBU biotechnik GmbH)

Chloroform (Roth)

Coverslips for *in situ* hybridization (Roth)

CTP, GTP, ATP, UTP (Roche)

Dextran Sulfat (Sigma)

DNAse (deoxyribonuclease), RNAse free (Roche)

dNTPs (2'-Deoxynucleoside 5'-triphosphates) (Roche)

DPX Mountant for histology (Fluka)- DPX Mountant for histology (Fluka)

Eosin Sigma

Ethanol (Roth)

Ethidiumbromide (Serva or Roth)

Fatfree milk (Instant-Magermilchpulver, Neuform, Germany)

Ficoll 400 (Pharmacia)

Forceps 5, 55 Dumont, Switzerland

Glass coverslips (Menzel-Glaeser, Germany)

Glutaraldehyde (Sigma)

Glycerol (Merk)

Glycogen (Roche)

Hematoxylin Sigma

Isopropanol Roth

Kanamicin Sigma

Nuclear fast red (Sigma)

Orange G (Sigma)

O.C.T. (Optimal Cutting Temperature), Tissue Tek

Paraffin-paraplasts (Sherwood Medical Co, USA)

PFA (Paraformaldehyde) (Merck)

Phenol (Roth)

Proteinase K (Roche)

[P^{32}]-dCTP (3000 Ci/mmol) AmershamPharmacia, Freiburg

[P^{33}]-UTP (3000 Ci/mmol) AmershamPharmacia, Freiburg

[P^{33}]-UTP (2000 Ci/mmol), Hartmann Analytic, Braunschweig, Germany

Restriction endonucleases (NEB, Roche)

Ribonuclease A, RNAse A (Roche)

RNAse inhibitor (Roche)

Superfrost plus slides (Menzel-Glaeser, Germany)

Taq-DNA polymerase (Eppendorf)

TEA, triethanolamine (Merck)

Toluidine Blue O (Sigma)

TRIZOL Reagent (Invitrogen)

Tryptone (Difco)

T7, T3, SP6 RNA-polymerase (Roche)

T4 DNA Ligase (Roche 1U/µl)

Yeast extract (Difco)

Xylol (Roth)

2.1.2 Kits, buffers and reagents

Table 1: Kits.

QIAprep plasmid mini prep kit	Qiagen, Germany
Gene Racer Super Script II RT Module	Invitrogen
Super Script III First-Strand Synthesis System for RT-PCR	Invitrogen
Rediprime II Random Prime Labelling System	Amersham Biosciences
TOPO TA Cloning Kit for Sequencing	Invitrogen
Lumin Kit	Roth
Alkaline phosphatase (AP), Leukocyte	Sigma
TRAP (acid phosphatase, leukocyte)	Sigma

Table 2: Buffers for genomic DNA preparation from mammalian tissue.

solution A	25 mM EDTA, pH8.0 75 mM NaCl
solution B	10 mM EDTA, pH8.0 10 mM Tris-HCl, pH 8.0 1% SDS (w/v) 400 µg/ml Proteinase K

Table 3: Buffers for DNA agarose gel electrophoresis.

50X TAE buffer	2M Tris/acetate 50mM EDTA pH 7.5- 8.0 used as 1X solution
10X TBE buffer	0.89M Tris base 0.89M Boric acid 2mM EDTA pH 8.0 used as 1X solution
10X loading buffer	
Ethidium bromide	Roth, used at the concentration 0.5 µg/ml

Table 4: Reagents and buffers for southern blot hybridization.

Denaturation solution	1.5 M NaCl 0.5 N NaOH
Neutralization solution	1.5 M NaCl 1M Tris (pH 7.4)
20X SSC	300 mM Sodiumcitrate 3 M NaCl; pH 7.0
3MM Whatman filter paper	VWR
Nylon membrane	Hybond
micro spin columns	Amerscham
Sodium –Phosphate (**Na-P**)	1M Na_2HPO_4 1M NaH_2PO_4

	pH7.2 (reached using the same solutions)
Church buffer (prehybridization)	7% SDS 0,5 M **Na-P**, pH 7.2 1 mM EDTA
Church (hybridization) buffer	Church buffer 0.1 µg/ml fish sperm DNA 500µg/ml Cot-DNA
DNA from Hering sperm	Serva electrophoresis
Mouse Cot-1 DNA	Invitrogen
wash solution I	100 mM Na-P, pH 7.2 0,1 % SDS
wash solution II	50 mM Na-P, pH 7.2 0,1 % SDS

Table 5: Buffers for mice genotyping.

Tail lysis buffer:	50 mM Tris-HCl, pH 8.0 100 mM EDTA 1% SDS 100 mM NaCl
DirectPCR® Lysis Reagent (Tail)	Peqlab

Table 6: Reagents and buffers for in situ hybridization.

10x transcription buffer	Roche
Proteinase K:	stock solution 10mg/ml resuspended in 50 mM Tris-HCl, pH 8,0; 1 mM CaCl2, stored at -20°C; working solution is 20 µg/ml
PBS ((Phosphat Buffered Saline)	1.5 mM KH_2PO_4 140 mM NaCl 3 mM KCl, pH 7.4
PFA	Paraformaldehyde 4% (w/v) in PBS
Hybridization buffer:	50% Formamid

	3 M NaCl 20 mM Tris-HCl; pH 7.4 5 mM EDTA 10 mM NaH2PO4-H2O; pH 8.0 10% Dextran Sulfat (w/v) 1x Denhardt's 0,5 mg/ml Yeast RNA (total)
50x Denhardt's reagent:	50g Ficoll 5g polyvinylpyrrolidone 5g BSA H2O to 500 ml
RNAse free water (DEPC water)	0,1% DEPC (Diethylpyrocarbonat)
10xWash buffer:	4 M NaCl 0.1M Tris-HCl, 0,05 M EDTA; pH 7.5
RNAse A	stock solution 10mg/ml; 100µl dissolved in 400ml 1X wash buffer
20x SSC (standard saline citrate):	300 mM Sodiumcitrate 3 M NaCl; pH 7.0
Photoemulsion (autoradiography emulsion type NTB2)	Kodak, USA
Kodak-developer D-19	Kodak, USA
Kodak-fixer	Kodak, USA
Kodak Scientific Imaging Film	Kodak, USA
DPX Mountant for histology	Fluka

Table 7: Reagents and buffers for X-gal staining.

Potassium Ferricyanide ($K_3Fe(CN)_6$)	Sigma
Potassium Ferricyanide ($K_4Fe(CN)_6x3H_2O$)	Sigma
NP-40	Roth
X-Gal	Roth stock solution 40mg/ml in DMSO

Fixing solution	1XPBS 1% formaldehyde 0.2% glutaraldehyde 0.02% (v/v) Nonidet P40
Staining solution	1X PBS 2mM $MgCl_2$ 5mM $K_3Fe(CN)_6$ 5mM $K_4Fe(CN)_6$ 1mg/ml X-gal

Table 8: Reagents and buffers for skeletal preparation.

Alcian Blue 8 GX	Sigma
Alizarin Red S	Sigma
Alcian Blue solution	15mg of Alcian Blue 8GX 80ml of 95%Ethanol 20ml of glacial acetic acid
Alizarin Red solution	50mg Alizarin Red 1L of 1% or 2% KOH in water

Table 9: Reagents and media for the cell culture.

DMEM (Dulbecco's Modified Eagle Media): high glucose, with L-glutamine	GIBCO (Invitrogen)
FBS (FCS)	GIBCO (Invitrogen)
Penicilin/Streptomicin, 100X solution (contains 10,000 U of Penicillin, 10,000 µg of Streptomycin)	GIBCO (Invitrogen)
Trypsin, 10 X solution	GIBCO (Invitrogen)
COS-7 growth medium	DMEM, high glucose 5% FBS Pen/Strep (1/100 of stock solution)
6- or12-well plates, pipetts	Corning
15mm glass coverslips	Roth

Polyfect Transfection Reagent	QIAGEN
Vectashield mountig medium with Dapi	Vector

2.1.3 Bacterial strain

DH5α™

F- φ80*lac*ZΔM15 Δ(*lac*ZYA-*arg*F)U169 *rec*A1 *end*A1 *hsd*R17(rk-, mk+) *pho*A*sup*E44 *thi*-1 *gyr*A96 *rel*A1 λ-

TOP10

F- *mcr*A Δ(*mrr-hsd*RMS-*mcr*BC) Φ80*lac*ZΔM15 Δ*lac*X74 *rec*A1 *ara*D139 Δ(*araleu*) 7697 *gal*U *gal*K *rps*L (StrR) *end*A1 *nup*G

2.1.4 Plasmids and vectors

pBluescript II KS (+) Stratagene
pCR4-TOPO, Invitrogen
pEGFP-N3, Clontech
pWH9, kindly provided by Reinhard Fässler

2.1.5. DNA-probes for in situ hybridization

Table 10: Mouse DNA probes for in vitro transcription.

Probe	Vector	Insert size	Restriction endonuclease (for antisense)	RNA-polymerase (for antisense)	Reference
mIhh	pBSK	1800 bp	*Xba* I	T7	Bitgood and McMahon, 1995
mCol10a1	pBSK+	400 bp	*Cla* I	T3	Jacenko et al., 1993
mOsx	pBS II KS+	660 bp	*Not* I	T3	Nakashima et al., 2002
MMP13	pCR-21	1000	*Hind* III	T7	Yamagiwa et al., 1999

mBspI	pCR	~900 bp	*Not* I	SP6	(Young et al., 1994)
mOsc	pBSK	500 bp	*Xba* I	T3	Desbois et al., 1994
Tmem16f	pBS II SK	220bp	*Bam H I*	T7	Chinenkova and Vortkamp

2.1.6 Mouse lines

Wild type NMRI mice were derived from Harlan Winkelmann (Germany branch)

Wild type C57Bl/6J mice were derived from Harlan Winkelmann (Netherlands branch)

Ihh deficient mice, *Col-IIGal4* and *UAS-Ihh* transgenic mice were kindly provided by Andrew P. McMahon (Long et al., 2001; St-Jacques et al., 1999).

Runx2 deficient mice were kindly provided by Stephan Mundlos, MPI Berlin

Fixed limbs of Osx deficient mice were kindly provided by Knakashima

2.1.7 Gene trap ES cells

Bay Genomics California, USA

2.1.8 Bioinformatics resources

NCBI Blast http://www.ncbi.nlm.nih.gov

Ensemble genome browser http://www.ensembl.org/index.html

MGI, mouse genome informatics http://www.informatics.jax.org

TMHMM- Prediction of transmembrane helices in proteins

http://www.cbs.dtu.dk/services/TMHMM-2.0

UniProt database http://www.uniprot.org

PSORT- Prediction of protein subcellular localization http://www.psort.org

2.2 Methods

2.2.1 Total RNA purification

RNA was isolated using Trizol reagent (Invitrogen). The extraction was performed according to the manufacturer protocol. Limbs of E 16.5 or E 18.5 NMRI mouse embryo were collected and homogenized in 1 ml of Trizol. To remove insoluble

material from the homogenate, the mixture was centrifuged for 10 min at 12000 x g at 4°C. To separate the RNA from the genomic DNA and proteins 0,2 ml of chloroform was added to the homogenate, the sample was shaken, incubated at RT for 2-3min and centrifuged at 12000 x g for 15 min at 4 ^{0}C. This step separated the mixture into a lower, phenol-chloroform phase, an interphase and an upper aqueous phase. RNA remains in the aqueous phase, which was then precipitated by mixing with isopropyl alcohol (0,5ml) followed by the 10 min incubation at RT and centrifugation at 12000 x g for 10 min at 2 to 8 ^{0}C. RNA pellet was washed with 75% ethanol, mixed by vortexing and centrifuged at 7500 x g for 5 min at 4 ^{0}C. The pellet was air-dried for 5-10 min and solved in 30µl to 50 µl RNAse free H_20 (DEPC treated or Millipore water). The quantity of the isolated RNA was determined by photometric measurement. The quality was monitored by electrophoresis on an agarose gel stained with ethidium bromide: two distinguishable bands of 28S and 18S ribosomal RNA (~5kb and ~2kb respectively) were visible, which provided test for the sufficient amount of total RNA.

2.2.2 Reverse transcription

The Super Script III First-Strand Synthesis System (Invitrogen) for the cDNA synthesis from mRNA template was used following manufacturer protocol. 3 to 5 µg of total RNA was mixed with Oligo$(dT)_{20}$ primer or gene specific primer (GSP) and dNTPs. Mixture was heated and cooled down for primer annealing. cDNA Synthesis mixture containing 10X transcription buffer, 25mM $MgCl_2$, 0.1M DTT, 40U of RNaseOUT and 200U of SuperScript III RT was added to RNA mix. cDNA synthesis was performed at 50^{0}C for 50 min in 20µl reaction volume and terminated by heating at 85^{0}C for 5 min. To remove RNA template 1µl of RNAseH was added to the sample for 20 min (37^{0}C). After the synthesis, 2µl of the reaction product was used for PCR.

2.2.3 5’ RACE

This method allows to amplify full-length transcripts via elimination of truncated mRNA from the amplification process (Maruyama and Sugano, 1994; Schaefer, 1995; Volloch et al., 1994. Fig. 6). At first step purified total RNA from E16.5 limbs is treated with calf intestinal phosphatase (CIP). This enzyme removes 5’ phosphate group from truncated RNA and non-mRNA (but has no effect on full length, capped mRNA), thus allowing to prevent subsequent ligation with the GeneRacerRNA Oligo. The dephosphorylated RNA is treated with tobacco acid pyrophosphatase (TAP) to

remove the 5'cap structure from the full-length mRNA. This enzyme leaves a 5'phosphate required for ligation to the GeneRacerRNA Oligo. The GeneRacerRNA Oligo is then ligated to the 5'end of the mRNA using T4 RNA ligase. Ligated mRNA was reverse-transcribed to create RACE-ready first-strand cDNA with known priming site at 5' end. To amplify the 5' ends of cDNA a reverse gene specific primer (GSP) and GeneRacer 5'Primer (complementary to the GeneRacerRNA Oligo) were used. Additionally, gene specific nested primers (NGSP) are used to amplify the 5' cDNA end. Control primers, complementary to the 3'region of the Tmem16f gene were used to confirm presence and sufficient amount of the cDNA. Several clones, obtained from the 5'RACE were chosen for the sequencing.

Primers for the amplification of the 5' part of Tmem16f:

GSP1 (complimentary to the 5'-end of the Tmem16f)
5'- GATAAGGTTAGATTCGTATGCTTGTC-3'
NGSP1 (complimentary to the 5'-end of the Tmem16f)
5'-GTTCAGCAGGACCTTCCTAGTCATC -3'
GeneRacer RNA Oligo
5'- CGACUGGAGCACGAGGACACUGACAUGGACUGAAGGAGUAGAAA -3'
GeneRacer 5'Primer 5'-CGACTGGAGCACGAGGACACTGA-3'

Control Primers to the 3' region of Tmem16f cDNA
contr_fw 5'-ACCCCACGATGGGAACAGGATTACC-3'
contr_rev 5'-TCGGAAGTCACGGTACCTGCACAAG-3'

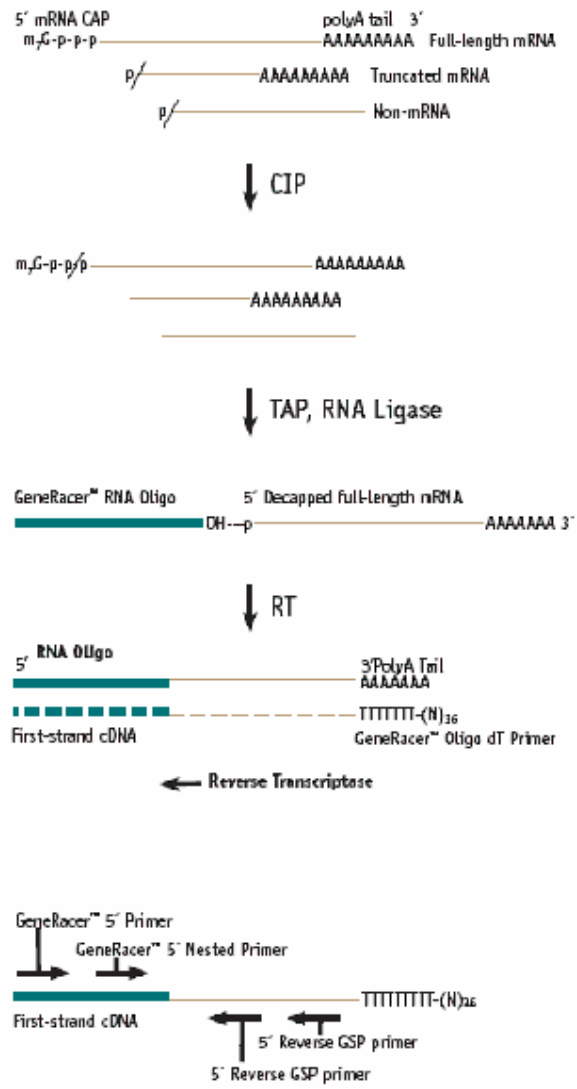

1. RNA (mRNA or total) is treated with calf intestinal phosphatase (CIP). CIP removes the 5′ phosphate from partial transcripts, preventing the GeneRacer™ RNA Oligo from ligating. CIP does not affect capped mRNA.

2. RNA is treated with tobacco acid pyrophosphatase (TAP), which removes the cap from capped mRNA and exposes the 5′ phosphate, permitting ligation of the GeneRacer™ RNA Oligo.

3. The GeneRacer™ RNA Oligo is ligated to the TAP-treated mRNA with T4 RNA ligase.

4. A cDNA template is generated by reverse transcription using SuperScript™ II RT or AMV RT and either the GeneRacer™ Oligo dT Primer, your gene-specific primer, or random primers.

5. 5′ ends are PCR amplified from these cDNA templates with a primer for the GeneRacer™ RNA Oligo (GeneRacer™ 5′ Primer) and your gene-specific primer. Only cDNA containing the GeneRacer™ RNA Oligo sequence will be amplified.

Figure 6: Scheme of the 5' RACE.

Accepted from "GeneRacer^{tm} Kit" manual, Invitrogen.

2.2.4 Proof of the Tmem16f cDNA

Primers for different Tmem16f exons were used in PCR to confirm intron-exon structure of the Tmem16f gene:

Exon-3	5'-AGCAGGACTTCAGGACTCCA-3'
Exon-6	5'-AGTGCTGTGCACCTATGCTG-3'
Exon-8	5'-AGGGAACGCTGCTTTGTAGA-3'
Exon-11a	5'-CGAAGATCAGGGTTCCAAAA-3'

Exon-11b	5'-TTTTGGAACCCTGATCTTCG-3'
Exon-16	5'-CGTCAGCTGTGTGGTCAGTT-3'

2.2.5 Preparation of genomic DNA from mammalian tissue

Mouse liver (500mg up to 3g) was rapidly frozen in liquid nitrogen and crushed to produce readily digestible pieces. It was important to avoid taking gallbladder, since it contains high levels of degradative enzymes. The tissue was suspended with 2ml of solution A (25mMEDTA pH8.0, 75 mM NaCl) per each 500mg of tissue, followed by the addition of 2ml of solution B (10 mM EDTA pH8.0, 10 mM Tris-HCl pH 8.0, 1% SDS (w/v), 400 µg/ml Proteinase K) for the same amount of tissue. Digestion by Proteinase K took place overnight at 55^0C in water bath on a shaking platform. After that 2ml of solution A and 2 ml of solution B were added to the suspension and incubated for 2 hours at 55^0C to allow most of the cellular proteins to degrade. In order to remove RNA, 10 µl of RNAseA (stock solution 10mg/ml) was added per 2 ml suspension and incubated for 1 hour at 37^oC. Phenol/chloroform extraction was performed twice with gentle rotation of the tube using equal volume of reagents and slow centrifugation at 5000rpm for 10min helped to remove proteins from the DNA. DNA was precipitated from the aqueous phase by adding 5M NaCl (to final concentration of 250mM) and 0.7V isopropanol. DNA became visible as a white "threads" after gentle rotation of the mix and could be easily removed from the solution by a glass stick. DNA was placed into clean eppendorf tube, dried, and left overnight in 250 µl of water or TE-buffer at 4^0C to dissolve. The quality of genomic DNA was analysed by gel electrophoresis and the quantity was measured with a photometer (Pharmacia Biotech). This quantity can be also estimated by the A260/A280 ratio. Ratio >1.8 shows highly pure DNA, while 50%protein/50%DNA mixtures have A260/A280 ratios of ~1.5.

2.2.6 Southern Blot: DNA transferring onto a nylon membrane with high-salt buffer

Southern Blotting is the transfer of DNA fragments from an electroforesis gel to a membrane support (Southern, 1975). The protocol is divided into three stages. First, the agarose gel is pretreated by soaking in a series of solutions that depurinate, denature, and neutralize the DNA and gel matrix. The second stage is the transfer itself, which occurs by upward capillary action. Third, the DNA is immobilized on the membrane by UV irradiation (Ausubel et al., 1987-1999).

Preparation of the gel

Genomic DNA was digested with appropriate restriction enzyme. The mixture contained 5 to 15 µl of genomic DNA in 30 to 50µl volume, 20 to 40 U of restriction enzyme, 0.1mM DTT, 1mM Spermidine and 100µg/ml BSA. After 2 hours of incubation another portion of the restriction enzyme was added to complete digestion. The sample was incubated for another 2 to 4 hours. 0.8% agarose gel was run in 0.5 X TBE buffer overnight with appropriate DNA size markers, stained with ethidium bromide. The gel was photographed with a ruler laid alongside so that band positions can later be identified on the membrane. Then the gel was rinsed in distilled water, placed in a clean glass dish containing ~10 gel volumes of 0.2 N HCl and shaken slowly for 30 min. This partial depurinization of the DNA fragments led to strand cleavage and thus to the length reduction, which improves the transfer of longer molecules. After depurinization the gel was placed in ~10 volumes of denaturation solution (1.5M NaCl/ 0.5N NaOH) for 45 min to 1 hour. Denaturation gives single stranded molecules which are suitable for subsequent hybridization. For neutralization the gel was placed in 1.5M NaCl/1M Tris (pH 7.4) solution to bring the gel pH down to <9.0.

Set up the transfer

Transfer buffer (10 X SSC) was put into reservoir of an appropriate size. The glass plate with a sheet of long 3MM Whatman filter paper (soaked in 10 X SSC) was placed on to the reservoir so, that the ends of the filter paper were submerged into transfer buffer. Another couple of short sheets of Whatman paper (slightly larger than the gel) soaked in 10 X SSC was placed onto the glass plate. Air bubbles were carefully removed from the paper sheets. The gel was placed onto the sheets and covered with the nylon membrane (Hybond) soaked in 6XSSC. The membrane was the same size as the gel. 3 more pieces of Whatman paper were placed on the nylon membrane, soaked into 6 X SSC. Four strips of plastic wrap were placed over the edges of the gel to prevent the buffer from “short-circuiting”. Paper towels were placed on Whatman sheets and a weight of 0.3-0.4 kg was placed on a top of them. The transfer took place overnight. After the transfer, the position of the slots was marked on the filter and the same bottom corner was cut as on the gel to distinguish the direction of the membrane later.

Immobilization of the DNA: UV crosslinking

Nylon membrane was shortly rinsed in 6 X SSC and completely dried on Whatman Paper. DNA crosslinking was performed at 245-nm wavelength in Stratalinker

(Stratagene). UV crosslinking leads to covalent attachment and enables the membrane to be reprobed several times.

2.2.7 Preparing the radioactive labeled probe for hybridization

Procedure was performed using Rediprime II Random Prime Labelling System (Amersham), based on the method, introduced by Feinberg and Vogelstein (Feinberg and Vogelstein, 1983 and 1984). Following the manufactures protocol, DNA for hybridization was diluted to a concentration of 25ng in 45µl of TE-buffer (10mM Tris HCl pH 8.0, 1mM EDTA), denaturated at 95^0C for 5 min and cooled immediately by placing on ice for 5min after denaturation. Denatured DNA and 5µl of Redivue [^{32}P]dCTP were added to the reaction tube (pre-made by manufacturer) and mixed well by pipetting. Reaction was incubated at 37^{o}C for 1 hour. Addition of 5µl of 250mM EDTA stopped the reaction and the probe was cleaned using micro spin columns (Amerscham) following manufactures protocol. 500µl of hybridization buffer (Church buffer containing fish sperm DNA (0.1 µg/ml) and Cot-DNA (500µg/ml) was added to the cleaned DNA probe. The mixture was heated at 95^0C for 5 min to denaturate DNA probe and added directly to the membrane in preheated hybridization buffer. Fish sperm DNA and mouse Cot-DNA serve to prevent non-specific binding of DNA-probe by annealing to nonspecific sequences and repetitive elements.

2.2.8 Southern Blot hybridization

Nylon membrane carrying digested genomic DNA was prehybridized in 15-20 ml of hybridization buffer for 6 hours or overnight at 65^{o}C. The solution was changed to the 5ml of hybridization solution with radioactive labeled probe (Church buffer+ fish sperm DNA+ Cot-DNA+ labeled DNA probe). Hybridization took place overnight at 65^{o}C, followed by 3 step- washing: 30 min at 65^{o}C in 200 ml of solution I, 30 min at 65^{o}C in 200-300 ml of wash solution II, two times. The phosphoimager cassette was exposed overnight to the wet filters packed in to the plastic foil.

2.2.9 PAC library hybridization

Mouse genomic PAC library (RPCI21 High Density Gridded Filters) was used.

The source of the library was the female 129/SvevTACfBr mouse spleen genomic DNA. Seven filters PAC1 to PAC7 covered the whole library. Each filter was prehybridized in 100 ml of hybridization buffer at 65^{o}C overnight. Prehybridization

solution was removed and 30ml hybridization solution containing labeled probe was added immediately. Hybridization took place at 65^{0}C overnight. Filters were washed in three steps. The first wash in 200ml of solution I was performed for 30min at 65^{o}C followed by the second and third washes in 500 ml of solution II for 30 min at 65^{o}C.

Primers for the amplification of the 714bp DNA-probe:

Primer1_fw	5'-GGGAGACATGCAGATGATGA-3'
Primer1_rev	5'-GGTGCAGAGCCTTAACTTGC-3'

2.2.10 Tmem16f gene targeting

The targeting vector for Tmem16f gene was electroporated into R1 ES cells (derived from 129/Sv mice). These cells were subsequently grown in the presence of Geneticin (G418). Resultant colonies were isolated, expanded, and further analyzed by Southern blot hybridization for the correct integration site. ES cells of chosen clones were injected into the blastocysts from black C57Bl/6J mice. The injected blastocysts are transfered into the uterus of foster mice, where they develop into chimeric mice. Germ-line transmission was recognized by mating these chimeric mice to C57Bl/6J mice. ES-cell-derived germ cells result in agouti animal, since agouti is dominant over black.

2.2.11 ES cell clones analysis

The analysis of 360 ES cell clones was performed by Southern blot hybridization using 5'- and 3'- external probes (Fig. n+1). Genomic DNA purified from the ES cell clones was digested in a total volume of 30µl with 40 units of appropriate restriction enzyme. Incubation took place at least 6 hours at the optimal condition for given enzyme. 120 ES cell clones were analyzed on one filter. Each filter was prehybridized in 90 ml of hybridization solution. 20 ml of hybridization solution containing 2 radioactive labeled probes was used for this hybridization. The two-steps washing routine was performed at 65^{o}C for 30 min (washing solution I) and at 55^{o}C for 10 min (solution II).

Primers for the 5' probe:

ST2-5'probe5'	5'-CCTAGAACATGCCCTTCAGATAC-3'
ST2-5'probe3'	5'-TCCAGTATGGTGAGCCAGTGAG-3'

Primers for the 3' probe:

3‘ES_ST2_fw	5'-AAA TGC ACG CAA GAT TAT GCT-3'
3‘ES_ST2_rev	5'-ACT GGA CCT GGA AAC CTG AAA G-3'

2.2.12 Cloning techniques

2.2.12.1 PCR

Polymerase chain reaction was performed in 25-50µl volume mixture containing 1XPCR Buffer, two primers 0.5µM each, 200µM dNTPs mix, 10-100ng DNA template, 2.5U of Taq-polymerase. 30 cycles were used to amplify the DNA fragment.

2.2.12.2 Restriction digestion

To digest DNA, chosen restriction enzyme was added in a ratio 1U of enzyme to 1 µg of DNA in 50µl of reaction. Buffer and temperature condition were used according the manufacturer data (NEB).

2.2.12.3 Ligation

Reaction was performed at 16^{o}C or room temperature for 4 to 16 hours. 10µl of reaction mixture contained 10X ligation buffer, 5mM DTT, ~100ng of the fragment, ~50ng of the vector and 1 U of the T4-DNA ligase (Roche). The ligase was inactivated by heating at 65^{o}C for 10min.

2.2.12.4 Transformation

Heat-shock competent cells (Invitrogen) were used followed manufacturer protocol. An aliquot of the cells (50µl) was thawed on ice and 1-3 µl of the ligation mix were added to the cells. After 30 min of the incubation on ice the cells were placed into 37^{o}C water bath for 30 seconds and then immediately on ice. 1 ml of SOC-medium was added to the cells and incubated for 1 hour at 37^{o}C on shaking platform. Different amount of the suspension (5, 50 or 200µl) was plated onto agar-plate containing an appropriate antibiotic for the clone-selection.

2.2.12.5 Clone analysis

To pick up the right clone, containing correct sequence of DNA fragment, up to 60 clones were analyzed. The analysis was performed by colony-PCR and restriction digestion.

2.2.12.6 DNA sequencing

The sequencing of DNA was performed by Seqlab (Sequence Laboratories Göttingen GmbH), Göttingen.

2.2.12.7 Cloning of Tmem16f into pEGFP-N3 vector

The small fragment of the 3'end (~300bp) of the Tmem16f gene was amplified and inserted in to the pEGFP-N3 plasmid, digested with *Kpn*I and *BamH*I restriction enzymes

Primers:

CTD_*Kpn*I 5'-CTTGTGCA**GGTACC**GTGACTTCC-3'

CTD_*BamH*I 5'-AAAT**GGATCC**TTCGAGTTTTGGC-3'

Larger 5' part of the gene was cut out from the RZPD clone, containing most of the Tmem16f cDNA sequence. The *EcoR*I- *Kpn*I fragment was inserted into pEGFP-N3 infront of the cloned 3'part of Tmem16f ORF.

Sequences in bold represent sites of restriction enzymes.

2.2.12.8 Cloning strategy for ST2-C6 KO construct (in to pWH9)

5' arm cloning:

XhoI primers were used for amplification of the 5' arm sequence. Ligation with pWH9:*Xho*I vector. Result: pWH9-ST2-5'arm construct

Primer sequences:

ST2-5'arm5' 5'-GAAAA**CTCGAG**TGGAGCTGTTACTTGG-3'

5'armST2_XhoI_1 5'-AAAA**CTCGAG**CTTCTATGAGCTCACGAGGGTC-3'

3' arm cloning was done in two steps:

Step I: cloning of the 3' arm in to pBS II SK in 2 pieces:

1) *Sal*I-*BamH*I fragment (4,3 kb PCR-product)

Primer sequences:

ST2_3'arm _SalI 5'-AAATT**GTCGAC**TGAGCTGTCTGTAACTTGGGA-3'

ST2_3'arm BamHI_rev 5'-TATTT**GGATCC**AAAGCATCAAGAAGAGAGAATGAG-3'

2) *BamH*I-*Xba*I PCR-fragment (3,58 kb)

Primer sequences:

3'armST2_BamHI_fw	5'-GCTTT**GGATCC**AGATGTAGAACTCTCAGTTCCTTC-3'
3'armST2_XbaI	5'-TCACA**TCTAGA**ATACAAACTGCACCAAAGGTGG-3'

Step II: subcloning of the 3'arm fragment from pBS II SK vector into pWH9-ST2-5'arm construct using *Sal*I & *Not*I enzymes

2.2.12.9 Preparation of the murine Tmem16f-probe for the in situ hybridization

Primer sequences

BamH I_1ex5'	5'-AAA**GGATCC**TCGCACGCTGAGCAGCGCCTG-3'
EcoR I_1ex3'	5'-AAA**GAATTC**CAATGTCTCCATCCTCATCG-3'

PCR fragment of 220bp was cloned into pBS K II

2.2.13 Genomic DNA preparation from mouse tail

Piece of mouse tail was placed in 500 µl of lysis buffer (50 mM Tris-HCl, pH 8.0, 100mM EDTA, 1% SDS, 100 mM NaCl) with 10 µl of 20 mg/ml proteinase K in 1.5 ml tube and incubated at 55°C overnight. The mixture was cooled down to room temperature and 250 µl of 5 M NaCl was added. Then, the mixture was shaken and incubated for 10 minutes on ice. Probes were centrifuged at 8,000 rpm for 8 minutes. Supernatant (0.5 ml) was transferred to the clean tube and DNA was precipitated by addition of 1 ml of 100% ethanol followed by centrifugation at 14,000 rpm for 10 minutes at room temperature. DNA pellet was resuspended in 70-100 µl of TE buffer at 65°C for 20 minutes.

2.2.14 Genotyping of the mice

Genotyping of the mice was performed by PCR. PCR mixture contained 100 ng genomic DNA, 0.02 µM of appropriate primers, 0.25 mM dNTPs, 0.5 U Taq-polymerase and 10x PCR-buffer.

Primers for ***Col II-Gal4*** mice

forward primer	5'-CTTCTATCGAACAAGCATGCG-3'
reverse primer	5'-GCCAATCTATCTGTGACGGC-3'

The PCR conditions for genotyping of *ColII-Gal4* mice were: 94°C for 5 minutes; 40 cycles of 94°C for 30 seconds, 58°C for 30 seconds, 72°C for 30 seconds; and 72°C for 5 minutes.

The resulting fragment of 322bp indicated a transgenic mouse.

Primers for ***UAS-Ihh*** mice

forward primer	5'-GGGCGGGCGCTGGCGACGCTG-3'
reverse primer	5'-CGGGCTGCACGTGGCTG-3'

The PCR conditions for genotyping of *UAS-Ihh* mice were: 94°C for 10 minutes; 35 cycles of 94°C for 30 seconds, 72°C for 30 seconds, 72°C 30 seconds; and 72°C for 10 minutes.

The resulting fragment of 300 bp indicated a transgenic mouse.

Primers for ***Ihh* deficient** mice

Neo	5´-TACCGGTGGATGTGGAATGTGTGCG-3´
Ihh- fw	5´-AGGAGGCAGGGACATGGATAGGGTG-3´
mIhh ex2 rv2	5'-TGTTCTCCTCGTCCTTGAAGA-3'

The PCR conditions for the wild -type allele were: 94°C for 5 minutes; 32 cycles of 94°C for 45 seconds, 59°C for 45 seconds, 72°C for 60 seconds; and 72°C for 7 minutes. The resulting 160 bp fragment indicated the wild-type allele. For genotyping of the transgenic allele the following PCR conditions were used to amplify a 300 bp fragment: 94°C for 5 minutes; 30 cycles of 94°C for 1 minute, 62°C for 1 minute, 72°C for 1 minute and 72°C for 7 minutes.

Primers for ***Runx2* deficient** mice

runx2neo	5'-TCTGGATTCATCGACTGTGG-3'
CBFA11fw	5'-CTTGAAGGCCACGGGCAGG-3'
MCBFA	5'-CAAGATGAGCGACGTGAGCC-3'

The PCR conditions were: 94°C for 5min, 5 cycles of 94°C for 1 min, 64°C for 45 sec, 72°C for 45 sec; 10 cycles of 94°C for 1 min, 62°C for 45 sec, 72°C for 45 sec; 20 cycles of 94°C for 1 min, 60°C for 45 sec, 72°C for 45 sec; and 72°C for 7 minutes.

The resulting fragment of 450 bp indicated a transgenic allele and the fragment of 320 bp indicated the wild type allele.

Primers for ***Tmem16f* deficient** mice

neo-3'fw_3 5'-CCTTCTATCGCCTTCTTGAC-3'

ST-3'arm_rev_5 5'-CTCCTCCTTACTTCTAAGACATC-3'

The PCR conditions were: 95°C for 5min, 30cycles of 95°C for 30sec, 58°C for 30 sec, 72°C for 30 sec, final elongation 72°C for 5min. The resulting 600bp fragment indicated transgenic allele.

Primers for ***Tmem16f* wild type** mice

ST2_wt_fw primer 5'-TTCTCTGTCCTCTTTCGGT- 3'

3'arm_rev_2 5'-GACTTACACTATACTCGACA- 3'

The PCR conditions were: 95°C for 5min, 30cycles of 95°C for 30sec, 58°C for 30 sec, 72°C for 40 sec, final elongation 72°C for 5min. The resulting 600bp fragment indicated wild type allele.

Primers for ***Tmem16f gene trap cassette***

ST2-ex13_gtreseq 5'-GGT CAC GCT GTG TGC GAG C-3'

GT-vec-70-R 5'-CAC TCC AAC CTC CGC AAA CTC-3'

The PCR conditions were: 95°C for 5min, 30cycles of 95°C for 30sec, 61°C for 30 sec, 72°C for 30 sec, final elongation 72°C for 5min. The resulting ~300bp indicated gene trap allele.

Primers for ***Tmem16f gene trap*** wild type mice

ST2-ex13_gtreseq 5'-GGT CAC GCT GTG TGC GAG C-3'

gt-wt-rev_3primer 5'-GCAATACTCCACGTGACAG-3'

The PCR conditions were: 95°C for 5min, 30cycles of 95°C for 30sec, 55°C for 30 sec, 72°C for 25 sec, final elongation 72°C for 5min. The resulting ~300bp indicated wild type allele.

2.2.15 In situ hybridization

2.2.15.1 Preparation of DNA template for in vitro transcription

Plasmid DNA was isolated from *E.coli* DH5 cells using QIAprep Plasmid Miniprep according to the manufacturer instructions. 5 µg of plasmid DNA was linearized with 5 U of the appropriate restriction endonuclease for 1 hour at the optimal temperature. Efficiency of the digestion was analyzed on a 1% agarose gel. Phenol/chloroform extraction was performed twice. The final aqueous phase was transferred to a clean

tube and was precipitated with 2.5 volumes of 100% ethanol. The mixture was centrifuged at 14.000 rpm for 15 minutes at 4°C. The DNA pellet was washed with cold 80% ethanol and resuspended in 10 µl of RNAse free water.

2.2.15.2 Labeling of antisense riboprobes

Transcription reaction was performed in 20 µl with the following components: 500 ng linearized DNA template for *in vitro* transcription, 1x transcription buffer, 0.5 mM NTP mixture, 5 U RNAse inhibitor, RNAse free water, 40 U RNA-polymerase and 80 µCi [P33]-UTP. The transcription reaction was carried out for 1.5 hours at 37°C. To remove the DNA template, 20 U of DNAse (RNAse-free) were added to the transcription mixture and incubated for 20 minutes at 37°C. The transcription mixture was then diluted with 4 volumes of RNAse free water, containing 20 ng/ml glycogen and 0.5 M LiCl, and precipitated with 2.5 volumes of 100% ethanol. Probes were incubated at -20°C for 30 min and then centrifuged at 14000 rpm for 15 minutes at 4°C. The RNA pellet was washed with cold 75% ethanol, resuspended in 50µl RNAse free water, and diluted with 1ml of hybridization buffer. The riboprobe was heated for 5 minutes at 95°C (denaturation) and chilled on ice (kept on ice until used).

2.2.15.3 Prehybridization and in situ hybridization

All solutions for the prehybridization procedure were prepared with RNAse free water. The sections were incubated in xylol for 20 minutes to remove the paraffin. To rehydrate the tissue, the sections were incubated in a descending ethanol series (100%, 95%, 80%, 75%, 50%, 30%) each for 2 minutes, followed by 0.85% NaCl for 5 minutes and PBS for 5 minutes. After rehydration the tissue was fixed in 4% PFA for 20 minutes. The sections were then incubated for 5 minutes in following solutions: PBS, 0.2N HCl and RNAse free water. The tissue was digested for 5 minutes with 0.02 mg/ml Proteinase K and rinsed with PBS for 5 minutes. Subsequently the sections were refixed in 4% PFA with 0.2% glutaraldehyde for 10 minutes and rinsed with PBS for 5 minutes. The sections were incubated in 0.2% Triethanolamine with freshly added 0.25% acetic anhydride for 10 minutes, then rinsed with PBS for 5 minutes and additionally incubated in 0.85% NaCl for 5 minutes. Sections were dehydrated with the following ethanol solutions: 30%, 50%, 75%, 100%. The sections dried at RT for at least 15 minutes. A minimal volume of labeled riboprobe (50 µl) was distributed evenly on the slide and the sections were covered with plastic coverslips to prevent evaporation. Hybridization was performed

at 70°C overnight.

2.2.15.4 Washing of slides and dipping in photoemulsion

After hybridization the sections were washed in 5xSSC for 30 minutes at 55^{o}C and coverslips were removed from the slides. The sections were washed in 2xSSC for 30 minutes at 55^{o}C, followed by treatment with 0.02mg of RNAse A in 1x Washing buffer for 30 minutes at 37^{o}C. Stringent washing procedure was performed in 2xSSC with 50% formamide for 30 minutes at 55^{o}C followed by washing in 2xSSC for 30 minutes at 55^{o}C twice. The sections were dehydrated in an ascending ethanol series (30%, 50%, 75%, 80%) containing 0.3M ammonium acetate. Finally, the sections were briefly incubated in 100% ethanol and dried for 10 minutes at RT. X-ray film (Kodak Scientific Imaging Film) was placed on the slides for overnight exposition at RT to estimate the intensity and the signal strength of each probe. The sections were dipped into photoemulsion NTB2 at 42°C in the darkness. Dried sections were stored at 4°C in darkness for the time predicted from the developed X-ray film. The dipped sections were developed using Kodak-developer for 5 minutes at 15°C, rinsed in water and fixed in Kodak-fixer for 15 minutes at RT. The sections were counterstained with 0.2% Toluidin blue O and dehydrated in ethanol solutions 30%, 50%, 75%, 80%, 95% and 100%. The sections were placed into 100% xylol for at least 20 min and then covered with glass coverslips using minimal volume of mounting medium (DPX mountant for histology). The slides were dried overnight. The sections were analyzed and photographed by dark-field microscopy.

2.2.16 The gene trap integration site

The integration site for the gene trap cassette was initially defined by Bay Genomics as approximate site of cassette insertion. To confirm this data the integration site was proven by PCR with the primers annealed at the end of exon 13 of Tmem16f and to the gene trap cassette. The sequence of PCR product confirmed integration of the cassette into 13th intron, 300b.p. beyond the exon 13. The same pair of primers was used for the genotyping of the gene trap mice.

2.2.17 Alcian Blue-Alizarin Red staining

Embryos or adult mice were dissected and skin and fat were carefully removed. The specimens were fixed in 95% Ethanol for 3 days and placed in acetone for one day to remove the rest of the fat. Acetone was removed and specimens were washed with 95% ethanol. Ethanol was replaced by Alcian Blue solution for one day at room

temperature. Alcian Blue solution was replaced with 95% ethanol for one day followed by replacement with Alizarin Red solution. The skeletons were stained for 1 day with Alizarin Red followed by the clearance with 1% KOH (for the embryos) or 2% KOH (for adult mice) for one to two days. The specimens were placed in 20% glycerol/1%KOH (2% KOH for adult specimens) until they were cleared. For longer storage the skeletons were placed in 40% glycerol/1%KOH followed by the 60% glycerol /1%KOH, 80% glycerol /1%KOH and finally 100% glycerol (at least one day for each solution). Alcian Blue stains cartilage in blue and Alizarin Red stains bone in red.

2.2.18 X-gal staining

The E. coli lacZ gene encoding ß-Galactosidase (ß-Gal) is the classical histochemical reporter gene. The activity of ß-Gal can be detected by X-gal (5-bromo-4-chloro-3-indolyl-ß-D-galactoside). X-gal staining is used to detect ß-galactosidase activity in transgenic mice. E14.5 or E15.5 embryos were put into the fixing solution for 30min at 4^{o}C, cut in two pieces, washed with 1XPBS and incubated further in fixing solution for another 30min. The embryos were washed two times in 1X PBS for 20min at room temperature. PBS solution was removed and staining solution was added followed by the incubation for one to two days at 30^{o}C. After staining the samples were stored in 1X PBS for several days while photographing.

2.2.19 Von Kossa staining

The von Kossa technique is a histochemical method for detection of calcium, associated with phosphate and carbonate (Kiernan, 2008). The reaction is carried out in bright light (or UV light), which leads to reduction to metal of silver ions in the crystals of the insoluble silver phosphate and carbonate. Unreduced ionized silver is removed by treatment with sodium thiosulphate followed by subsequent counterstaining for the nuclei of the cells. In more details, the paraffin sections were deparaffinized and rehydrated to water through the descending ethanol raw and rinsed several times in distilled water. The sections were incubated with 1% silver nitrate in clear glass coplin jar for 20 min under UV light. The slides were rinsed several times with distilled water and un-reacted silver was removed by 5% sodium thiosulfate for 5min. The sections were rinsed with distilled water and counterstained with Nuclear Fast Red for 5min. Slides were rinsed with water and then dehydrated through the ascending ethanol and placed in Xylol. The slides were covered using

DPX mounting medium. Calcium salts can be visualized as black or dark brown precipitate and nuclei are stained in red or pink.

2.2.20 Hematoxylin Eosin staining

This histological staining method stains nuclei blue (Hematoxylin) and the cytoplasm red (Eosin). Sections were deparaffinized, rehydrated and subsequently incubated for 45seconds in Hematoxylin, rinsed shortly with tap water and then incubated for 2 to 3 minutes in Eosin. Finally slides were rinsed with tap water, dehydrated by an increasing ethanol series, transferred into Xylol and embedded in DPX mounting medium.

2.2.21 TRAP staining

The tartrate resistant acid phosphatase (TRAP) is the marker for the osteoclasts. Compared to other nonspecific phosphatases, this enzyme has optimal activity in acidic conditions (pH<5) and can be distinguished from other phosphatases by its resistance to inhibition by tartrate. Naphtol AS-BI, released by enzymatic hydrolysis, couples immediately with fast garnet GBC forming insoluble dark-red dye deposits at sites of activity. The acid phosphatase kit (Sigma) was used for osteoclasts detection, following manufacturer protocol. In brief, the sections were fixed in Citrate/Aceton solution for 30sec at room temperature, rinsed in deionized water and dried at least for 15 min. The staining solution was prepared by mixing water, Acetate solution, Naphthol AS-BI phosphoric acid and Tartrate solution. Contents of one capsule Fast Garnet GBS salt was added to the mixture, and prepared solution was finally filtered through Whatman No. 54 paper. The solution was placed in the 37^{o}C water bath until it reaches the same temperature. The samples were incubated in the staining solution for 1 hour at 37^{o}C in dark. The slides were washed in deionized water, counterstained in Acid Hematoxylin Solution for 5min, and dried before imbedding in the aqueous mounting medium.

2.2.22 Preparation of the cryosections

The limbs were embedded in to the O.C.T. medium (Optimal Cutting Temperature, Tissue Tek) at -40^{o}C to -60^{o}C. 10µM cryosections were done at -20^{o}C and dried at room temperature for several hours. The tissue on slides was stored at -80^{o}C if not used immediately. The tissue was fixed in acetone for 10 min at 4^{o}C and washed in the buffer used for the appropriate staining or water.

2.2.23 Detection of Alkaline Phosphatase activity

To detect the activity of Alkaline Phosphatase the 8µM cryostat sections of the forelimbs were fixed in acetone for 10 min at 4^{o}C and rinsed with water. The tissue was stained using Alkaline Phosphatase (AP) kit from Sigma. 1ml of Sodium Nitrite Solution and 1ml of FBB-Alkaline Solution were mixed and incubated for 2min at room temperature. This mix was added to 45ml of the deionized water (forming diluted diazonium salt solution). 1ml of Naphtol AS-BI Alkaline Solution was added to the diluted diazonium salt solution. This alkaline-dye mixture was added to the fixed slides and incubated for 15min. After incubation the slides were rinsed for 2 minutes in deionized water and counterstained for another 2 minutes with Neutral Red solution, Buffered. The aqueous mounting media (Kaiser gelatine) was used for coverslipping.

2.2.24 Transient transfection of COS-7 cells

Approximately 4x10^{4} of COS-7 cells were seeded the day before transfection on the round (15mm) glass coverslips laying on the bottom of the 12-well plate in 1ml of growth medium and incubated at 37^{o}C and 5% CO_2. The cells were about 40-80% confluent before the transfection. 0.6 to 1.2µg of DNA was diluted in 40µl of DMEM without serum or antibiotics. 4µl of PolyFect Reagent was added, followed by mixing (vortexing) for 10sec. To allow complex formation, the mixture was incubated for 5-10 min at room temperature. During the incubation, the COS-7cells were washed with PBS and growth medium was exchange for 600µl of new medium, containing serum and antibiotics. 250µl of serum- and antibiotic-containing growth medium were added to the DNA complex, mixed by pipetting, and transfered to the cells. The well-plate was gently swirled to ensure uniform distribution of the complexes. Incubation took place for 24-48 hours at 37^{o}C and 5%CO_2. After incubation the cells were washed in 1X PBS and fixed in 4% PFA in 1X PBS for 15min at room temperature. The cells were washed 3 times with PBS and placed on the slide (coverslip upside-down) with 7µl of Vectashield mounting medium for fluorescence, containing Dapi. Dapi stains the nuclei of the cells in blue, whereas GFP indicates the localization of the protein. The cells were then analyzed under fluorescent microscope with Dapi- and GFP-filters

Results

3.1 Identification of the Tmem16f transcript structure

3.1.1 EST clone sequencing

In a screen for Ihh target genes an osteoblast-specific cDNA of 769 base pairs was discovered, which was a part of a novel protein-coding gene (Wenzel, 2003). This gene was later called Tmem16f or Anoctamin-6 (Ano6) (Kato and Katoh, 2004; Galindo and Vacquier, 2005). To identify the full cDNA sequence of Tmem16f/Anoctamin-6 we used BLAST algorithm of the NCBI database. We searched the Expressed Sequence Tag (EST) libraries for EST clones which aligned with the 769 bp sequence. Overlapping EST clones were then obtained from RZPD Deutsche Zentrum für Genomforschung GmbH. These clones were sequenced from the 5' and 3' ends and with new designed internal primers and thus new sequences aligned by DNA star program. Finally, we revealed a 5680 bp transcript of Tmem16f gene (Fig. 7).

3.1.2 5' RACE

Although the 3' end of the mRNA is readily verifiable due to the presence of the poly-A tail sequence, it is not immediately obvious that the set of the overlapping ESTs really includes the 5' end of the gene's transcript sequence. To verify that we did not miss further extensions on the 5' end we used the 5'RACE method (see chapter 2.2.3). A total mRNA was purified from E 16.5 mouse limbs. GeneRacerRNA Oligo was ligated to the 5'-end of full-sequence mRNA. cDNA synthesis was performed from these templates with subsequent RT-PCR using specific primers to the GeneRacerRNA Oligo and gene specific primer (GSP) designed to match exon 5. Resulting fragments were cloned into the TOPO vector and sequenced (see chapter 2.2.3). The results of the sequencing of the PCR product clones were aligned to the established cDNA sequence (Contig 2 on Fig.7). Eight clones exhibited perfect matches to the previously defined sequence, but none of them extended the previously assembled 5' end of cDNA sequence. Two clones 23 and 29 revealed additional sequences, which were not homologous to the cDNA contig but were found to be homologous to sequences in the 1st intron of Tmem16f (shown in red on Fig. 8), and thus were attributed to alternative splicing of the second exon.

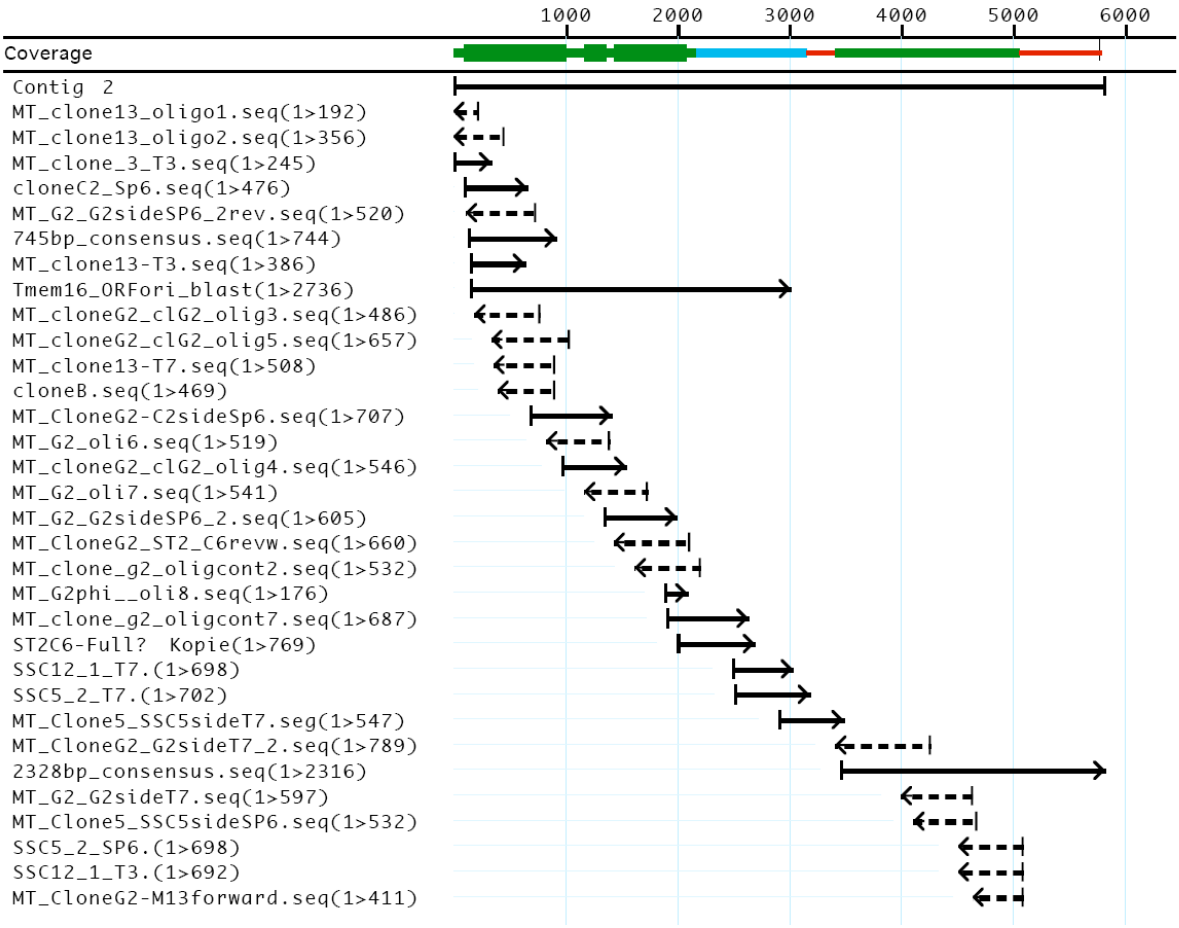

Figure 7: Assembly of the full length cDNA sequence.

On the left side there are clones or consensus sequences which perfectly aligned to assemble a complete cDNA sequence of Tmem16f gene. “ST2C6-Full” is the sequence, fished from the screening for Ihh-target genes. “Contig2” is the resulting sequence, assembled from sequenced fragments of EST clones.

These two clones (clone 29 and 23 (XM-178415-contig) contained additional sequences in the genomic region of the 1st intron of Tmem16f. They might then represent two potential alternative splicing variants of Tmem16f (Fig. 9).

There were more ESTs and 5’RACE clones detected which did not contain the 2nd exon and only a few clones were found containing the 2nd exon. Therefore we conclude that Tmem16f transcript without exon 2 had by far the highest level of expression compared to the alternatively spliced variants with the 2nd exon. Because the gene-specific primer was inside the 5th exon, we could potentially detect splicing variations of exons 1, 3 and 4. We did not observe such variations. This indicates that exons 1, 3 and 4 are not alternatively spliced when exon 5 is present in Tmem16f (Fig. 9).

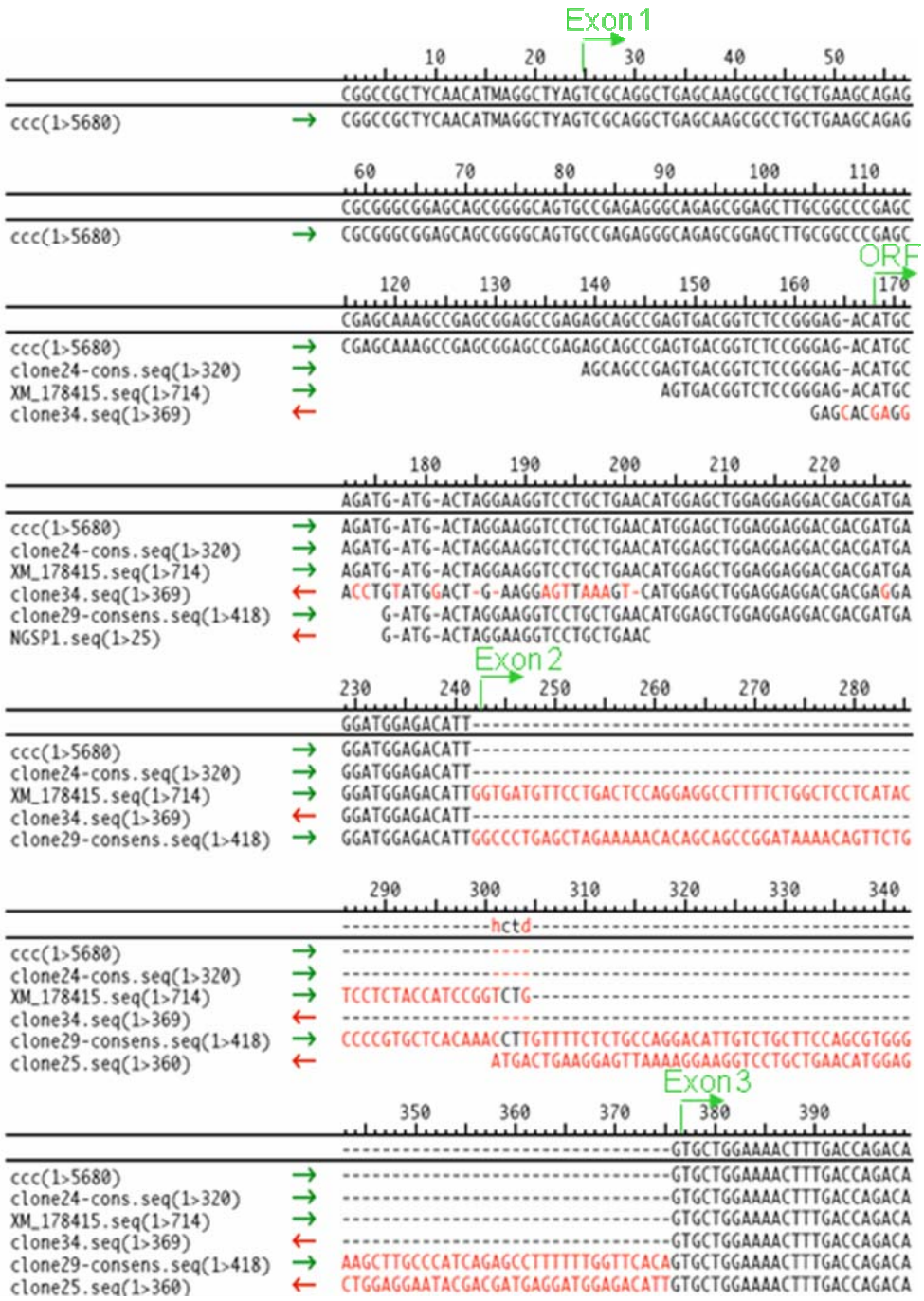

Figure 8: Alignment of the 5‘-RACE clones.

On the left side: ccc- is the sequence received from sequenced EST clones, XM_178415 is a consensus obtained from computer Data Base, other names are for clones of the 5’-RACE experiment. Green marks Exon1, 2, 3 show start positions of the appropriate exons. ORF is the Tmem16f open reading frame. Sequences in red represent alternative spliced variants of exon 2 of Tmem16f.

Figure 9: Alternative splicing variants of Tmem16f.

On the left side: clone 24 represents the majority of Tmem16f transcripts which skip second alternatively spliced exon. XM_178415 sequence represents the alternatively spliced exon 2a and clone 29 sequence represents the alternatively spliced exon 2b. Green signs Exon1, 2, 3, 4, 5 show the beginning of the appropriate exons. ORF is the Tmem16f open reading frame. Sequences in red represent alternative spliced variants of exon 2 of Tmem16f.

3.1.3 Genomic organization of Tmem16f, transcript and protein structure

Aligning the cDNA consensus region of the mouse gene to human EST libraries and subsequently comparing the protein-level homology of the corresponding human

sequence to the mouse Tmem16f protein, we were able to determine an ORF of 2736 nucleotides in mouse Tmem16f encoding a protein of 911 amino acids. The Tmem16f gene consists of 21 exons (Table 11), where a fraction of transcripts undergoes alternative splicing of exon 2 (represent exon2a and 2b, based on XM-178415 ESTs contig and 5'RACE results). The Tmem16f covers 184 kb of genomic sequence on chromosome 15 (Chr 15F1, nucleotides 95621274 to 95805180 of genomic sequence).

Table 11: Genomic location of Tmem16f exons.

Exon number	Start	End	Exon length
1	95,621,274	95,621,487	214
2a	95,661,074	95,661,136	63
2b	99,663,851	99,663,984	134
3	95,694,656	95,694,738	83
4	95,724,844	95,724,972	129
5	95,742,736	95,742,801	66
6	95,743,803	95,744,087	285
7	95,744,303	95,744,416	114
8	95,746,384	95,746,499	116
9	95,750,675	95,750,809	135
10	95,757,955	95,758,060	106
11	95,762,214	95,762,274	61
12	95,771,641	95,771,783	143
13	95,773,829	95,773,906	78
14	95,778,703	95,778,928	226
15	95,779,922	95,780,091	170
16	95,780,290	95,780,387	98
17	95,786,322	95,786,452	131
18	95,792,507	95,792,712	206
19	95,796,252	95,796,454	203
20	95,798,054	95,798,159	106
21	95,802,926	95,805,180	2,255

The open reading frame starts in exon 1 and ends in exon 21 of Tmem16f (Fig. 12). RT-PCR using primers complementary to the parts of different exons of Tmem16f confirmed the cDNA to be expressed (Fig. 10 A, C). Bioinformatics analysis

(ENSEMBL) revealed that the 3' sequence of Tmem16f (exons 16 to 21) codes for a domain of Unknown Function (DUF 590, ENSEMBL ID IPR007632, Fig 10A, Table 12). This domain was found to be highly conserved among different species such as human, rat, drosophila and C. elegans (NCBI-BLAST).

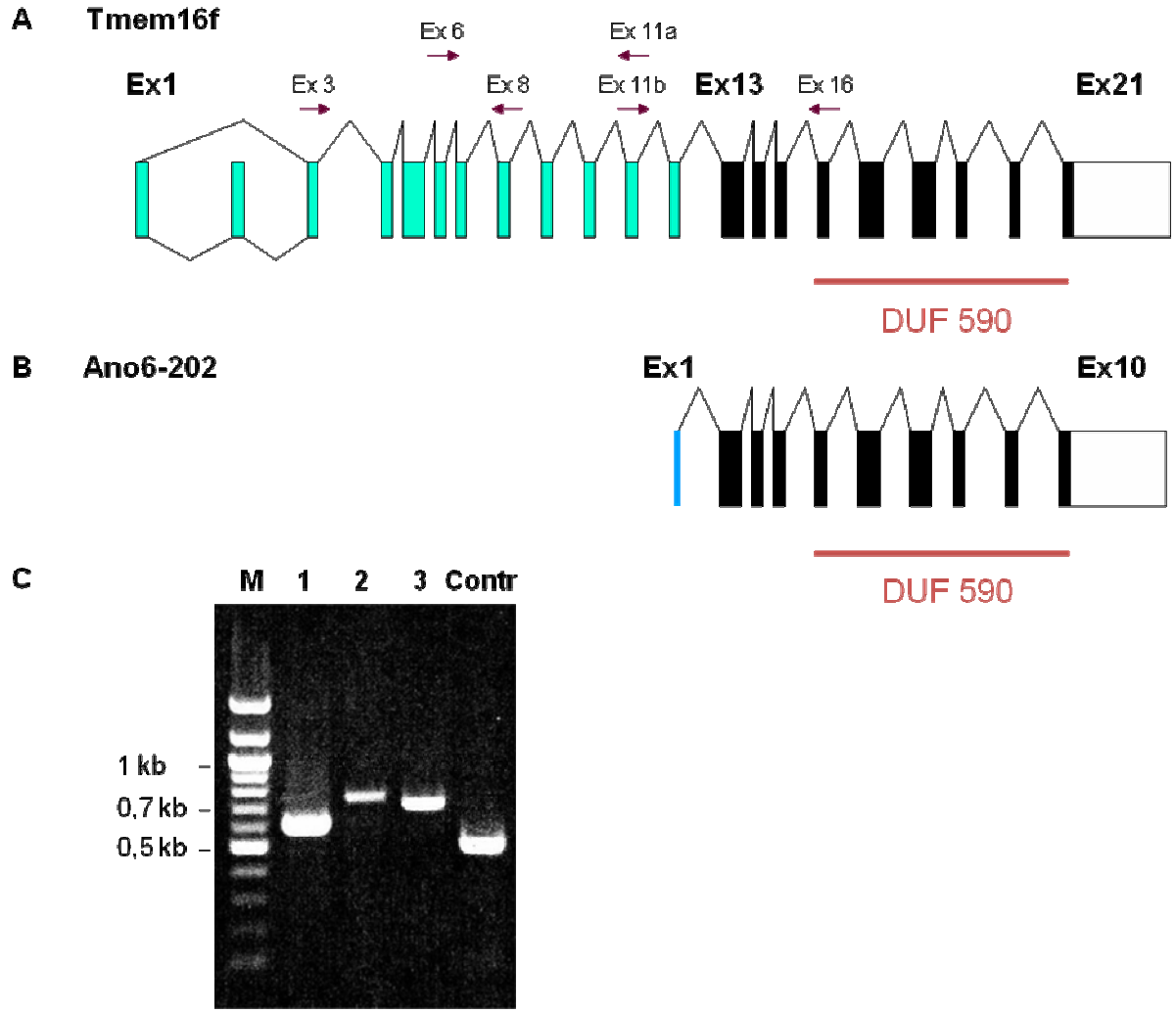

Figure 10: Genomic structure of Tmem16f gene.

Transcript structure of Tmem16f (A). Arrows show the position of the primers used in RT-PCR. Red underline shows the position of the DUF590 domain. Ano6-202 is a shorter isoform of Tmem16f (B). RT-PCR on cDNA derived from E16.5 mouse bone tissue with primers covering different regions of Tmem16f (C). M- marker, lanes 1, 2, 3- PCR products with primers covering exon 3 to exon 8, exon 6 to exon 11a and exon 11b to exon 16 respectively. Contr- control primers were used to the fished 3' region of Tmem16f (exon 17- exon 20).

A shorter isoform of Tmem16f named Ano6-202 was predicted by Ensembl (Chr 15F1, nucleotides 95773585 to 95805180 of genomic sequence). It represents the 3'-sequence of Tmem16f containing exon13 to exon 21 of Tmem16f and an alternative spliced exon 12b on the 5'-end containing the start codon (nucleotides 95,773,585 to 95,773,614 of genomic DNA) (Fig. 10B). Ano6-202 encodes a

polypeptide of 484 amino acid residues and contains the DUF 590 domain (from amino acid 182 to 446). The first nine amino acids of Ano6-202 do not match the sequence of Tmem16f protein.

Tmem16f protein is a highly hydrophobic protein, which contains eight potential transmembrane domains predicted by the TMHMM algorithm (Table 12) (Sonnhammer et al., 1998; Krogh et al., 2001). The DUF domain is on the C-terminus end of Tmem16f protein (from amino acid residue 609 to 873). Ano6-202 predicted protein represents the shorter version of Tmem16f protein. It contains only 6 transmembrane domains. The DUF domain is also fully represented in Ano6-202 (Table 12).

Table 12: Predicted domains of Tmem16f and Ano6-202 proteins.

Tmem16f domains	Position	Ano6-202 domains	Position
Transmembrane domain 1	296-316		
Transmembrane domain 2	377-397		
Transmembrane domain 3	456-476	Transmembrane domain 1	32-54
Transmembrane domain 4	515-535	Transmembrane domain 2	79-101
Transmembrane domain 5	553-573	Transmembrane domain 3	129-146
Transmembrane domain 6	671-691	Transmembrane domain 4	245-267
Transmembrane domain 7	727-747	Transmembrane domain 5	295-317
Transmembrane domain 8	826-846	Transmembrane domain 6	399-421
DUF 590	609-873	DUF 590	182-446

Another prediction from TMHMM is that if Tmem16f is plasma membrane protein with both, the N- and C-terminal ends of the protein, exposed to the cytoplasm (Fig. 11). The transmembrane domains 6, 7 and 8 are part of the DUF590 domain. Using the UniProt database six predicted N-linked glycosylation sites were found at the amino acid residues 330, 362, 494, 778, 785 and 803 which might be identified in extracellular loops of Tmem16f (Fig. 11).

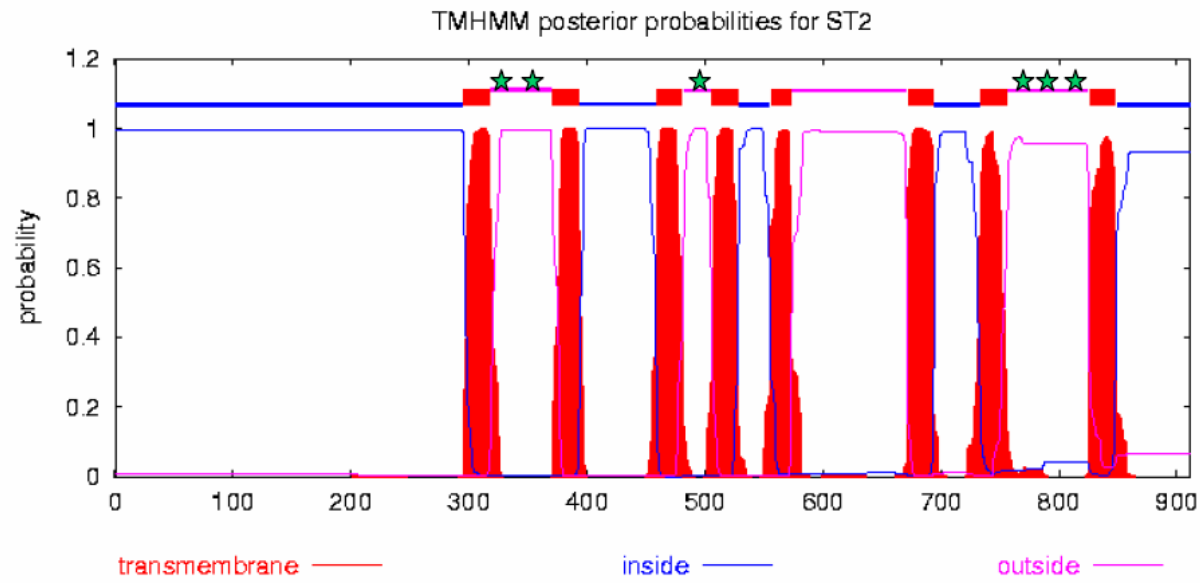

Figure 11: Prediction of transmembrane domains and membrane orientation of Tmem16f.

Blue and pink lines represent protein backbone, facing inside or outside the membrane, respectively. Regions in red represent the potential transmembrane regions of Tmem16f protein. Green asterisks show the predicted glycosylation sites present in extracellular loops.

3.2 Expression analysis of Tmem16f

To analyze the expression pattern of Tmem16f during embryonic mouse development, a P_{33}-labeled antisense riboprobe complementary to the 1st exon of Tmem16f was hybridized on the sections of E14.5 and E16.5 wild-type mouse embryos (Fig. 12 B). As Tmem16f had initially been identified in a screen for Ihh target genes, it was further important to know if Tmem16f and Ihh are expressed in the same or adjacent tissues. To compare the expression domains of Tmem16f and Ihh, an antisense riboprobe to Ihh was hybridized on parallel sections. Ihh is expressed in prehypertrophic chondrocytes of endochondral bones such as bones of vertebrae and long bones of the limbs and ribs (Fig. 12 A and Fig. 13 A). Tmem16f was specifically expressed by the osteoblasts in the bone and periosteum surrounding the Ihh expressing domains (Fig. 12 B and Fig. 13 E).

Further we analyzed expression of Tmem16f in different mutant mouse lines, which have bone malformations.

It has been shown that in Ihh-deficient mice no endochondral bone is formed indicating that Indian hedgehog is essential for endochondral ossification (St-Jacques et al., 1999).

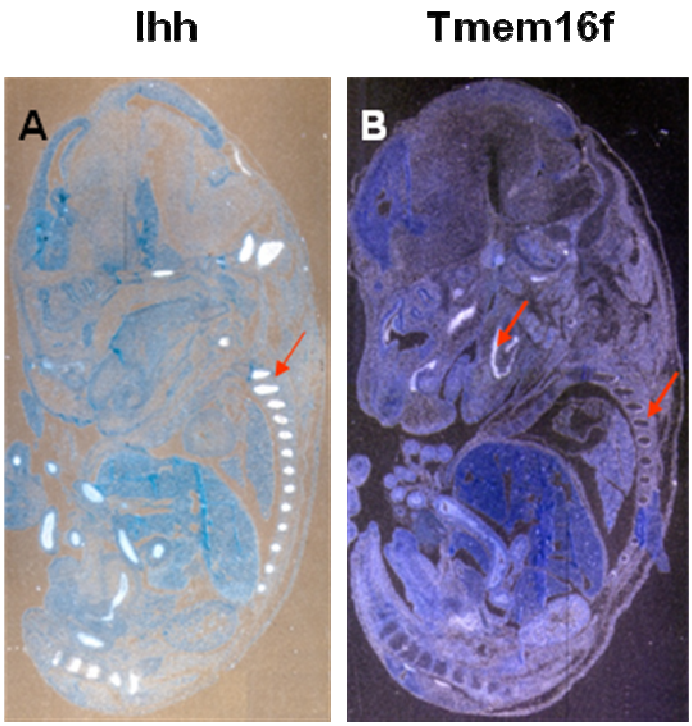

Figure 12: Expression of Tmem16f.

Longitudinal sections of wild type mice at E16.5 were hybridized with antisense riboprobes for Ihh (A) and Tmem16f (B). Ihh is expressed in the cartilage (A, red arrow), whereas Tmem16f is expressed in the bone and periosteum (B, red arrows).

To analyze if Tmem16f acts downstream of Ihh the Tmem16f riboprobe was hybridized on the sections of E 16.5 mouse limbs of Ihh deficient mice and of mice expressing Ihh under Coll II promoter (Coll-II/Ihh mouse line). No expression of Tmem16f was detected in Ihh deficient mice (Fig. 13 C, G). In Ihh-overexpressing mice the expression of Tmem16f was expanded adjacent to Ihh domain (Fig. 13 B, F). These results show that Tmem16f acts downstream of Ihh.

Two transcription factors Runx2 and Osx have been shown to be required for osteoblast differentiation. Mice deficient for these factors develop a cartilaginous skeleton with complete absence of osteoblasts (Ducy, et al., 1997; Komori et al., 1997; Otto et al., 1997; Nakashima, et al., 2002). To understand whether Tmem16f is acting upstream or downstream of the transcription factors Runx2 and Osx, *in situ* hybridization was performed on the limbs of Runx2 and Osx deficient mice. We detected no Tmem16f expression in these mutants (Fig. 13 D, H, I). This indicates that Tmem16f acts downstream of these transcription factors in osteoblasts.

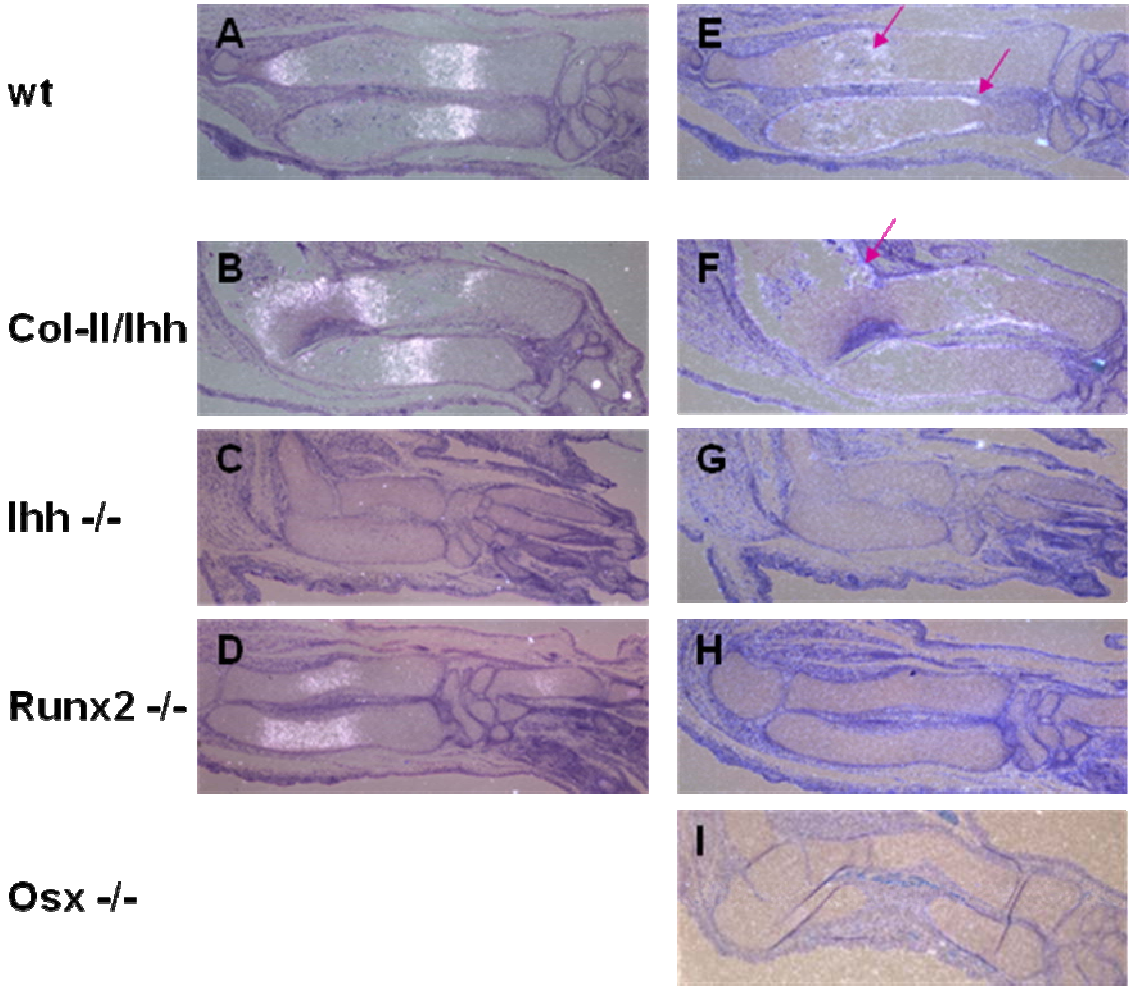

Figure 13: Tmem16f acts downstream of Ihh, Runx2 and Osx.

Ihh- and Tmem16f riboprobes were hybridized on the sections of E16.5 limbs of wild type (A, E), Ihh oversxpressing (B, F), $Ihh^{-/-}$ (C, G), $Runx2^{-/-}$ (D, H) and $Osx^{-/-}$ (I) mice. Ihh is expressed in prehypertrophic chondrocytes of wt (A), Col-II/Ihh (B), $Runx2^{-/-}$ (D) and $Osx^{-/-}$ (not shown) mice. No Ihh expression could be detected in Ihh-/- mice (C). Tmem16f is expressed in the newly formed bone and the periosteum, flanking the Ihh expression domain (E, pink arrows). Tmem16f expression is upregulated in osteoblasts of Ihh overexpressing mice adjascent to Ihh expression domain (F, arrow). No Tmem16f expression could be detected in $Ihh^{-/-}$ (G), $Runx2^{-/-}$ (H) and $Osx^{-/-}$ (I) mice.

3.3 Localization of Tmem16f in the cell

To define the localization of Tmem16f protein, COS-7 cells were transfected with Tmem16f-EGFP fusion constructs. The ORF of Tmem16f was cloned into the pEGFP-N3 vector in front of the EGFP gene. The stop-codon of Tmem16f was removed to enable the synthesis of the Tmem16f-EGFP-fusion protein (Fig. 14 A). Transient transfection of COS-7 or CHO cells with this construct showed, that Tmem16f is localized in the cytoplasm, but not in the nucleus (Fig. 14 C). Control transfection of the same cells with the vector, expressing only EGFP showed equal distribution of EGFP protein throughout the cell, including nucleus (Fig. 14 B).

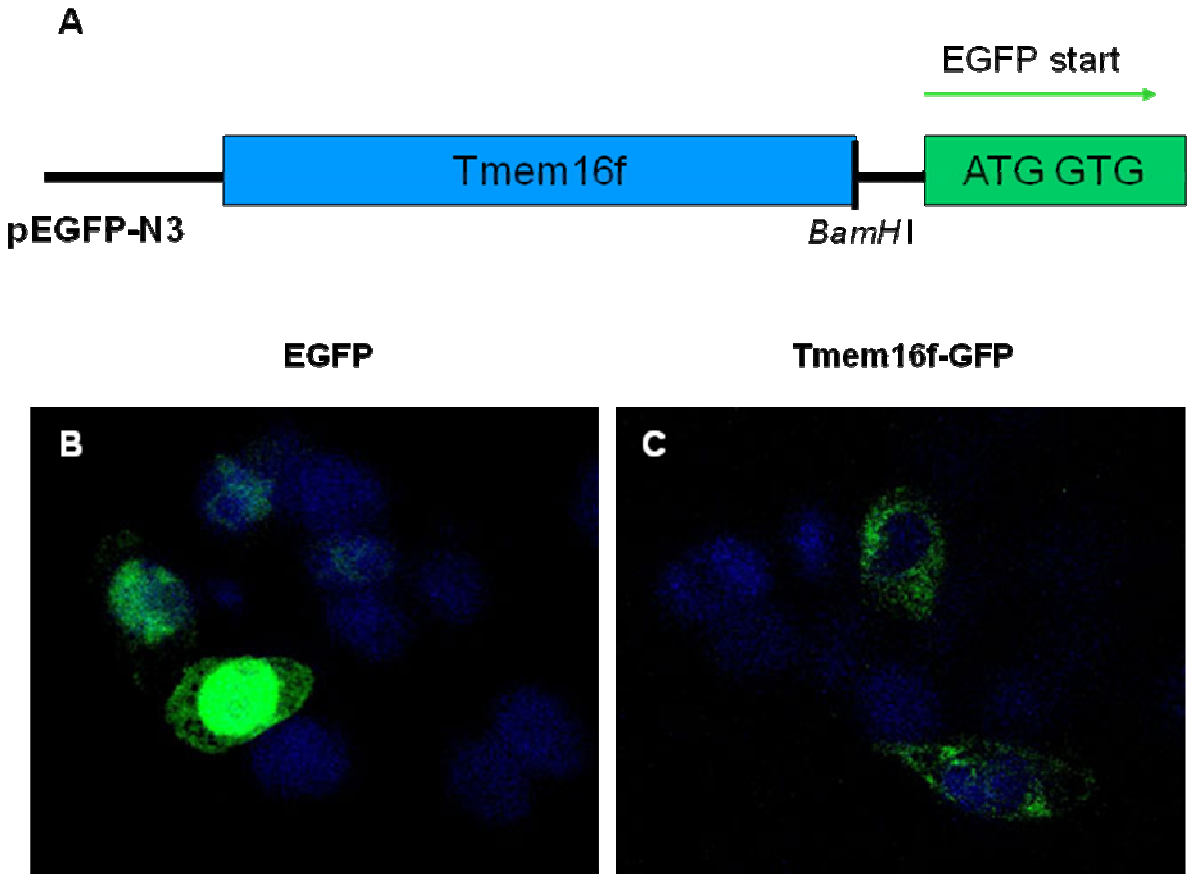

Figure 14: Localization of Tmem16f.

Tmem16f gene was cloned into pEGFP-N3 to generate a Tmem16f-EGFP fusion protein (A). COS-7 cells were transiently transfected with EGFP control and Tmem16f-EGFP expression plasmids. EGFP is distributed throughout the whole cell including the nucleus (B), whereas Tmem16f is localized in the cytoplasm and absent from the nucleus (C).

3.4 Inactivation of Tmem16f

One of the common approaches for analysis of the gene function is inactivation of the gene in mouse. There are two major strategies used to inactivate a gene of interest: a targeted deletion of the gene and a gene trapping. To analyze the function of Tmem16f we decided first to create a Tmem16f deficient mouse.

The necessary steps of gene targeting procedure are:

- screening of PAC library
- cloning of the targeting construct
- electroporation of the targeting vector into appropriate ES cells
- screening for the positive ES clones (for homologous recombination event)
- blastocyst injection
- transfer of injected blastocysts into the uterus of foster mice
- breeding for germline transmission

We used an approach in which the targeting vector with a positive selection cassette replaces the gene of interest. Important elements of a replacement vector are the homology to the targeted locus, a positive selection marker, bacterial plasmid sequence and a linearization site outside of the homologous sequence of the vector (Hasty, et al., 2003). A common strategy of gene targeting is to replace the complete gene of interest. In mice most people delete single or several exons due to the size of the genes. The strategy in that case is to delete exons containing the start codon of the ORF or sequences encoding critical functional domains. Due to a large intron sequences between the exons of Tmem16f and presence of the alternatively spliced exons 2a and 2b we decided to delete the first exon of Tmem16f which contains the only identified translation initiation site thus preventing the synthesis of all possible isoforms of Tmem16f.

An alternative approach to the targeted deletion of a gene is a gene-trap. This was established for large scale random mutagenesis in mice and the rapid identification of the mutated genes. The basic gene trap vector contains a splice-acceptor sequence upstream of the reporter gene ß-Geo, a fusion of ß-galactosidase and neomycin phosphotransferase II (Stryke et al., 2003). This vector inserts randomly into the genome. If inserted into the intron of a gene, the splice acceptor will be used by the splicing machinery. The fusion transcript will contain sequences from exons upstream to the insertion site joined to the ß-Geo marker.

Here we used the gene trap approach in parallel to the straight deletion strategy. As ES cells carrying an integrated gene trap cassette are commercially available long and difficult procedures of cloning and screening of ES clones can be avoided. The gene trap also allows investigating the function of the truncated form of the gene product, thus possibly predicting functional domains of N-terminal end of a protein. It is easy to follow the gene expression pattern in mouse embryos performing X-gal staining. With the gene trap approach it is possible to compare the long version of Tmem16f to the shorter version, Ano6_202.

3.4.1 Screening for PAC clones containing Tmem16f genomic region

To create a targeting construct it is needed to clone the genomic sequences upstream and downstream of the targeted locus into the targeting vector. These sequences are called 5'- and 3' arms, respectively. It was demonstrated that the frequency of homologous recombination is adversely affected by the presenceof vector-target mismatches (teRiele, et al., 1992; Wurst, Auerbach and Joiner, 1994).

To avoid such mismatches targeting vectors are generated using "isogenic" DNA to optimize the efficiency of gene targeting. ES cells used for electroporation were derived from 129/Sv mice. Therefore, the PAC library of the same mouse strain was chosen. P1-derived Artificial Chromosome (PAC) cloning systems are specifically designed for cloning of large genomic DNA fragments ranging in size from 60 kb to 150 kb. PACs are plasmid-based and thus DNA is easily isolated and manipulated (Sambrook and Russell, 2001). Therefore, a genomic library was purchased to identify a PAC clone, which would contain a large fragment of at least first exon of Tmem16f and surrounding genomic sequences.

A DNA probe of 714bp complementary to the start of the first intron of Tmem16f was prepared by PCR amplification (Fig. 15 A). This probe was hybridized on the filters of mouse genomic PAC library RPCI21 (Osoegawa et al., 2000). Seven filters PAC1 to PAC7 covered the whole library. Eight clones gave positive signal after hybridization (Fig. 15 B) and were subsequently analyzed for the presence of Tmem16f genomic region.

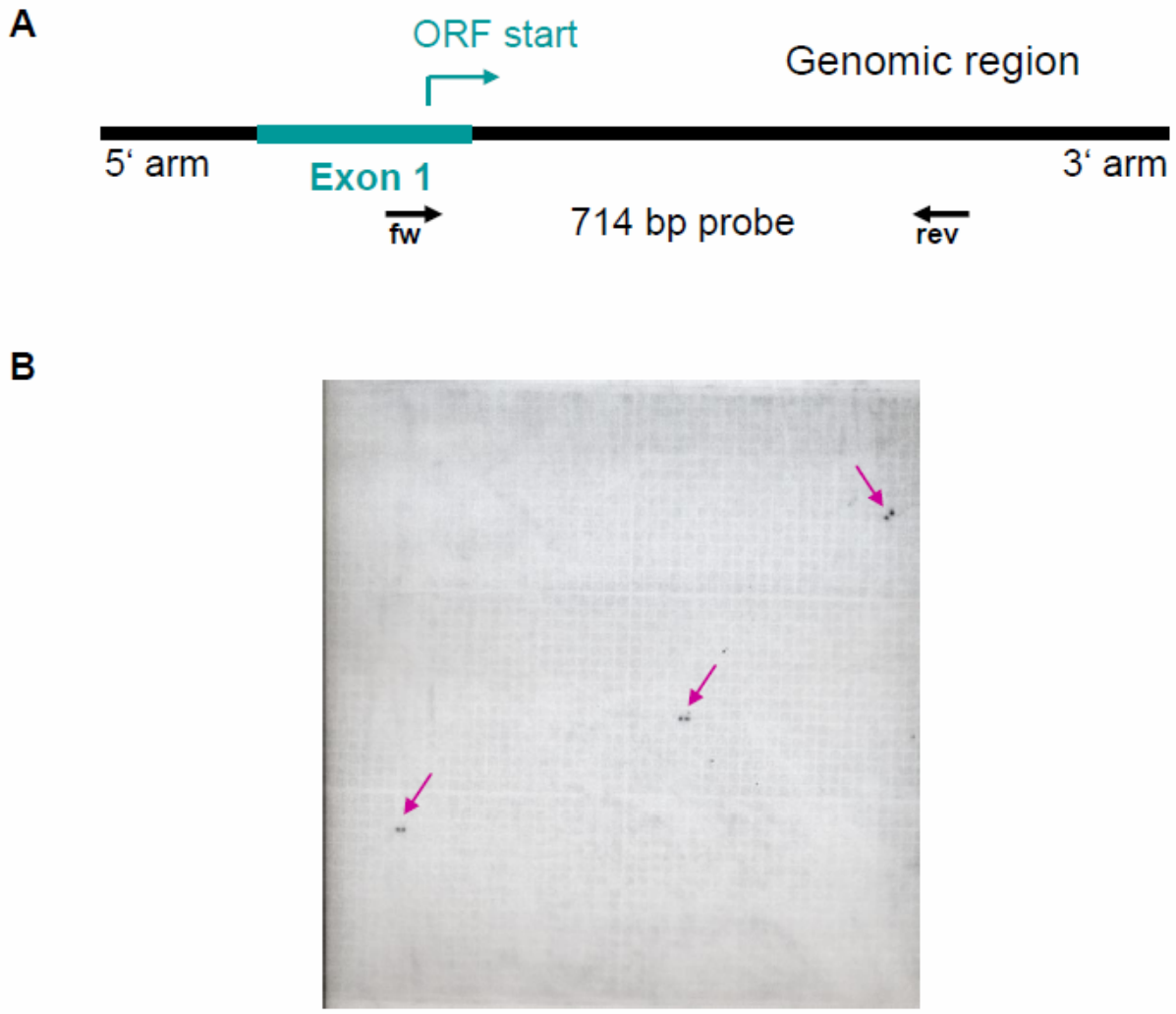

Figure 15: Hybridization of 714bp probe on the mouse genomic PAC library RPCI 21.

Design of 714bp probe for Southern blot hybridization (A). The primer fw was designed to match the end of the 1st exon of Tmem16f and the primer rev located 714 bp downstream. (A) Positive clones were detected after Southern blot hybridization of 714bp probe on PAC filters (B, arrows)

DNA was purified and digested with three different restriction enzymes producing DNA fragments of specific length. After hybridization with the 714bp probe only three PAC clones 379, 449 and 473 contained DNA fragments of the correct size: 4.2 kb fragment after the digestion with *Bgl*II, 3.5 kb fragment after the digestion with *Xba*I and 10 kb fragment after the digestion with *Hind*III restriction enzymes (Fig. 16 A). To confirm that these clones contain the entire 5’ genomic part of Tmem16f DNA, a PCR with the primer pairs for 5’- and 3’-arms was performed. It revealed that only clone 379 included both 5’- and 3’- sequences of genomic region of the 1st exon (Fig. 16 B). The 5’-arm sequence was also present in clones 449 and 473, however, the 3’-arm sequence was absent in these clones (Fig. 16 B). Other five clones detected

by PACs analysis seem to be false positive. Thus, clone 379 was the only one, which was suitable for further cloning of a targeting construct.

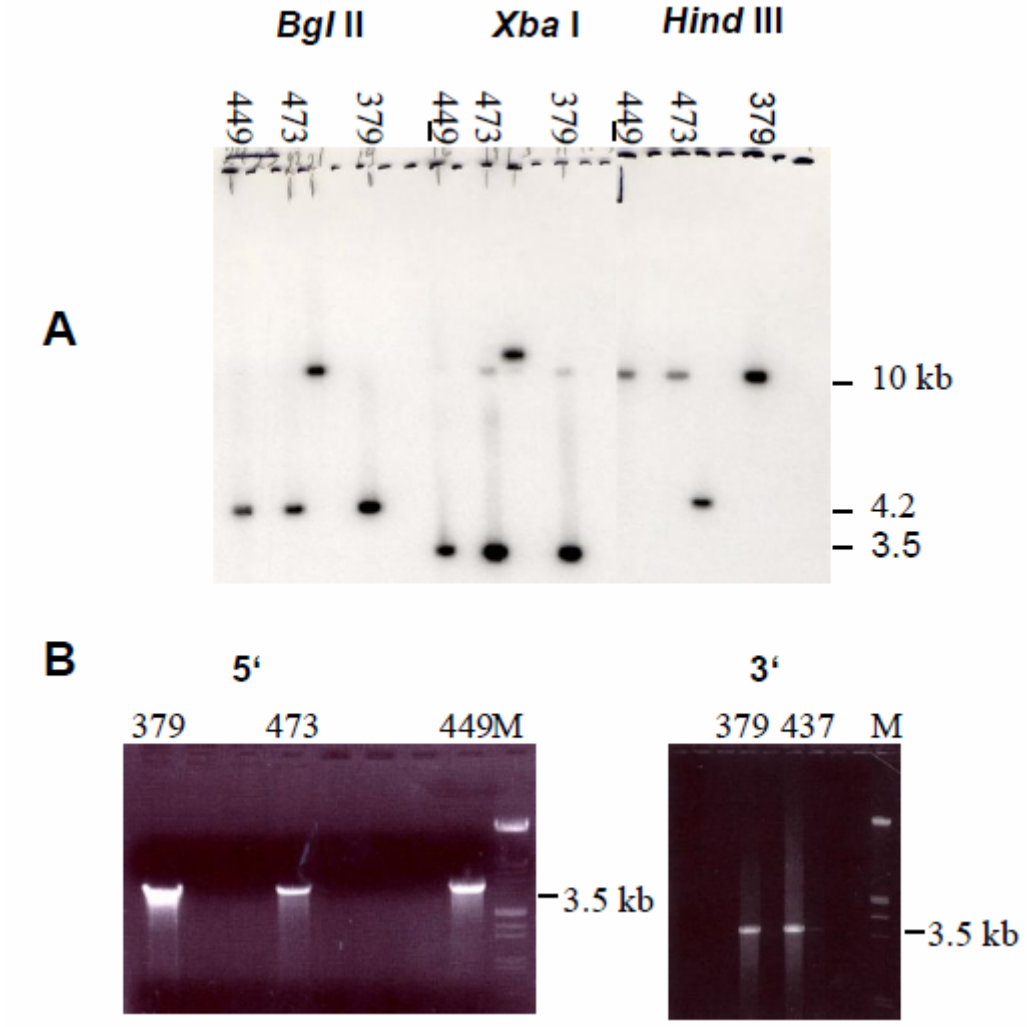

Figure 16: Analysis of PAC clones.

Southern blot hybridization of PAC clones DNA with 714bp probe. Correct size bands of ~4.2 kb appear after *Bgl*II digestion, ~3.5 kb after *Xba*I digestion and ~ 10kb fragment appear after digestion with *Hind*III restriction enzyme of PAC clones number 379, 473, 449 (A). Amplification of the 5'- and 3'-armsequences of the first exon. Only clone 379 gave positive result for both 3' and 5' genomic regions (B).

3.4.2 Cloning of the targeting construct

It was shown that the ideal length of homologous sequences in the targeting vector is in the range of 5 to10 kb- the greater is the length of homology the higher is the targeting frequency (Thomas and Capecchi, 1987; Hasty, et al., 1991). Another necessary condition is that the targeting vector should include one short arm and one long arm of homologous sequences in purpose to screen ES cell for correct

integration site of the selection cassette. Considering these guidelines, we cloned 5' arm sequence of 3,5 kb and 3' arm sequence of 7,9 kb into the targeting vector pWH9 (Fig. 17) upstream and downstream of the positive selection cassette, respectively (Fig. 17 and Fig. 18 A).

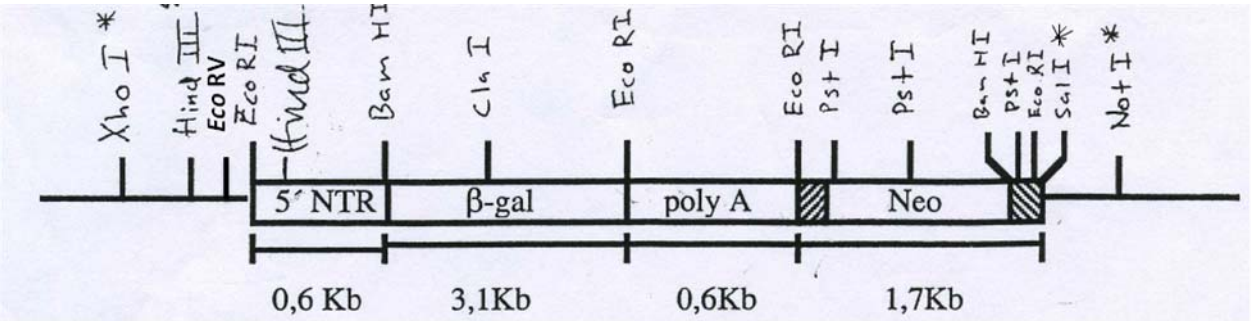

Figure 17: Scheme of the targeting vector pWH9.

The cassette, including ß-Gal and Neo was inserted into pBSSK vector using *Eco*RI and *Sal*I sites resulting in pWH9 vector. Only unique *Xho*I site is available for cloning of the 5' arm and *Sal*I and *Not*I sites for cloning of the 3' arm (asterisks). pWH9 vector was kindly provided by R. Fässler.

Since the 5' arm was shorter than the 3' arm, we first cloned it into pWH9. Primers containing *Xho*I sites on their ends were used to amplify the 3,5 kb of 5' homologous sequence of the 1st exon from the PAC clone 379 DNA. The fragment was directly cloned into pWH9 previously linearized with *Xho*I restriction enzyme resulting in pWH9 -5'arm construct. Since the 3' arm was 7,9 kb long we first cloned it in to pBSII SK vector. Two fragments of 3'arm were amplified using primers containing *Sal*I and *Bam*HI sites (4,3 kb fragment) and *Bam*HI and *Xba*I sites (3,6 kb fragment). *Sal*I-*Bam*HI fragment of the 3'arm was first cloned into pBS II SK and then *Bam*HI- *Xba*I fragment was ligated to the resultant construct thus assembling the complete 3'- arm sequence. The complete 3' arm fragment was subcloned into pWH9 using the *Sal*I and *Not*I sites present in pBS II SK vector (Fig. 18 A).

The targeting construct was linearized and electroporated into R1 ES cells (derived from 129/Sv mice). The cells were grown for several days under selection condition (G418). Picked clones were analyzed for the proper recombination event (Fig. 18 B).

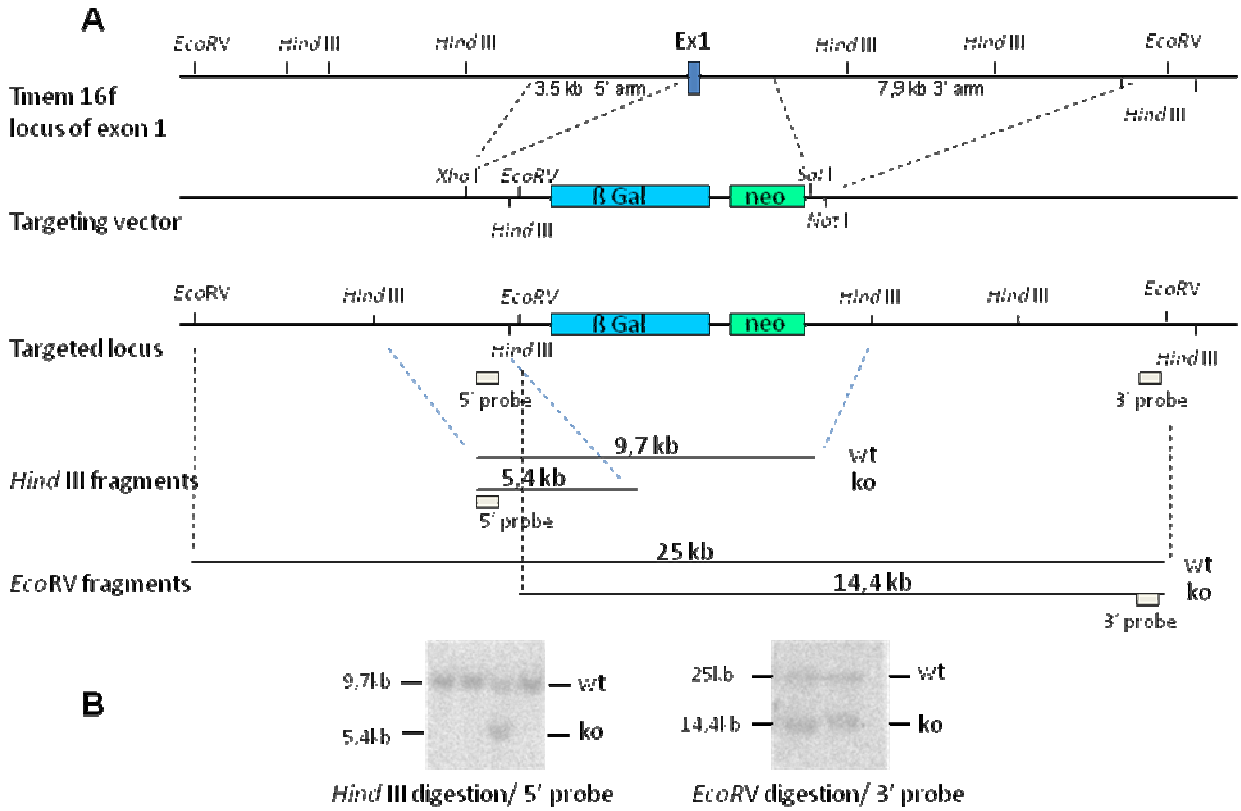

Figure 18: Cloning strategy for the targeted deletion of Tmem16f gene.

The first exon of Tmem16f gene was replaced with positive selection cassette, which included ß-Galactosidase and neomycin resistance genes (A). The integration of the cassette led to the insertion of the additional sites for *Hind*III and *EcoR*V enzymes which served for ES cell clone analysisby Southern blot (B). 9,7kb and 25kb fragments indicate the wild type allele after digestion of genomic DNA with *Hind*III and *EcoR*V respectively. 5,4kb and 14,4 kb fragments detect the knockout allele after digestion of genomic DNA with *Hind*III and *EcoR*V respectively (B).

3.4.3 Screening for homologous targeting events by Southern blot

To confirm the correct integration of the knockout cassette, the ES cell clones were analyzed by Southern blot using 5' and 3' probes (Fig. 18 B). The integration of the neo cassette led to the insertion of additional *Hind*III and *EcoR*V restriction sites which were used for the analysis of the ES cell clones for the integration site by Southern blot (Fig. 18 B). The external probes for the hybridization were chosen so that they would hybridize close to the site of integration, but outside of the homologous regions to detect the integration site at the correct genomic locus. In case of correct site of cassette integration, the fragments of 5.4 kb and 14.4 kb should be produced after digestion of genomic ES cell DNA with *Hind*III or *EcoR*V, respectively (Fig. 18 A, B, *Hind*III and *EcoR*V fragments).

In a first step 360 ES clones were analyzed for the 5' side using *Hind*III enzyme for genomic DNA digestion (Fig. 18 B). Second, positive clones number 77, 103, 104,

122, 127, 153, 180, 220, 222, 269 and 283 were selected for the analysis for the 3' side of integration. Their genomic DNA was digested with *EcoR*V. All of them demonstrated the correct integration site (Fig. 18 B). Finally, two ES cell clones number 77 and 127 were chosen for further blastocyst injection, which was done by the group of R. Fässler. The injected blastocysts from black C57Bl/6J mice are transferred into the uterus of foster mice, where they develop into chimeric mice. Germ-line transmission was recognized by mating these chimeric mice to C57Bl/6J mice. ES-cell-derived germ cells result in agouti animal, since agouti is dominant over black.

3.4.4 Gene trap allele of Tmem16f

By searching the gene trap databases we have found ES cells, containing gene trap cassette inserted into intron 13 of Tmem16f available. These cells were subsequently ordered from Bay Genomics company. The position of the integration site of the cassette was first provided by Bay Genomics database. We confirmed this data by PCR using forward primer complimentary to the 3'-end of exon13 and the reverse primers complimentary to the integration cassette (Fig. 19 A, B). Sequencing of the PCR-products identified the integration of the gene trap cassette into intron 13, approximately 300 bp downstream of exon 13 (Fig. 19 B). The same pair of primers was used for the genotyping of the gene trap mice (chapter 2.2.14). Considering the shorter isoform, Ano6-202, the gene trap cassette is inserted into the second intron (Fig. 19 C). Therefore, the truncated form of both isoforms of Tmem16f protein would be produced. Since the conserved DUF590 domain starts in exon 16 of Tmem16f, both truncated isoforms of Tmem16f would lack the DUF 590 domain (Fig. 19 A, C).
To create a Tmem16f gene trap mice, ES cells carrying the gene trap cassette in the 13th intron of Tmem16f were injected into C57Bl/6J mouse blastocysts, which in turn were transferred into the uterus of foster mice where they develop into chimeric mice (performed in the laboratory of R. Fässler). Chimeric mice were crossed with C57Bl/6J to follow the germ-line transmission. ES-cell-derived germ cells result in agouti animals.

3.4.5 X-gal staining of the Tmem16f gene trap embryos

Due to the presence of ß-galactosidase in the gene trap cassette it is possible to follow the expression of the Tmem16f gene in vivo with X-gal staining.

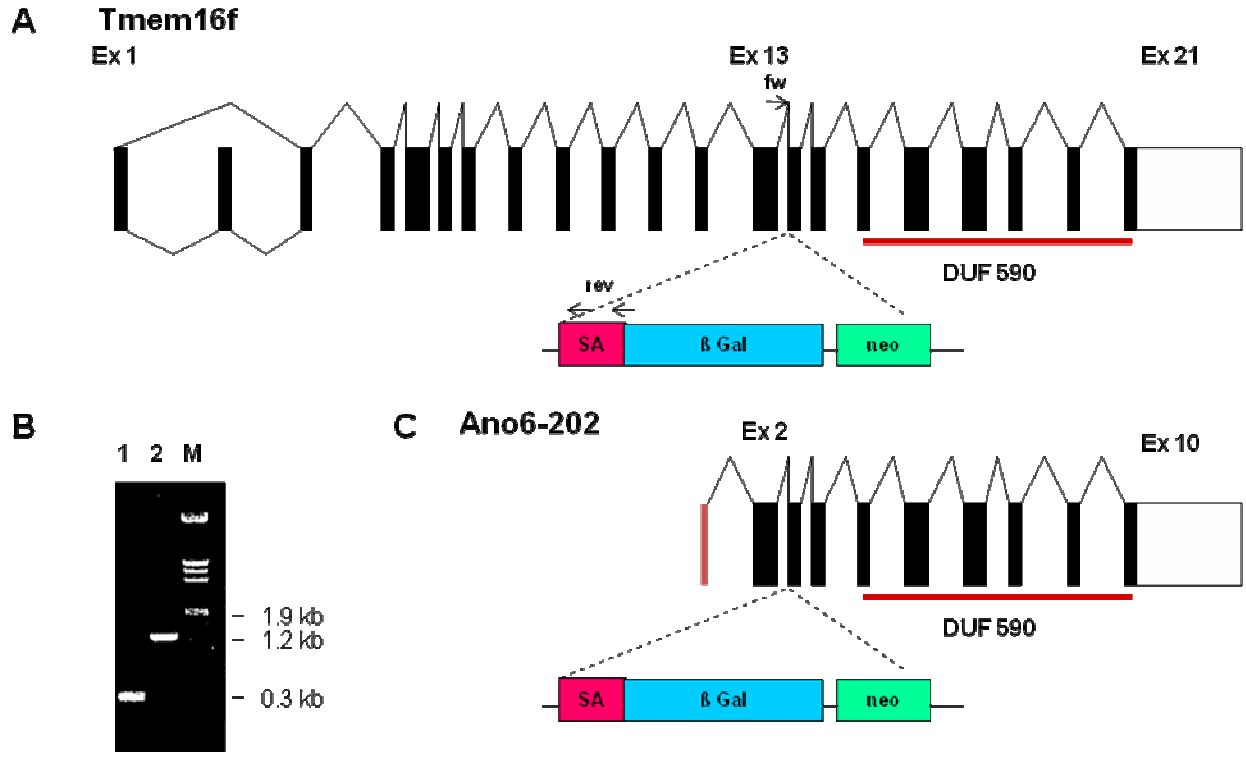

Figure 19: Gene trap integration site.

The gene trap cassette was inserted into intron 13 of Tmem16f (A).Forwardprimer to the 3'- end of the exon 13 of Tmem16f and two reverse primers to the gene trap cassette were used to define a gene trap integration site (A, arrows). PCR fragments of these primer pairs (B). The gene trap cassette was inserted into intron 2 of the shorter isoform Ano6-202 (C).DUF590- domain of unknown function starts in the exon 16 of Tmem16f, SA- splice acceptor, ß-Gal is ß-galactosidase gene, neo- neomycin resistance. M- DNA molecular weight marker

To investigate the expression of Tmem16f in vivo, E14.5 embryos of Tmem16f$^{gt/gt}$ mice were stained with X-gal to detect ß-Gal activity. Cells which normally express Tmem16f gene would express ß-galactosidase gene instead. Staining with X-gal (a substrate for ß-Gal) reveals those cells in which the Tmem16f is normally expressed. The pattern of ß-Gal expression was identical in heterozygous and homozygous Tmem16f mutants. This pattern reproduced the results of expression of the endogenous Tmem16f gene detected by *in situ* hybridization in the ossification centers of ulna and radius, in the ossified parts of ribs and in the skull bones where the ossification process has also taken place (Fig. 20 A, arrows).Closer look at the ulna and radius of E 14.5 mouse embryos reveals that Tmem16f is expressed in the osteoblasts of periosteum (Fig. 20 B, C, arrows).

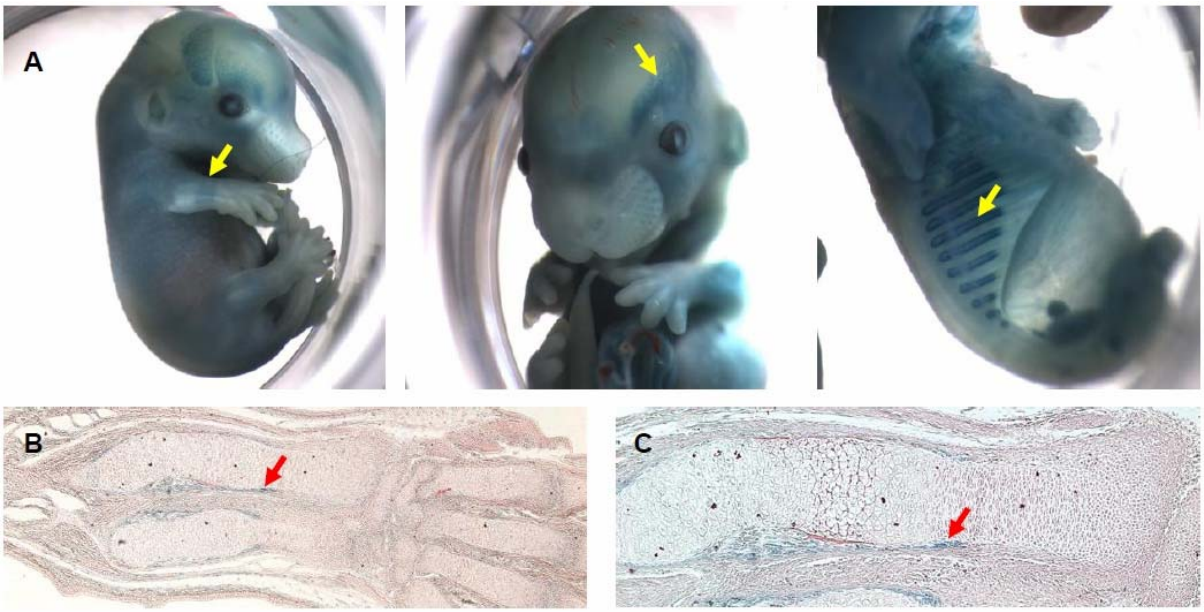

Figure 20: X-gal Staining of E 14.5 Tmem16fgt/gt embryo.

The whole embryos were stained for ß-Galactosidase. Tmem16f is expressed in osteoblasts of the bone formed by endochondral (limbs, ribs) and intramembranous (bones of the skull) ossification (A, yellow arrows). Osteoblasts in the periosteum express ß-Gal (B, red arrow, magnification 5X). Expression of ß-Gal in the osteoblasts, higher magnification (C, red arrow, magnification 10X).

3.5 Analysis of the phenotype of Tmem16f deficient and Tmem16f gene trap mice

Since Tmem16f is expressed in osteoblasts, one would expect disturbed bone formation in Tmem16f deficient and Tmem16f$^{gt/gt}$ mice. On the other hand, different targeting strategies were used to create both mouse lines, one deleting entire gene, and splice for the other- deleting only 3'-end of the gene. Therefore, the first goal was to reveal and compare the phenotypes of Tmem16f deficient and Tmem16f gene trap mice.

3.5.1 Skeletal phenotype of Tmem16f gene trap mice

Skeletal preparation and staining for bone and cartilage indicated that Tmem16f$^{gt/gt}$ mice have delayed endochondral and intramembranous ossification. Long bones are curved and generally shorter in Tmem16f$^{gt/gt}$ mice (Fig. 21). The heterozygous mice were phenotypically normal (data not shown). In E15.5 wild type and heterozygous mice the ossification has already started in endochohndral and intramembranous bones (Fig. 21, A). In contrast, E 15.5 Tmem16f $^{gt/gt}$ mice had no or rarely few ossification centers (Fig. 21, C, arrows). The long bones of E 16.5 Tmem16f$^{gt/gt}$ mice

are ossified, but bent (Fig. 21, G, H, arrows). The bones of the skull are also ossified in mutant mice at E16.5.

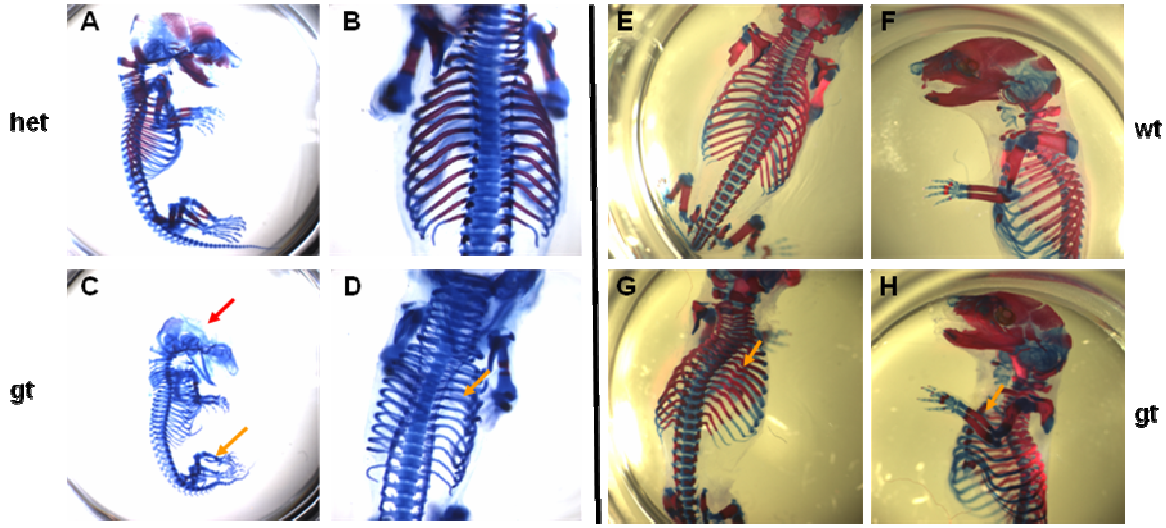

Figure 21: Skeletal phenotype of Tmem16f gene trap mice.

Skeletons of E15.5 (A, B, C, D) and E16.5 (E, F, G, H) mice were stained with Alcian Blue and Alizarin Red for cartilage and bone, respectively. The skeletons of Tmem16f$^{gt/gt}$ embryos (C, G) are shorter than skeletons of heterozygous (A) and wild type (E) embryos. The long bones of mutant mice (C, H, yellow arrows) are shorter compared to heterozygous (A) and wild type mice (F). They are also bent and less ossified (C, H, yellow arrows). The rib cage is generally smaller in mutant mice (D, G) compared to wild type (B, E). The ribs of E 15.5 Tmem16f$^{gt/gt}$ mice are not ossified (D, arrow), while ossification takes place in heterozygous mice (B). The ribs of E 16.5 Tmem16f gt/gt mice are ossified, but curved (G, arrow). Intramembranous ossification is severely delayed in E 15.5 Tmem16f gt/gt mice (C, red arrow).

Analysis of later stages, E18.5 and P0, showed dynamic changes in the ossification of Tmem16f$^{gt/gt}$ mice. First, most of the bones are ossified similar to those of the wild type. Second, the long bones are not that dramatically curved as they were at the early stages. The skull bones of Tmem16f$^{gt/gt}$ mice are strongly ossified as well, but the sutures are wider than the sutures of wild type mice (Fig. 22).

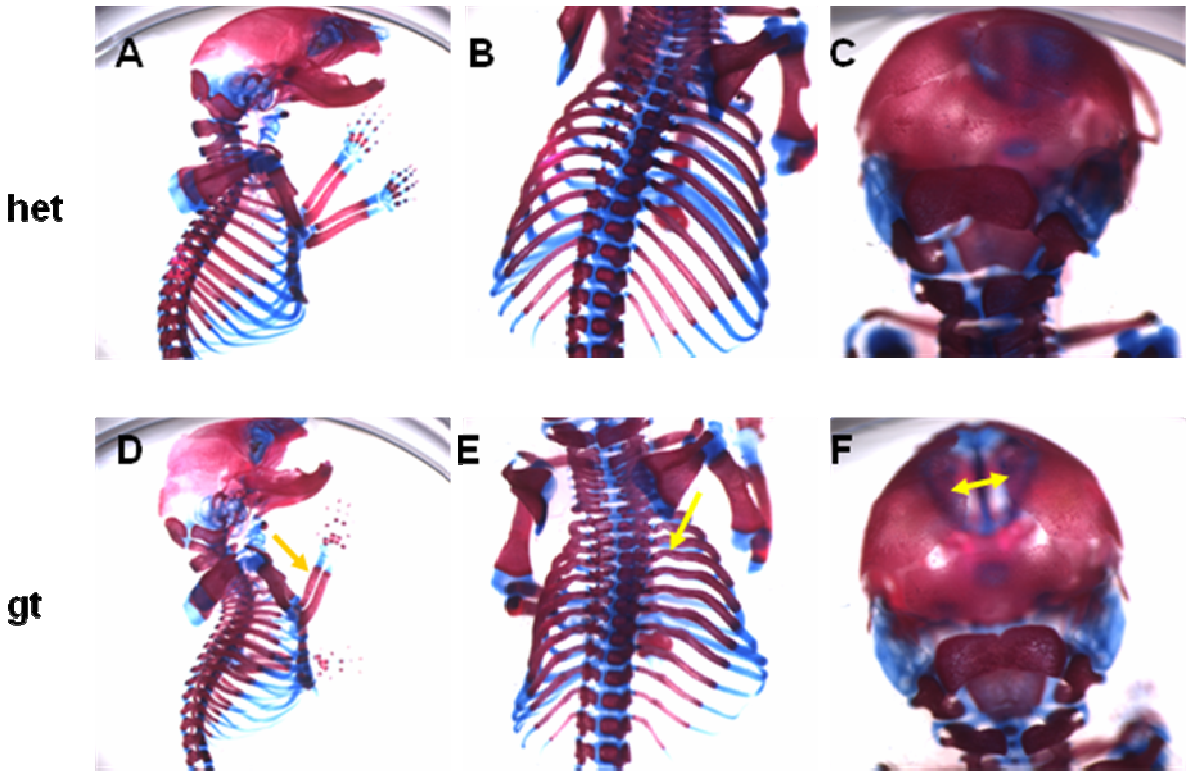

Figure 22: Alcian Blue and Alizarin Red staining of Po wild type (A, B, C) and Tmem16fgt/gt (D, E, F) skeletons.

The long bones of mutant mice are well ossified and slightly curved (D, E, arrows) compared to the long bones of wild type mice (A, B). The skull bones of mutant mice are ossified similarly to those bones of the wild type, but the sutures are wider (F, arrow).

3.5.2 Skeletal phenotype of Tmem16f deficient mice

Analysis of the skeletons of Tmem16f null mice revealed the same phenotype as of Tmem16f$^{gt/gt}$ mice: ossification was delayed in mutant mice compared to heterozygous and wild type mice.

At the embryonic stage E14.5 no bones are ossified in the mutant embryos while both, intramembranous and endochondral ossification have already taken place in wild type embryos as well as in heterozygous mice(Fig. 23). Mutant embryos are smaller in size and the cartilage anlagen of long bones, such as ribs and limbs, resemble the shape of bones of wild type mice (Fig. 23). Heterozygous mice are phenotypically normal.

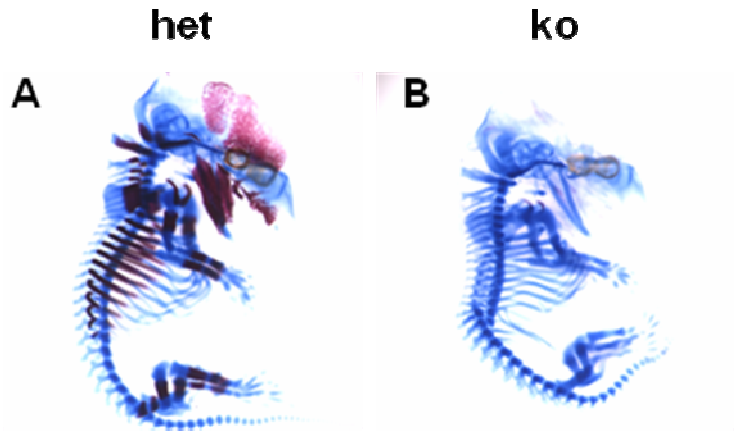

Figure 23: Alcian Blue and Alizarin Red staining of E14.5 Tmem16f heterozygous and deficient skeletons.

In E 14.5 wild type and heterozygous mice (A) the ossification has already taken place (bone is stained red). The embryos of Tmem16f deficient mice are smaller in size (B). No ossified bones can be seen in Tmem16f-/- embryos (B).

At E15.5 the skeletons of Tmem16f null mice remain to be smaller compared to wild type mice (Fig. 24). At this stage there is no or rarely very little ossification in Tmem16f mutant mice. The cartilage anlagen of long bones are shorter and the limbs and ribs are bent (Fig. 24).

At E 16.5 the bones of Tmem16f deficient mice become ossified. However, they are smaller in size than those of wild lype. The bones of Tmem16f$^{-/-}$ limbs and ribs are curved (Fig. 24). Heterozygous mice are phenotypically normal (data not shown).

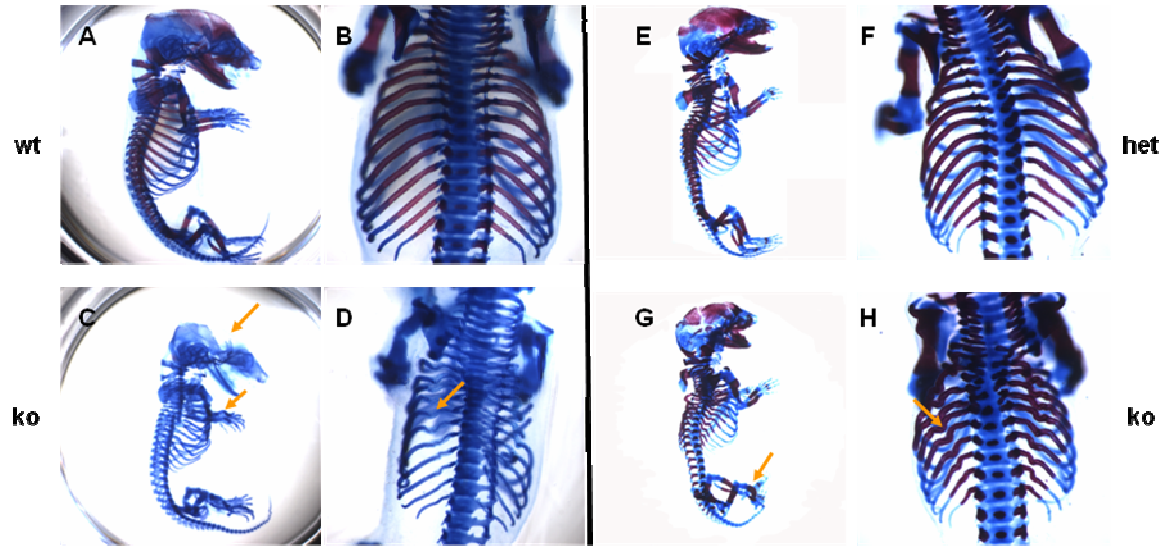

Figure 24: Skeletal phenotype of E 15.5 and E16.5 Tmem16f null mice.

Skeletons of E15.5 (A, B, C, D) and E 16.5 (E, F, G, H) mice were stained with Alcian Blue and Alizarin Red for cartilage and bone, respectively. The skeletons of Tmem16f$^{-/-}$ mice are significantly smaller than those of the wild type (C, G). There is no visible endochondral or intramembranous ossification taking place in E 15.5 mutant mice (C, D, arrows). The ribs are curved, but not ossified yet in mutant mice (D, arrow), compared to straight ossified ribs of wild type mice (B).The long bones of E 16.5 Tmem16f$^{-/-}$ mice (G) are shorter compared to wild type or heterozygous mice (E). They are also bent and less ossified (G, H, arrows). The rib cage is generally smaller in mutant mice (H) compared to wild type or heterozygous mice (F). The ribs of E 16.5 Tmem16f null mice are ossified, but curved (H, arrow).

Endochondral ossification in the forelimbs of Tmem16f deficient mice.

Analysis of different stages of forelimb development revealed several differences between wild type and Tmem16f deficient mice. At all stages the mutant limbs are generally shorter than wild type limbs (Fig. 25 A). During embryonic development, the forelimbs of Tmem16f deficient mice have normal shape but are not ossified at E14.5, whereas the limbs of the wild type embryos have already started to ossify. At E15.5 the forelimbs of mutant mice are still not ossified, but already display a malformed shape (bending). At E16.5 the mutant limbs are ossified, but keep their malformed shape of E15.5 stage, whereas wild type limbs are straight (Fig. 25 A). At E18.5 and after birth (P0) the limbs remain slightly bent. Analysis of forelimbs of one month old mice revealed shortened bones and a smaller olecranon processes in limbs of mutant embryos compared to those of the wild type mice (Fig. 25 B, red arrows). Additionally, the ulna and radius are no longer bent, but twisted around each other, whereas ulna and radius of wild type mice are parallel to each other (Fig. 25 B, black arrows). Analyzing early stages of limb development we found that the olecranon process of Tmem16f deficient mice was normal at E14.5. Starting from E15.5 the size of olecranon process of mutant mice was reduced but the elbow joints developed normally, suggesting a reduction of chondrocyte proliferation in olecranon process (Fig. 25 A, arrows). The cartilage anlagen of olecranon processes become ossified after birth and are completely ossified at the age of one month (Fig. 25 B, red arrows).

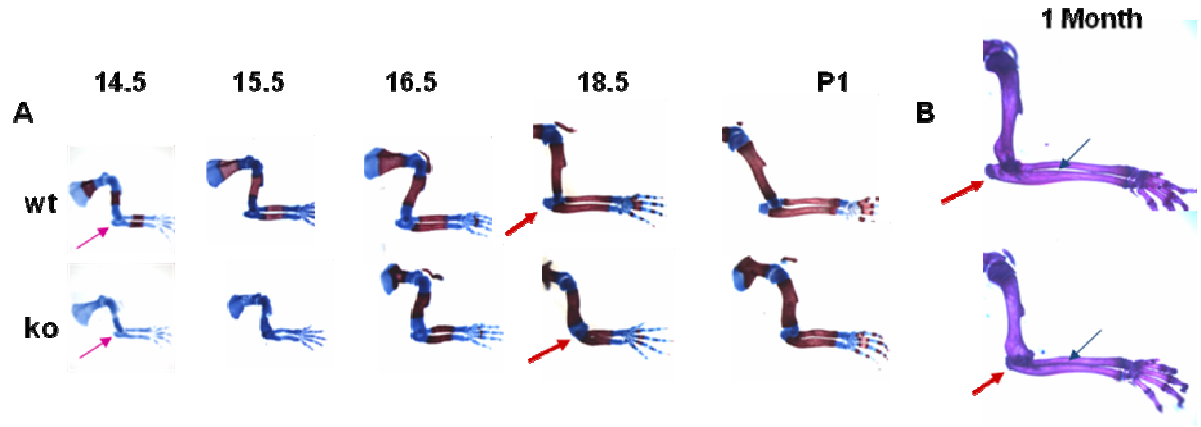

Figure 25: Endochondral ossification in the forelimbs of Tmem16f deficient mice.

The limbs were stained with Alcian Blue and Alizarin Red for cartilage and bone, respectively. The limbs in the upper row are from wild type mice, the limbs in the lower row are from Tmem16f deficient mice. The forelimbs of Tmem16f mutant mice are generally smaller in size, they are not ossified at E14.5 and E15.5. The bones are bent at E15.5 and at the later stages compared to the wild type limbs of corresponding stages (A). The olecranon process of Tmem16f deficient mice is formed properly at E14.5 (pink arrows). It is reduced in size at later stages compared to the wild type limbs (A, red arrows). The long bones of the one month old mutants are shorter than those of the wild type mice. The ulna and the radius are twisted around each other in mutant mice, whereas these bones are parallel in the wild type mice (B, black arrows). The olecranon process is fully ossified in the limbs of Tmem16f deficient mice and is reduced in size compare to the wild type limbs.

3.5.3 Comparison of endochondral ossification in Tmem16f deficient and Tmem16f$^{gt/gt}$ mice on molecular level

To investigate, whether Tmem16f deficient and Tmem16f$^{gt/gt}$ mouse lines have the same phenotype we analyzed them in greater detail at the molecular level. Analyzing limbs at the stage of E15.5, we compared chondrocyte markers (Ihh, Col10a1) and, additionally, bone markers, such as MMP13 and Dkk. The zones of prehypertrophic and hypertrophic chondrocytes can be distinguished by expression of Ihh and Col10a1, respectively. MMP13 marks the terminal hypertrophic chondrocytes and bone. The region of expression of these markers was not altered in mutant mice compared to the wild type mice (Fig. 26). However, the expression of Dkk1, a marker for osteoblasts, was reduced in Tmem16f deficient and Tmem16f$^{gt/gt}$ mouse limbs, indicating that less bone is formed at that time point of development (Fig. 26).

The comparison of endochondral ossification in Tmem16f deficient and Tmem16f$^{gt/gt}$ limbs on a molecular level confirmed the identical bone phenotype of both mouse lines.

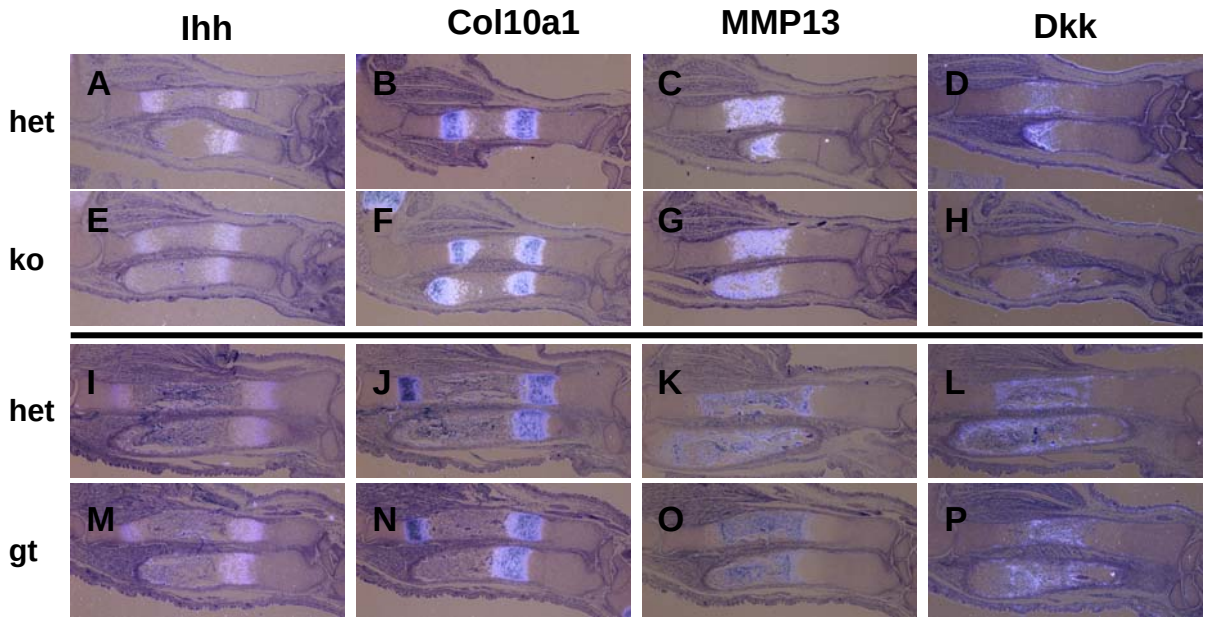

Figure 26: Ossification in the forelimbs of E15.5 mice.

Ihh, Col 10a1, MMP13 and DKK1 riboprobes were hybridized on the sections of E15.5 limbs of heterozygous mice (A, B, C, D, I, J, K, L), Tmem16f deficient (E, F, G, H) and Tmem16f$^{gt/gt}$ (M, N, O, P) mice. No significant differences were found between Ihh (A, E, I, M) and Col 10a1 (B, F, J, N) expression in mutant and heterozygous mice. MMP13 expression was also not altered in mutant mice (C, G, K, O) compared to the wild type mice. The region of Dkk1 expression (D, H, L, P) was reduced in both, Tmem16f deficient and Tmem16f$^{gt/gt}$ mutant mice.

3.5.4 Mineralization and bone resorption in Tmem16f deficient and Tmem16f$^{gt/gt}$ mice

The formation of bone is the result of the balance between the function of osteoblasts and osteoclasts. Osteoblasts form the bone, osteoclasts resorb it. Performing von Kossa and TRAP histological stainings we compared the mineralization and osteoclast number in Tmem16f deficient and Tmem16f$^{gt/gt}$ mice. In wild type mice the strongly mineralized periosteum and trabeculae were distinguishable at E16.5, whereas the periosteum and trabeculae of Tmem16f deficient and Tmem16f$^{gt/gt}$ mice were markedly less mineralized (Fig. 27, von Kossa staining). To determine whether this was caused by increased number of osteoclasts in the mutant limbs, we performed tartrate resistant acid phosphatase (TRAP) staining. TRAP is produced by the osteoclasts. We found no significant difference in number of osteoclasts between wild type and mutant mice (Fig. 27, TRAP staining).

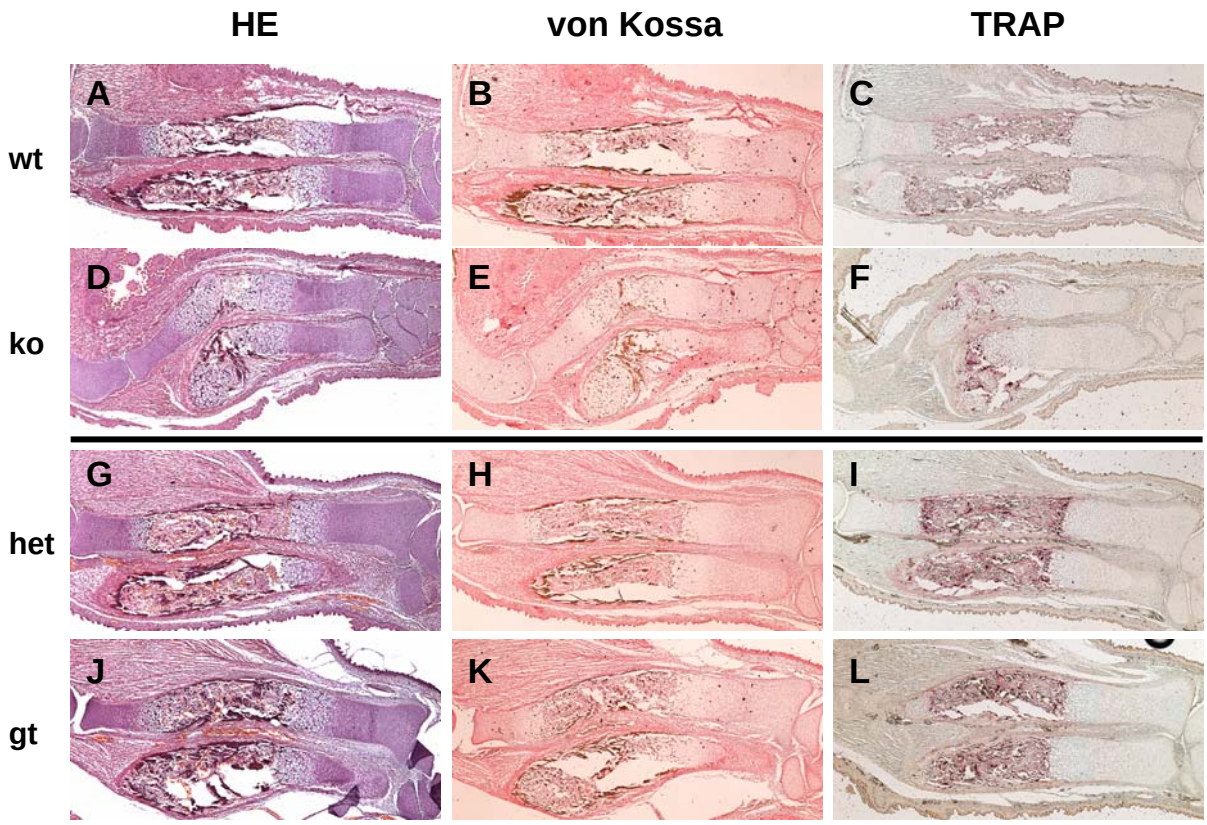

Figure 27: Histological analysis of E16.5.

The sections of E16.5 limbs of wild type mice (A, B, C, G, H, I), Tmem16f deficient (D, E, F) and Tmem16f$^{gt/gt}$ (J, K, L) mice were stained with Hematoxylin and Eosin (HE) for the morphology (A, D, G, J), with von Kossa staining for calcium ions (B, E, H, K). TRAP staining (C, F, I, L) was performed to detect the oseoclasts. The size of trabeculae and the front of mineralization were markedly reduced in both mouse mutant lines (D, E, J, K) compared to the wild type mice (A, B, G, H), even though the number of osteoclasts was not altered.

3.5.5 Delayed ossification in Tmem16f deficient mice

To investigate the mechanism which regulates the ossification in the Tmem16f deficient mice, we analyzed more osteoblast markers to test whether the reduced mineralization is due to the smaller number or to the reduced activity of the osteoblasts. In situ hybridization of Osterix (Osx) and Bone sialoprotein (Bsp) riboprobes on E14.5 forelimbs showed no alteration in expression of these osteoblast markers between wild type and Tmem16f deficient mice (Fig. 28). At this stage both, Osx and Bsp, are expressed in the periosteum. In mutant mice the intensity of the expression of both osteoblast markers and the distance from periarticular region to the domain of their expression in periosteum were equal to those of the wild type mice. However, no mineralization was detected at this time point of development in the limbs of Tmem16f deficient mice (Fig. 28).

The same chondrocyte and osteoblast markers were used to analyze limbs of E15.5 Tmem16f deficient mice. As at the earlier stage, no differences were seen in chondrocyte proliferation or differentiation (Fig. 29, Ihh and Col 10a1 riboprobes). Expression of Osx and Bsp was also not altered in Tmem16f deficient mice, which suggests normal development of early osteoblasts. However, von Kossa staining showed weaker mineralization of the limbs of Tmem16f deficient mice, the trabeculae are less mineralized. On the Fig. 29 one can see that the front of mineralized periosteum in Tmem16f deficient limb (Fig. 29 J) does not expand as far up to Ihh expression domain as in wild type limb (Fig. 29 E). The same is true for the averages taken over ten wild type and ten Tmem16f deficient limbs, however this difference is not statistically significant in our experiments at the stage E 15.5.

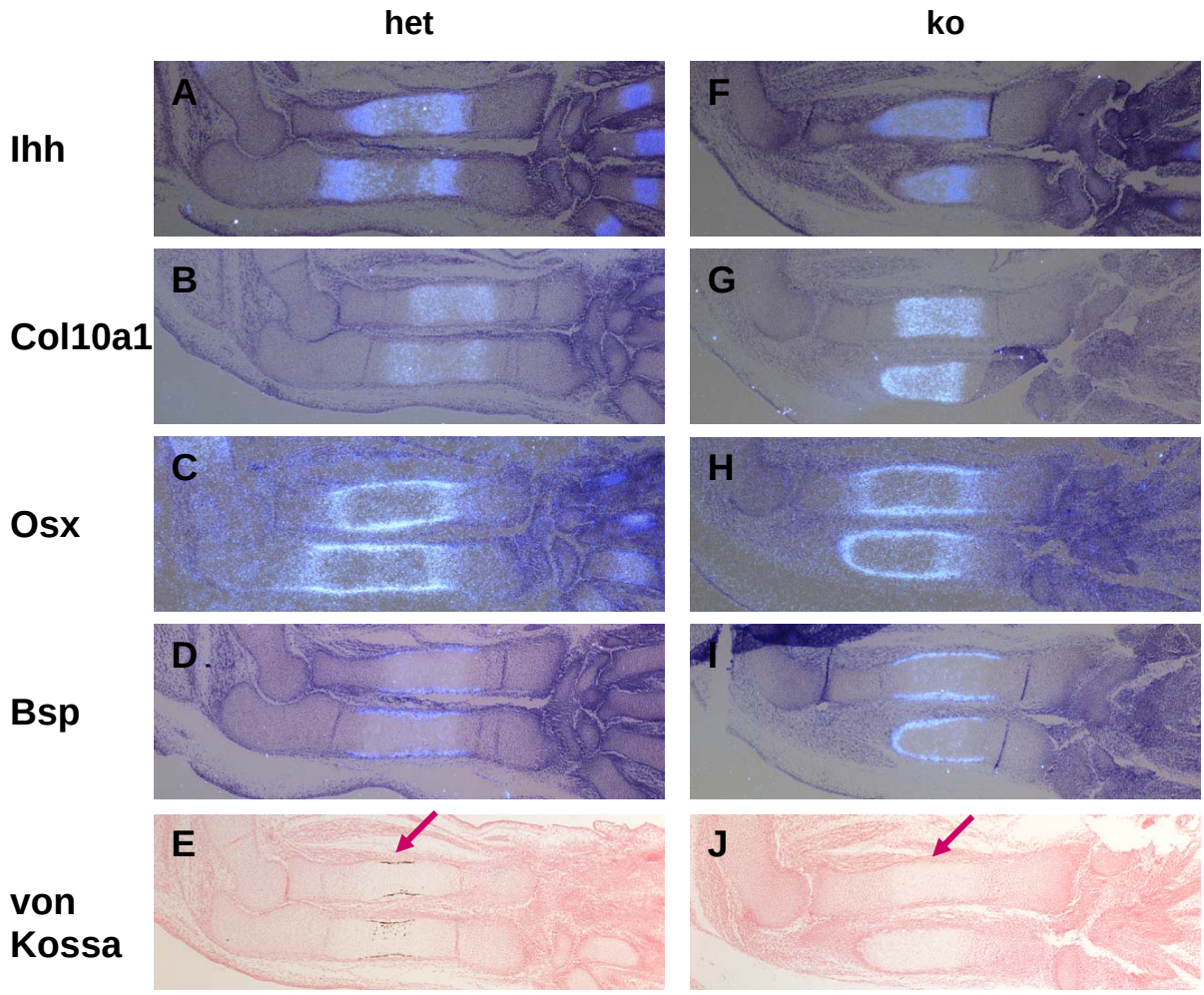

Figure 28: Ossification in E14.5 Tmem16f deficient mice.

Ihh, Col 10a1, Osx and Bsp riboprobes were hybridized on the parallel sections of E14.5 limbs of heterozygous (A, B, C, D) and Tmem16f deficient (F, G, H, I) mice. The mineralization was detected by von Kossa staining of the parallel sections of heterozygous (E) and Tmem16f deficient (J) mice.

Hypertrophic differentiation is not affected in Tmem16f deficient mice (Ihh and Col 10a1 probes). Expression of the osteoblast markers such as Osx and Bsp in the periosteum is not affected in the mutant mice, whereas no calcification of the periosteum was detected in the Tmem16f deficient mice (arrows). The magnification is 5X.

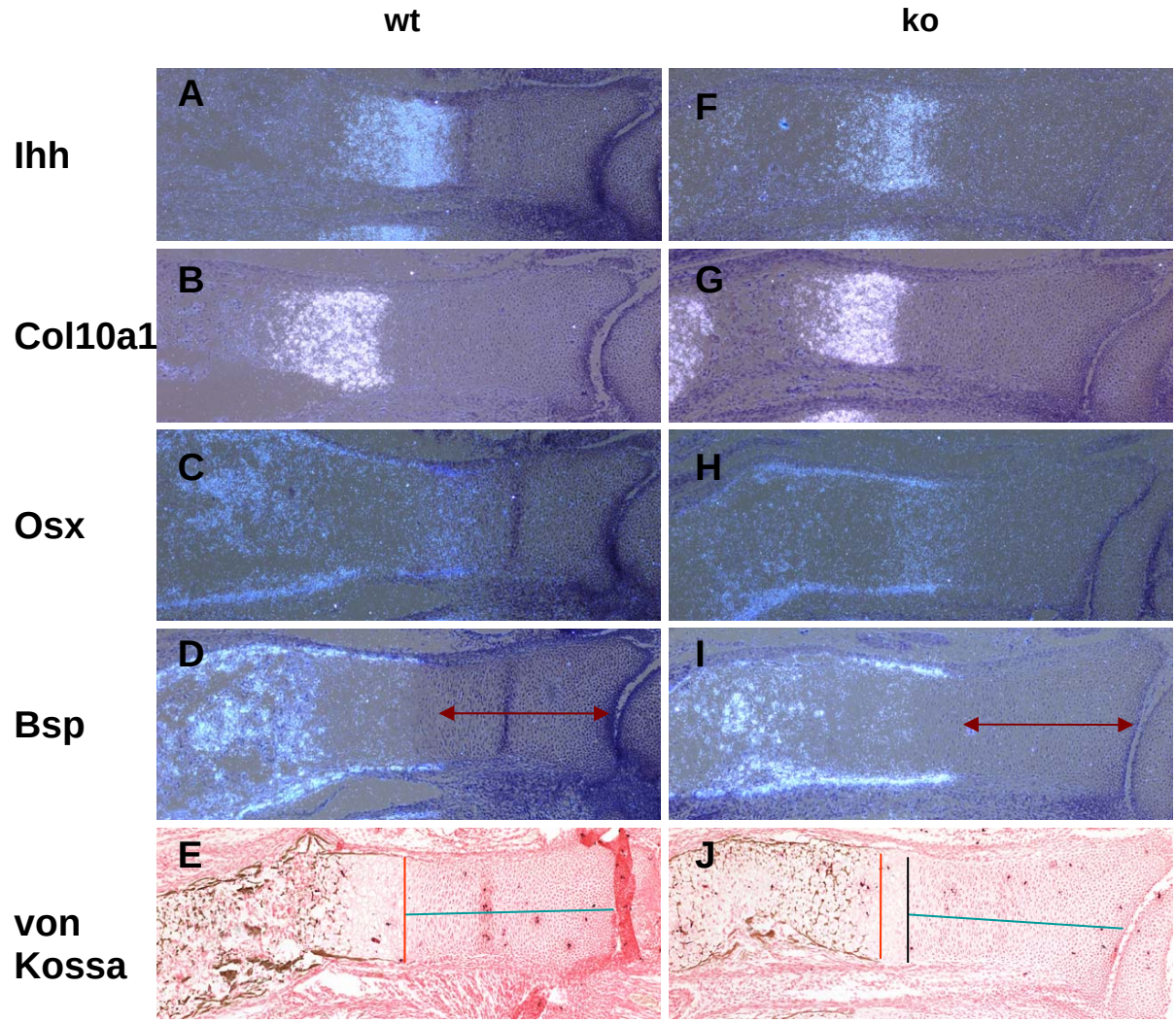

Figure 29: Ossification in E15.5 Tmem16f deficient mice.

Ihh, Col 10a1, Osx and Bsp riboprobes were hybridized on the parallel sections of E15.5 limbs of wild type (A, B, C, D) and Tmem16f deficient (F, G, H, I) mice. Von Kossa staining was performed on the parallel sections of wild type (E) and Tmem16f deficient (J) mice. Expression of markers for chondrocytes (Ihh, Col 10a1) and for osteoblasts (Osx, Bsp) showed no difference in the development of early osteoblasts between the wild type and Tmem16f deficient mice. The distance from the periarticular region to the border of Bsp expression in the periosteum is not altered (D, I, red arrows), whereas the distance from the periarticular region to the border of ossified periosteum is larger (green line shows the distance from periarticular region to the border of calcified periost, orange line shows the ossification border of mineralized periost, black line represents the border of mineralized periost in wild type limbs, transferred to the picture of Tmem16f deficient mice). The radius is shown at the magnification of 10X.

Further we analyzed the limbs of E16.5 Tmem16f deficient mice. The bone is formed in the centre of the anlage in both Tmem16f deficient and wild type mice. The expression pattern of chondrocyte specific markers such as Ihh and Col 10a1 in the Tmem16f deficient mice were similar to those of the wild type mice (Fig. 30). This indicates that there is no alteration in the chondrocyte proliferation and differentiation in Tmem16f deficient mice. The early osteoblast markers Osx and Bsp are expressed clearly in the periosteum surrounding Ihh expression domain in prehypertrophyc chondrocytes and also in the trabeculae of wild type mice. However, their expression is much weaker in the trabeculae of Tmem16f deficient mice (Fig. 30). E16.5 is the earliest stage of embryonic development, when the expression of late osteoblast marker Osteocalcin (Osc) can be detected. In the wild type it is strongly expressed in the periosteum which borders trabecular bone and it is weaker in the trabeculae. However, Osc expression is markedly reduced in the limbs of Tmem16f deficient mice (Fig. 30). This evidence indicates delayed maturation of osteoblasts in Tmem16f deficient mice. Moreover, the trabeculae of Tmem16f deficient mice are much weaker, smaller and more dispersed than the trabeculae of wild type mice (Fig. 30).

Molecular analysis of endochondral ossification in Tmem16f mutants revealed that proliferation and differentiation of chondrocytes is not affected, whereas the ossification process is severely delayed. Interestingly, the expression of early osteoblast markers like Osx and Bsp is unaffected in the periosteum, but reduced in the trabeculae. Later osteoblast differentiation is disturbed as shown by a delayed onset of mineralization and reduced Osteocalcin expression.

To test whether the mineralization of the periosteum in Tmem16f deficient mice is significantly delayed compared to wild type mice, we performed several measurements. First, the distance from the periarticular region to the border of Bsp expression in the periosteum was measured in wild type and Tmem16f deficient mice (length “a”, onset of Bsp expression) (Fig. 31 A, C).

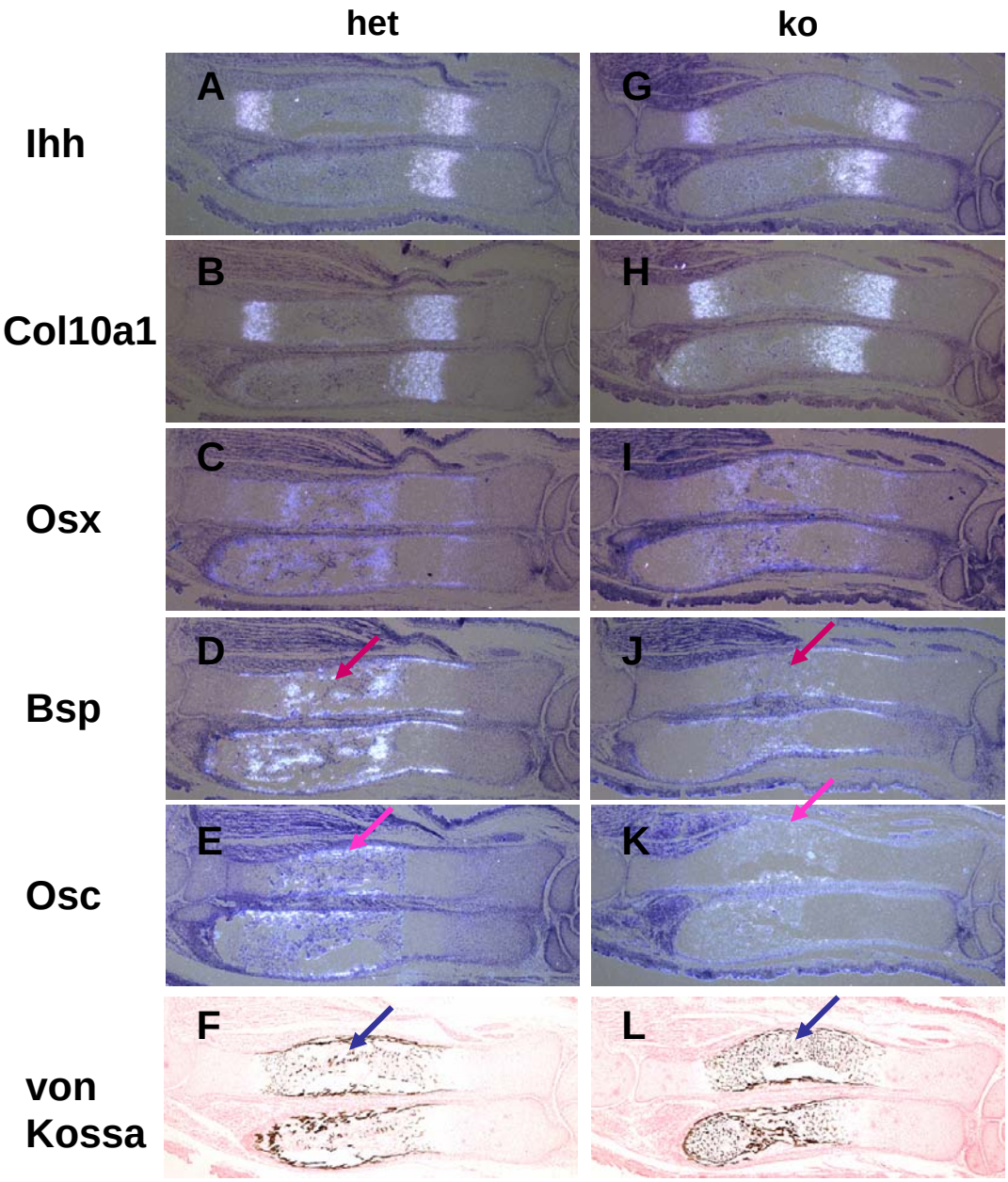

Figure 30: Ossification in E16.5 Tmem16f deficient mice.

Ihh, Col 10a1, Osx, Bsp and Osc riboprobes were hybridized on the parallel sections of E16.5 limbs of Tmem16f heterozygous (A, B, C, D, E) and Tmem16f deficient (G, H, I, J, K) mice. Von Kossa staining was performed on the parallel sections of wild type (F) and Tmem16f deficient (L) mice. Ihh (A, G) and Col 10a1 (B, H) riboprobes mark prehypertrophic- and hupertrophic chondrocytes, respectively. Osx (C, I) and Bsp (D, J) are expressed by early osteoblasts. Their expression in trabecular bone is downregulated in Tmem16f deficient mice compare to the wild type mice (D, J, arrows). The expression of Osc, a marker of the late osteoblasts is markedly reduced in Tmem16f deficient mice, compare to wild type mice (E, K, arrows). The trabeculae of Tmem16f deficient mice are smaller in size and weaker mineralized than those of the wild type (F, L, arrows). The ulna and the radius are shown at the magnification of 5X.

Second, the distance from periarticular region to the mineralized periosteum was measured in wild type and Tmem16f deficient mice (length “b”, mineralized periosteum) (Fig. 31 B, D). Subtracting the length “a” from the length “b”, we determined the distance from the border of Bsp expression in the periosteum to mineralized periosteum (length “c”). The distance between Bsp expression in the periosteum and mineralized periosteum (length “c”) was 71 % larger in Tmem16f deficient mice than in the wild type mice (length “c”, Fig. 31 B, D, E).

These results indicate that despite normal chondrocyte proliferation and differentiation in Tmem16f deficient mice the osteoblast maturation is retarded at the later stages of osteoblast differentiation process. Therefore, mineralization of the bone is also delayed.

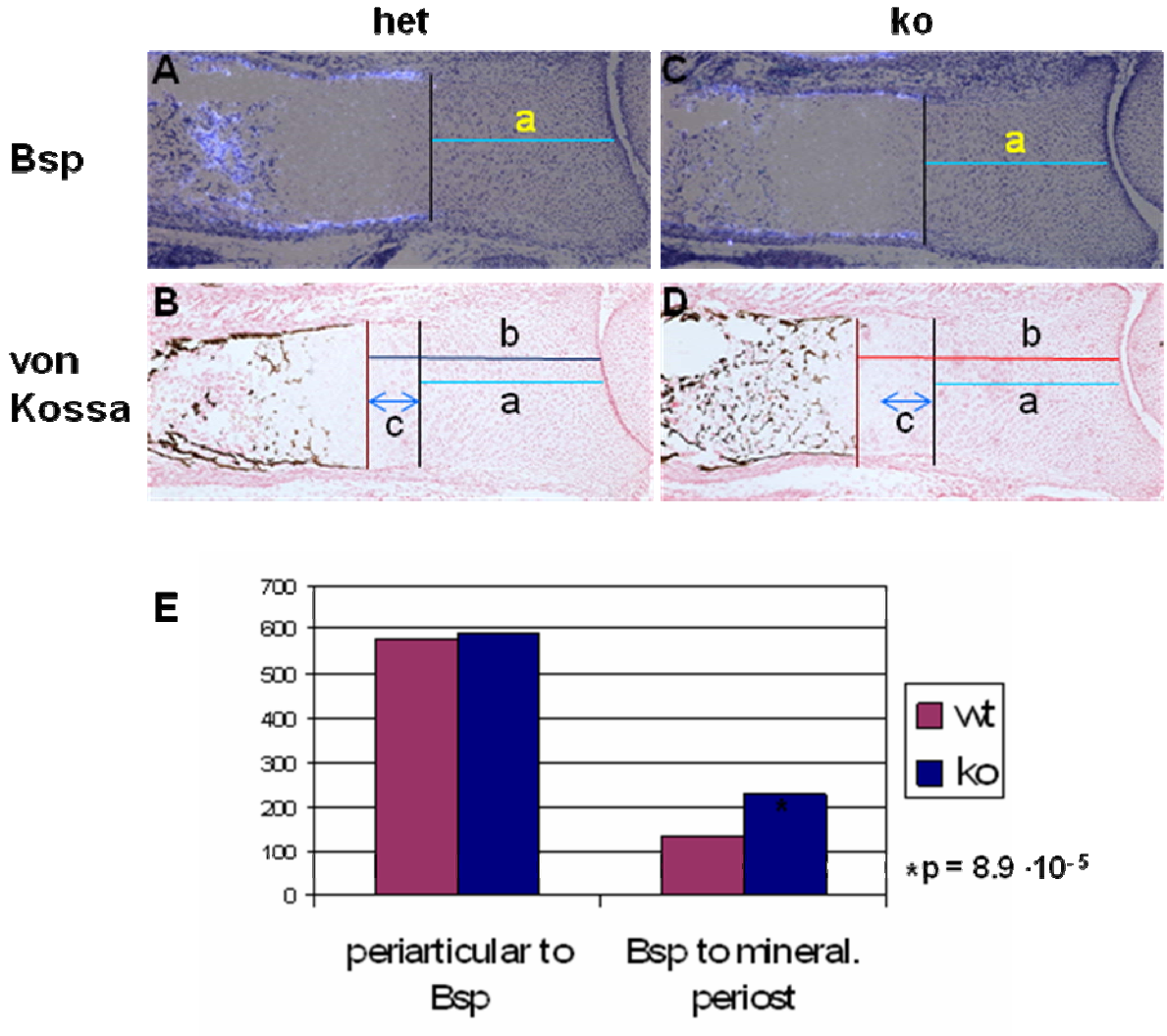

Figure 31: Mineralization in E16.5 Tmem16f deficient mice.

In Tmem16f mutants the onset of Bsp expression is unaffected (A, C, E), whereas the mineralized region of the periosteum is significantly shorter than in the wild type (B, D, E). n=10, unpaired student t test. The radius is shown at the magnification of 10X.

As a first hypothesis of why there is a delay in the mineralization during the development of endochondral bones, we suggested that there is a reduction in the synthesis and/or the activity of alkaline phosphatase (TNAP or AP). However, no dramatic changes were found in the activity of alkaline phosphatase in the limbs of E16.5 Tmem16f deficient mice compare to wild type mice (Fig. 32), suggesting other mechanisms acting downstream of Tmem16f gene.

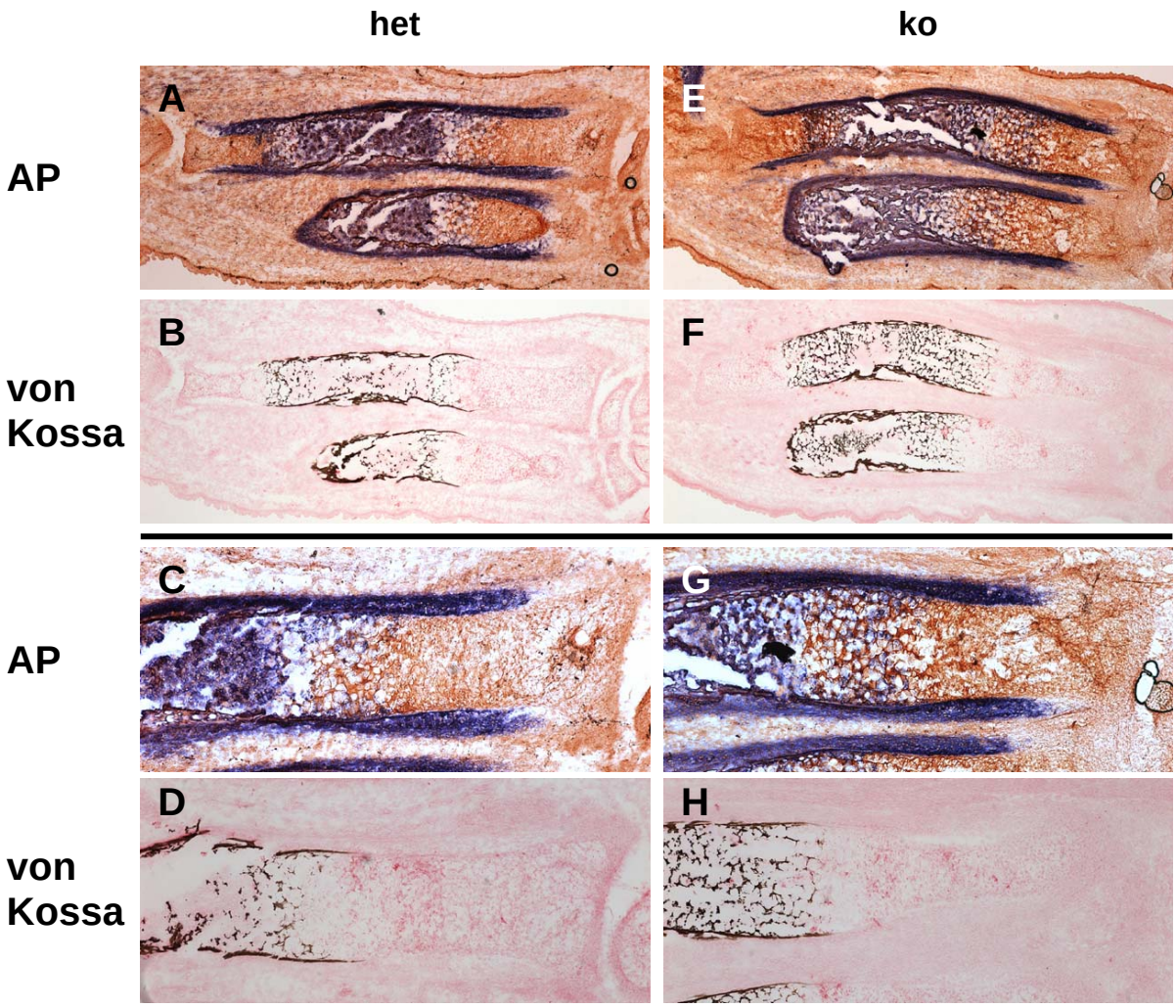

Figure 32: Alkaline phosphatase activity in E16.5 Tmem16f deficient mice.

Cryosections of E16.5 forelimbs of Tmem16f heterozygous mice (A, B, C, D) and Tmem16f deficient mice (E, F, G, H) were stained to detect alkaline phosphatase activity. No significant difference was found in alkaline phosphatase activity (A, E, C, G) between wild type and mutant mice. The parallel sections were stained for calcium ions (B, F, D, H). The magnification is 5X for (A, B, E, F) and 10X for (C, D, G, H).

3.5.6 Intramembranous ossification in Tmem16f deficient mice

As the first step to reveal the cause of the delayed ossification of skull bones, we analyzed the expression of early and later osteoblast markers such as Bsp and Osc. At stage E16.5 the expression of Bsp was upregulated, whereas the expression of Osc was downregulated in intramembranous bones of Tmem16f deficient mice (Fig. 33). Parallel sections of E16.5 mouse heads were also stained for calcium ions. The mineralization of intramembranous bones was markedly reduced as it was shown by von Kossa staining (Fig. 33).

Further we analyzed the width of the interfrontal suture. Sutures are the fibrous tissues uniting the bones of the skull. They are also the major sites of bone growth (Opperman, L. A., 2000). We measured the distances between Bsp and Osc expression zones in frontal bones and between the fronts of the mineralization of these bones (Fig. 33). The distance between two mineralized bones (the suture) was wider in Tmem16f deficient mice than in the wild type mice, but the distance between the zones of Osteocalcin expression in mutant mice was similar to those of the wild type (Fig. 33 C, F and B, E). Also it is interesting, that the distance between the Bsp expression domains of the frontal bones was smaller in Tmem16f deficient mice than in the wild type mice (Fig. 33, A, D). That suggests that there is some compensating mechanism for mineralization of intramembranous bones in Tmem16f deficient mice. Finding this mechanism demands the analysis of additional markers and later stages of mouse development.

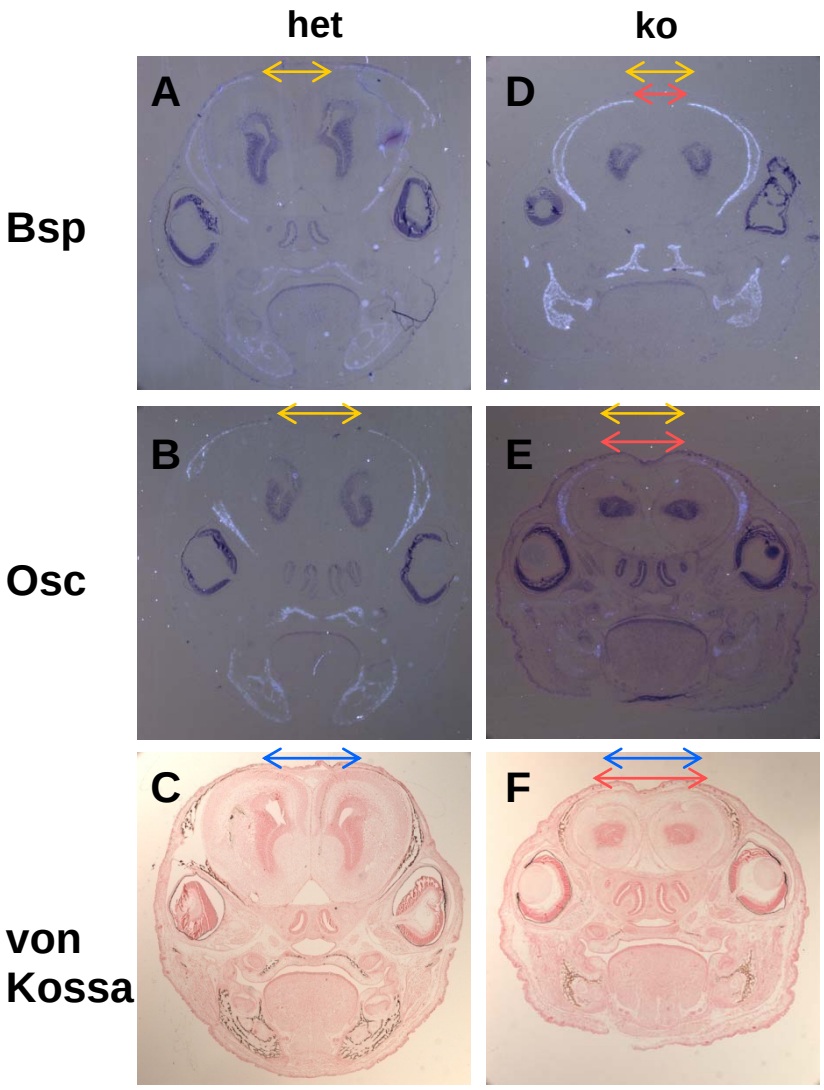

Figure 33: Intramembranous ossification in E16.5 Tmem16f deficient mice.

Bsp and Osc riboprobes were hybridized on the sections of E16.5 heads of heterozygous mice (A, B) and Tmem16f deficient mice (D, E). Von Kossa staining was performed on the parallel sections of the same heads of the wild type (C) and Tmem16f deficient (F) mice. The expression of Bsp is upregulated, whereas expression of Osc is downregulated in intramembranous bones of Tmem16f deficient mice. The distances between Bsp expression domains of frontal bones in Tmem16f deficient mice is smaller than in the case of the wild type (A, D, arrows). The distances between Osc expression domains of the same bones in mutant mice is comparable to the wild type case (B, E, arrows). Mineralization in the intramembranous bones of Tmem16f deficient mice is delayed. The distance between the ossification fronts (width of the suture) of frontal bones is larger in Tmem16f deficient mice than in the wild type (C, F, arrows). The magnification is 2.5X.

4. Discussion

4.1 Structure of Tmem16f

The complete cDNA sequence was obtained by combining two approaches. First, the EST clones matching the originally identified 769 bp region of Tmem16f were sequenced. Second, a 5'RACE method was used to verify the complete 5'-end sequence of Tmem16f. By now, we obtained the complete Tmem16f mRNA sequence by ESTs sequencing. The 5'end obtained using this method was longer than those resultant from 5'RACE. The 5'RACE experiment revealed an existence of the second alternatively spliced exon. Even more, there were two isoforms of the second exon found: 2a and 2b. Considering the number of clones obtained and sequenced during 5'RACE experiment (which is based on the extraction of the mRNA and synthesis of the cDNA) one can suggest that those two isoforms of the second exon are rarely expressed. Only single clones contained exons 2a or 2b, whereas the other exons, number 1, 3, 4, 5 were present in all clones. Our data indicate that Tmem16f consist of 21 exons, including the second alternatively spliced exon, whereas ensembl database has annotated a Tmem16f of 20 exons. The third exon resulting from our experiments represents the second exon of Tmem16f annotated by Ensembl database. It was found that Tmem16f covers 184 kb of the genomic region on mouse chromosome 15. The transcript of Tmem16f gene is 5680 bp.

Analysis of two other members of Tmem16 family by different research groups revealed several isoforms of Tmem16A and GDD1/TMEM16E (Caputo et al., 2008; Tsutsumi et al., 2005). For the GDD1/TMEM16E transcript 22 exons were identified forming the longest isoform. The other thirteen isoforms were comprised of different combinations of alternative exons 4, 6, 16b, 20 and 21 (Tsutsumi et al., 2005). These data indicate that there might be several other alternatively spliced exons detected for Tmem16f. Since the 5'RACE was performed using a gene specific primer to the 5^{th} exon of Tmem16f, the other possible isoforms could be detected by PCR using primers to different exons of Tmem16f starting from the 5^{th} exon. RT-PCR using primers complementary to the parts of different exons of Tmem16f confirmed *in silico* predicted intron-exon structure of Tmem16f but did not identify any other isoforms for Tmem16f (see chapter 3.1.3 and Fig. 10A, C). The PCR products were produced using primers covering exon 3 to exon 8, exon 6 to exon 11a and exon 11b to exon

16, exon 17to exon 20. We have determined Tmem16f ORF of 2736 nucleotides (in mouse) which was identical to those found later in the database (Ensembl). The open reading frame starts in the exon 1 and ends in the exon 21 of Tmem16f. It encodes a protein of 911 amino acids.

A short isoform of Tmem16f (Ano6-202) was predicted by Ensemble. It represents the 3'-sequence of Tmem16f starting from exon 13 of Tmem16f. Ano6-202 has an alternative start site in a genomic sequence of intron 12. An ORF for the Ano6-202 comprises 1455 nucleotides and encodes a polipeptide of 484 amino acid residues. First nine amino acids are encoded by the first exon of Ano6-202 and do not match the sequence of Tmem16F protein.

Analysis of amino acid sequence revealed that Tmem16F protein contains eight potential transmembrane domains. The domains 6, 7 and 8 are a part of the DUF590 domain. These domains are conserved among the members of TMEM16 family. For the plasma membrane both N- and C-terminal ends of the protein are exposed to the cytoplasm. There were six N-linked glycosylation sites predicted for Tmem16F at the amino acid residues 330, 362, 494, 778, 785 and 803 (data from UniProtKB/Swiss-Prot). For the GDD1/TMEM16E protein there were five putative glycosilation sites found using MOTIF and PSORT II programms (Tsutsumi et al., 2004). This data suggests that Tmem16f and GDD1/TMEM16E represent glycoproteins.

In present work the Tmem16F protein was analyzed only *in silico*. All data collected for Tmem16F protein was a prediction which might give a first clue about possible structure and function of Tmem16F protein. These results need to be further proved experimentally.

4.2 Tmem16f is expressed in osteoblasts

As Tmem16f was initially found in a screen for Ihh-target genes, it was important to know whether Tmem16f is expressed in the same or adjacent tissue as Ihh, by chondrocytes or osteoblasts or by other cell types. With *in situ* hybridization experiments on E 14.5 and E 16.5 mouse embryos it was established that Tmem16f is expressed by osteoblasts of newly formed bone and periosteum. However, in the study of another research group a broader expression of Tmem16f was detected. At E14.5 Tmem16f expression was detected in the epithelium of lung, and weak expression was observed in the lung mesenchyme. Tmem16f expression was also detected in the epithelium of small intestine at this stage and weak expression was

observed in the mesenchyme of the small intestine and in the epithelial and mesenchymal components of trachea, ovary, kidney and stomach. At E16.5 Tmem16f was found in the epithelium and mesenchyme of the esophagus (Rock and Harfe, 2008). We suggest that the differences in the detected patterns and sensitivity of detection may lie in the methods used by different groups.

The other members of Tmem16 family were also found to be expressed in various different tissues. Tmem16A was shown to be expressed in the epithelium of the trachea and lungs, esophageal mesenchyme, epithelium of the posterior stomach, thymus and the aorta, in the perichondria of the developing vertebrae and ribs (Rock et al., 2008; Rock and Harfe, 2008). Mouse GDD1/TMEM16E was shown to be strongly expressed in the bone (Tsutsumi et al., 2004). At E14.5 GDD1/TMEM16E was expressed in the mesenchyme surrounding the digits and carpal/tarsal bones (Mizuta et al., 2007). Weak GDD1/TMEM16E protein expression was detected in the bones of E14.5 limbs. GDD1/TMEM16E protein was detected later in the prehypertrophic chondrocytes of E18.5 limbs and in the hypertrophyc chondrocytes of epiphyseal growth plate of adult mice. In adult mice GDD1/TMEM16E was expressed by the osteoblasts of endosteum and periosteum, as well as in the articular cartilage cells. This protein was also found in the myofibers of the adult mouse heart (Mizuta et al., 2007).

Considering all data together, Tmem16f seems to be more bone-specific member of Tmem16 family than the others. Expression of Tmem16e by the chondrocytes and later in development by the osteoblasts gives an idea that both genes might function synergistically and that one gene can probably compensate for the absence of another.

4.3 Localization of Tmem16f in the cell

To get the first clue of where the protein of interest is localized in the cell we performed the fast method where the Tmem16f-EGFP fused construct was easily transfected into COS-7 or CHO cells. We have identified TMEM16F as localized in the cytoplasm and not in the nucleus. Which compartment of the cell Tmem16f resides is still remains unclear. This result is preliminary and need to be tested in other experimentst.

Similar results were initially shown for GDD1/TMEM16E which is homologous to the Tmem16f. COS-7 cells were transfected with an expression vector containing human GDD1/TMEM16E cDNA tagged with V5 epitope at it’s 3’-end. From this experiment it

was established that GDD1/TMEM16E is localized in endoplasmatic reticulum (Tsutsumi et al., 2004). However, in later study the same research group used GDD1-specific antibodies and revealed that GDD1/TMEM16E protein is residing mainly within intracellular membrane vesicles, and also in plasma membrane (Mizuta et al., 2007).

Another supportive data was established for Tmem16A protein. It was detected in plasma membrane (shown by transient and stable transfection of HEK-293 and FRT cells. Tmem16A protein had a FLAG epitope) (Caputo et al., 2008).

Taken all together these data seem to suggest that members of Tmem16 protein family are localized in plasma membrane and within intracellular membrane vesicles. To detect precise Tmem16f localization in the cell other experiments using specific antibody should be performed.

4.4 Targeting of Tmem16f gene: deletion and gene trap strategies

There are different strategies used by investigators to study the function of the gene. In our approach we have used two strategies to unravel the function of Tmem16f.

First, the targeted deletion was performed to eliminate the 1st exon of Tmem16f. Due to the large introns between the exons it was technically not possible to delete the whole gene. Therefore, only the first exon containing the start codon of Tmem16f was deleted thus preventing the synthesis of the long isoform of Tmem16f. However, this strategy does not eliminate the synthesis of the potential shorter isoform of Tmem16f (Ano6-202)

Second, ES cells carrying gene trap cassette inserted into intron 13 of Tmem16f gene were generated by Bay Genomics. That allowed to analyze mice in which the synthesis of both isoforms of Tmem16f would be disrupted. Therefore, the conserved DUF590 domain could be analyzed. Additionally, the presence of the ß-galactosidase gene in the gene trap cassette allow to follow the expression pattern of Tmem16f in mouse embryos by performing X-gal staining.

Taken together the results of two strategies allow for the comparison of two isoforms of the protein and possibly for the analysis of DUF590 domain and potential domains located on the N-terminus of Tmem16f.

4.5 Functional analysis of Tmem16f gene

First analysis of Tmem16f deficient and Tmem16f gene trap mouse lines during embryogenesis revealed identical phenotype discovered for both mouse lines.

Mutant mice had delayed start of ossification, shortening and bending of the long bones and delay in ossification of skull bones. The heterozygous mice of both mouse lines were phenotypically normal. In present study we have analyzed the bone phenotype of Tmem16f deficient mice on molecular level more in detail.

4.5.1 Impaired ossification in Tmem16f deficient mice.

The analysis of the phenotype of Tmem16f was performed in two steps. First, skeletal preparations were performed of mouse embryos of different stages, of newborn and 1 month old mice. Second, analysis on the molecular level was performed, using *in situ* hybridization and histological techniques.

The earliest time point for skeletal analysis was E14.5. At this stage we established that no ossification could be detected in the mutant embryos while both, intramembranous and endochondral ossifications have already taken place in wild type embryos. All limbs and ribs of mutant mice have normal shape. Mutant embryos are generally smaller in size than wild type embryos. At stage E15.5 there was still no (or rarely very little) ossification seen in Tmem16f mutant mice. The skeletons of Tmem16f mutant mice were smaller and the long bones are shorter compared to the wild type embryos. The limbs and ribs were bended in Tmem16f deficient mice. At E16.5 the bones of Tmem16f mutant mice started to ossify but the long bones (i.e. ribs and limbs) were still shorter and kept the curved shape seen at the stage E15.5. All bones of Tmem16f deficient mice were less ossified than the bones of wild type mice. At later stages, such as E18.5 and P0, most of the bones were ossified similar to those of the wild type. The long bones were not that dramatically curved as they were at the early stages. The skull bones of Tmem16f mutant mice were strongly ossified as well, but the sutures were wider than the sutures of wild type mice.

Analysis of one month old mice revealed slightly shortened bones and smaller olecranon processes of mutant limbs compared to those of the wild type mice. The ulna and radius were no longer bent, but twisted around each other in Tmem16f deficient mice, whereas ulna and radius of wild type mice are parallel to each other. The ribs of mutant mice were also not bent any more.

The finding of the shorter olecranon process in one month mutant mice led to additional analysis of olecranon process at early stages. We found that at E14.5 the olecranon process of Tmem16f deficient mice was the same shape and size as the olecranon process of wild type mice. Starting from E15.5 the size of olecranon

process of mutant mice was reduced but the elbow joints developed normally, suggesting a reduction of chondrocyte proliferation in olecranon process. The cartilage anlage of olecranon process become ossified later after birth and is completely ossified at the age of one month in wild type as well as in mutant mice. However, it remains to be much smaller than in wild type mice

Despite the severe embryonic skeletal phenotype Tmem16f deficient mice survive after birth and are fertile. These data indicates possible rescue by some other gene acting later or simultaneously with Tmem16f during the development.

We suggest that one hypothetical candidate for this role might be Tmem16E because it belongs to the same protein family and because of its expression pattern. It was shown that GDD1/TMEM16E protein is weakly expressed in the bones of E14.5 mouse limbs. Later this protein was detected in the prehypertrophic chondrocytes of E18.5 limbs and in the hypertrophyc chondrocytes of epiphyseal growth plate of adult mice. In adult mice GDD1/TMEM16E was expressed by the osteoblasts of endosteum and periosteum, as well as in the articular cartilage cells (Mizuta et al., 2007). To prove this idea Tmem16E/ Tmem16f double knockout mouse needs to be generated and analyzed.

4.5.2 Bone resorption and alkaline phosphatase activity are not affected in Tmem16f deficient mice

The comparison of mineralization in Tmem16f deficient and wild type mice revealed that the periosteum and trabeculae of Tmem16f deficient mice were markedly less mineralized compare to the wild type during embryogenesis. The formation of bone is the result of the balance between the function of osteoblasts and osteoclasts. These data led to a suggestion that reduced mineralization in mutant mice could be caused by increased number of osteoclasts. Staining for TRAP which is produced by osteoclasts revealed no significant difference in number of osteoclasts between wild type and mutant mice. Therefore we suggest that bone resorption is not altered in Tmem16f deficient mice.

As another hypothesis of why there is a delay in the mineralization during development of endochondral bones, we suggested that there is a reduction in the synthesis and/or the activity of alkaline phosphatase. However, no significant difference was found in alkaline phosphatase activity in the limbs of Tmem16f deficient and wild type mice. These facts led to suggestion that other steps of mineralization process are regulated by Tmem16f gene.

4.5.3 Delayed ossification in Tmem16f deficient mice

In attempt to identify the mechanism which regulates the ossification in the Tmem16f deficient mice, we analyzed forelimbs and skull of Tmem16f mice on molecular level. To investigate whether the reduced mineralization is due to the delay in hypertrophic chondrocyte differentiation or due to smaller number or the reduced activity of the osteoblasts we hybridized cartilage and bone markers on the forelimbs of Tmem16f deficient and wild type mice. An expression of Ihh (marker of prehypertrophic chondrocytes), Coll10 (hypertrophic chondrocytes) and MMP13 (marker of terminal hypertrophic chondrocytes) was not altered at any stage of embryonic development in Tmem16f deficient mice compared to wild type mice. There were also no changes found in expression of Runx2 (data not shown), which is normally expressed by prechypertrophic and chypertrophic chondrocytes and osteoblast progenitors and differentiated osteoblasts (Inada, et al., 1999; Kim, et al., 1999; Takeda, et al., 2001; Stricker, et al., 2002). This indicated that proliferation and differentiation of chondrocytes were not affected in Tmem16f mutants.

Analyzing the expression of the osteoblast markers such as Osterix (Osx), Bone sialoprotein (Bsp) and Osteocalcin (Osc) and comparing it to the mineralization of the limb (detected by von Kossa staining) we revealed that later osteoblast differentiation is disturbed in Tmem16f deficient mice. The expression of early osteoblast markers like Osx and Bsp was not altered in the limbs of E14.5 and E15.5 mutant mice, which indicates normal development of early osteoblasts. However, the limbs were less mineralized. At E16.5 the expression of Osx and Bsp was unaffected in the periosteum, but reduced in the trabeculae of Tmem16f deficient mice. The expression of osteocalcin was markedly reduced at this stage of development indicating that later osteoblast differentiation is disturbed in Tmem16f deficient mice. This is supported by the fact that onset of mineralization was delayed in mutant mice (it might be, that it is probably the cause of the delayed mineralization in mutant mice). The trabeculae of Tmem16f deficient mice are smaller and more dispersed than the trabeculae of wild type mice (shown by Von Kossa staining). The mineralization of the periosteum in Tmem16f deficient mice is significantly delayed compared to wild type mice while the Bsp or Osx expression is not altered in the periosteum.

Since the skull bones are formed by intramembranous ossification we analyzed the expression of early and later osteoblast markers such as Bsp and Osc in the skull bones and compared that with the front of ossification of these bones at stage E16.5

(the earliest stage when the skull bones of mutant mice get ossified). The expression of Bsp was upregulated and the distance between the Bsp expression domains of the frontal bones was smaller in Tmem16f deficient mice than in the wild type mice. The expression of Osc was downregulated but the distance between the zones of Osteocalcin expression in mutant mice was not changed compared to the wild type. The mineralization of intramembranous bones was markedly reduced and the distance between two mineralized bones (the suture) was wider in Tmem16f deficient mice than in the wild type mice. An unexpected upregulation and broader expression of Bsp together with downregulation and equal distribution of Osc suggest possible existence of some compensating mechanism for mineralization of intramembranous bones in Tmem16f deficient mice.

4.5.4 Tmem16f is important for proper mineralization of embryonic bones

Analyzing Tmem16f deficient mice we revealed that both, intramembranous and endochondral ossification are delayed in absence of Tmem16f. The ossification takes place but to a lesser extend in mutant mice than in wild type mice during embryogenesis. We suggest that Tmem16f is important for the proper mineralization of the embryonic bones but less important in adult life. The mechanism by which Tmem16f may promote the mineralization process during embryogenesis remains unknown. Since Tmem16E and Tmem16f constitute a subfamily among other Tmem16 proteins (Katoh, 2004 (a)) we propose that Tmem16E may act synergistically but later in time, overlapping with Tmem16f in the process of mineral deposition. These proteins were predicted to have similar structure where DUF590 domain is on C-terminal end. GDD1/TMEM16E was also shown to be strongly expressed in the bone (Tsutsumi et al., 2004). An additional analysis of Tmem16E deficient mice is necessary to unravel the function of Tmem16E. Tmem16E/Tmem16f double knock-out mice also need to be generated and analyzed for the possible synergistical role of these proteins in the process of bone mineralization.

Recent findings have revealed that Tmem16A, a member of Tmem16 protein family represents a novel calcium-dependent chloride channel (CaCC) (Caputo et al., 2008; Schroeder et al., 2008; Yang et al., 2008). Tmem16A is expressed differently than Tmem16F and plays role in proper tracheal cartilage formation (Rock et al., 2008). However, due to common predicted protein structure and similarity to other Tmem16

protein family members one can expect that Tmem16F and Tmem16E may also represent ion channels and play pivotal role in mineralization of the bone.

4.5.5 Tmem16f acts downstream of Ihh, Runx2 and Osx

Since Tmem16f was identified in a screen for Ihh-target genes we suggested that Tmem16f is most likely regulated by Ihh. It was previously shown, that Tmem16f expression is elevated by 7% in the E 14.5 mouse limbs treated with Shh in limb culture compared to non-treated limbs (activation of hedgehog signaling; Wenzel, 2003). The finding that Tmem16f expression was absent in mice lacking Ihh, and expanded in the mice overexpressing Ihh led to a suggestion that Tmem16f is regulated by Ihh. It is still to be confirmed whether this regulation is direct or indirect.

Since Tmem16f is expressed in osteoblast, it was important to analyze whether this gene acts downstream of essential transcription factors Runx2 and Osx. It has been previously shown that there are no osteoblasts formed in mice deficient for Runx2 or Osx (Ducy, et al., 1997; Komori et al., 1997; Otto et al., 1997; Nakashima, et al., 2002). It was also established that Osx is acting downstream of Runx2 (Nakashima, et al., 2002). We found that Tmem16f is not expressed in mice lacking Runx2 or Osx. However, both factors, Runx2 and Osx are expressed in Tmem16f null mice Therefore Tmem16f seem to act downstream of these transcription factors during osteoblast differentiation.

Summarizing these data we suggest that Tmem16f is positively regulated by Ihh. However, it is not known yet whether this occurs directly or indirectly through transcription factors Runx2 and Osx (Fig. 34). Unknown factors may also form independent pathway of Runx2 and Osx.

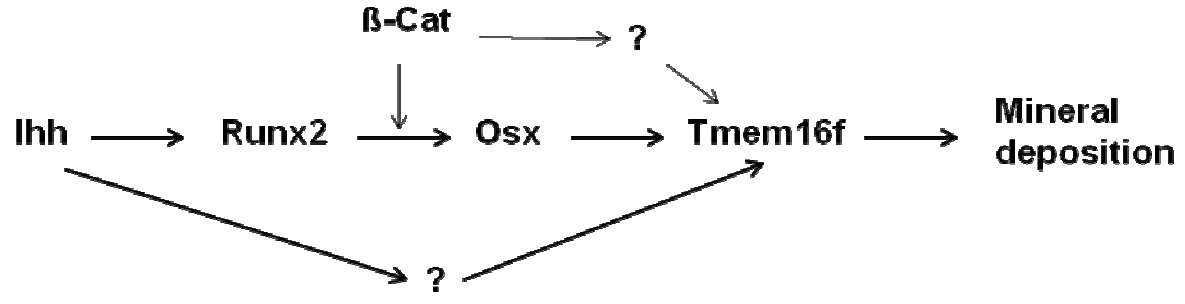

Figure 34: Positive regulation of Tmem16f by Ihh.

Ihh activates Runx2, which further promotes Osx expression. Osx positively regulates Tmem16f which in turn promotes mineral deposition. Ihh may also act directly on Tmem16f or through other unknown factors. ß-Catenin promotes and maintains the expression of Osx and therefore is involved in the regulation of Tmem16f indirectly.

ATF4 is another transcription factor which is required for terminal differentiation of osteoblasts and controls the transcriptional activity of mature osteoblasts (Yang, et al., 2004; Franceschi, et al., 2007). ATF4 and Runx2 cooperatively regulate osteocalcin transcription (Xiao et al., 2005). Therefore, Tmem16 can be regulated by ATF. This might be established later.

ß-Catenin, a central player in the canonical Wnt signaling might also potentially regulate Tmem16f. It was shown, that Wnt/ß-Catenin signaling promotes ossification acting downstream of Ihh (Day et al., 2005; Hill et al., 2005, Hu, 2005). Cells do not progress to osteoblasts expressing Osx if ß-Catenin is removed (Hill et al., 2005; Hu et al., 2005). It was established that ß-Catenin is also essential for maintenance of expression of Runx2 and Osx in osteoblasts (Rodda and McMahon, 2006). Therefore, we suggest that Tmem16f might be regulated by ß-Catenin (Fig. 34). That has to be investigated in the future.

5. Summary

The majority of skeletal elements are formed through endochondral ossification in which the signal molecule Indian hedgehog (Ihh) plays a key role. It regulates chondrocyte proliferation and differentiation and promotes osteoblast differentiation thus coordinating chondrogenesis with osteogenesis. In a previous study our group identified several candidate genes, which potentially act downstream of Ihh. In this study one of these genes, the transmembrane protein 16f (Tmem16f) was investigated in more detail and the skeletal phenotype of Tmem16f deficient mice was characterized.

First, the Tmem16f gene was analyzed *in silico* and mapped to the mouse chromosome 15 (15F1) covering 184 kb of the genomic region. Tmem16f consists of 21 exons and encodes a protein of 911 amino acids. By performing 5´-RACE we have discovered that the second exon is alternatively spliced. Additionally a shorter isoform of Tmem16f named Ano6-202 was predicted by the Ensembl database. It represents the 3´-sequence of the long isoform (exons 13 to 21) and an alternatively spliced exon 12b on the 5'-end. Furthermore the *in silico* analysis predicted 8 transmembrane domains and six N-linked glycosylation sites for Tmem16f.

Second, we defined an expression pattern of Tmem16f specifically in the developing bone and periosteum. In E14.5 and E16.5 wild-type mouse embryos Tmem16f is expressed by the osteoblasts of the forming bone and periosteum surrounding the Ihh expression domain. However, in mouse mutants, deficient for important regulators of bone development, such as Ihh, Runx2 or Osterix, the expression of Tmem16f was not detected, indicating that Tmem16f acts downstream of Ihh and the transcription factors Runx2 and Osx.

Third, the transient transfection of COS7-cells with Tmem16f-GFP fusion construct demonstrated that Tmem16f is localized in the cytoplasm.

The main focus of this study was to decipher the function of Tmem16f. Therefore a mouse line carrying a targeted deletion of the first exon of Tmem16f was generated. Additionally, we created a second mouse line carrying a gene trap cassette inserted into intron 13 of Tmem16f, which leads to disruption of both isoforms of Tmem16f.

Analysis of the skeletal preparations of Tmem16f mutant embryos revealed that both transgenic mouse lines display the same phenotype. The endochondral and intramembranous ossification was markedly delayed, the long bones of limbs and ribs were shortened and curved compared to those of wild type embryos. The sutures between the skull bones were wider in mutant embryos than those of wild

type embryos. At the age of 1 month the bones of Tmem16f mutant mice were slightly shorter and the olecranon processes of the ulna were smaller than those of the wild type mice. At this age, the long bones of the limbs and ribs were not bent any more as seen in the embryonic stage. However, the ulna and radius were twisted around each other in Tmem16f deficient mice.

Analysis of endochondral ossification on the molecular level revealed that proliferation and differentiation of chondrocytes is not affected, whereas the ossification process is severely delayed. The expression of early osteoblast markers is unaffected in the periosteum, but reduced in the trabeculae. Later osteoblast differentiation is disturbed as shown by a delayed onset of mineralization and reduced Osteocalcin expression.

These experiments indicate that Tmem16f is required for proper bone mineralization during embryogenesis but might have less important function in adult life.

6. Zusammenfassung

Die meisten Skelettelemente werden durch endochondrale Ossifikation gebildet. Das Signalmolekül Ihh spielt in diesem Prozess eine wichtige Rolle. Ihh reguliert die Proliferation und Differenzierung der Chondrozyten und die Differenzierung der Osteoblasten. Ihh koordiniert auf diese Weise die Chondrogenese mit der Osteogenese. In früheren Untersuchungen unserer Gruppe wurden verschiedene Kandidatengene identifiziert, die möglicherweise downstream von Ihh funktionieren. In der vorliegenden Arbeit wurde eines dieser Kandidatengene (Tmem16f) untersucht und der Skelettphänotyp der Tmem16f defizienten Mäusen charakterisiert.

Zuerst, wurde das Tmem16f Gen *in silico* analysiert. Es liegt auf dem Mauschromosom 15 in der Bande 15F1. Der Genlokus erstreckt sich über 185 kb und umfasst 21 Exons. Tmem16f kodiert für ein Protein mit 911 AS. Durch 5‘-RACE wurde festgestellt, dass das zweite Exon alternativ gespliced wird. Des Weiteren wird von der von Ensembl Datenbank eine kurze Isoform vorausgesagt, die als Ano6-202 bezeichnet wird. Diese entspricht dem 3‘-Sequenzbereich der langen Isoform (Exon 13 bis 21) mit einem alternative gesplictem Exon 12b am 5‘-Ende. Weitere *in silico* Analysen sagen für das Tmem16f Protein acht Transmembrandomänen und sechs N-verknüpfte Glycosilierungsstellen voraus.

Zweitens, wurde eine spezifische Genexpression von Tmem16f im sich entwickelten Knochen und im Periost nachgewiesen. In E 14,5 und E 16,5 Wildtyp Mäuseembryonen wird Tmem16f von Osteoblasten im sich entwickelnden Knochen und Periost neben der Ihh-Expressionsdomäne exprimiert. Da in Ihh-, Runx2- bzw. Osx- defizienten Mutanten keine Tmem16f Expression detektierbar ist, scheint Tmem16f downstream von Ihh, Runx2 und Osx zu agieren.

Drittens, durch transfektion von einem Tmem16f-GFP Fusionskonstrukt in COS-7 Zellen konnte eine zytoplasmatische Lokalisation von Tmem16f nachgewiesen werden.

Der Schwerpunkt dieser Arbeit lag auf der funktionellen Untersuchung von Tmem16f. Hierzu wurden Mausmutanten, die eine Deletion des ersten Exons des Tmem16f-Gens tragen generiert. Außerdem wurde eine zweite Mauslinie kreiert, die eine Genetrapkassette im 13. Intron enthält, wodurch es zur Unterbrechung beider Tmem16f Isoformen kommt.

Bei der Analyse von Skelettpräparationen der Tmem16f Mutantenembryonen wurde festgestellt, dass beide Mauslinien den gleichen Phänotyp, einer stark verzögerten

Endochondralen und Desmalen Ossifikation zeigen Die Langknochen der Gliedmaßen und die Rippen der Tmem16f-Mausmutanten sind gebogen und verkürzt im Vergleich zu Wildtypmäusen. Die Schädelnähte sind bei den Mutanten breiter als bei den Wildtypembryonen. Bei 1 Monat alten Mausmutanten sind die Knochen etwas kürzer als bei Wildtypmäusen. Die Langknochen der Gliedmassen und die Rippen sind nicht mehr gebogen. Jedoch sind Ulna und Radius bei den Mausmutanten umeinander gedreht, während diese bei Wildtypenmäusen sind parallel verlaufen.

Die Analyse der endochondrale Ossifikation auf molekularer Ebene zeigte, dass die Proliferation sowie die Differenzierung der Chondrozyten bei den Tmem16f-Mausmutanten unverändert, jedoch die Ossifikation stark verzögert ist. Die Expression der frühen Osteoblastmarkern ist im Periost unverändert, aber in den Knochenbälkchen reduziert. Durch den Nachweis einer verzögerten Mineralisierung und reduzierten Osteocalcin Expressions konnte gezeigt werden, dass die Differenzierung der späten Osteoblasten verlangsamt ist.

Diese Untersuchungen zeigen, dass Tmem16f für die korrekte Knochenmineralisierung während der embryonal Entwicklung notwendig ist, jedoch bei adulten Tieren eine untergeordnete Rolle spielt.

7. References

Abzhanov, A., Rodda, S. J., McMahon, A. P., Tabin, C. J. (2007). Regulation of skeletogenic differentiation in cranial dermal bone. Development 134(17):3133-44.

Alberts, B., Johnson, A., Lewis, J., Raff, M., Roberts, K. and Walter, P. (2002). Molecular biology of the cell, fourth edition.

Anderson, H. C. (1995). Molecular biology of matrix vesicles. Clin.Orthop. Relat. Res., 314, 266–280.

Anderson, H. C., Sipe, J. B., Hessle, L., Dhanyamraju, R., Atti, E., Camacho N. P. and Millan J. L. (2004). Impaired calcification around matrix vesicles of growth plate and bone in alkaline phosphatase-deficient mice. *Am J Pathol* 164 (3), 841-847.

Anderson, H. C., Garimella, R., Tague, S. E. (2005). The role of matrix vesicles in growth plate development and biomineralization. Frontiers in biosciense 10, 822-837.

Ausubel, F. M., Brent, R., Kingston, R. E., Moore, D. D., Seidman, J. G., Smith, J. A. und Struhl, K. (1987-1999). Current protocols in molecular biology (New York, Green and Wiley-Interscience).

Balcerzak, M., Malinowska, A., Thouverey, C., Sekrecka, A., Dadlez, M., Buchet, R. and Pikula, S. (2008). Proteome analysis of matrix vesicles isolated from femurs of chicken embryo. Proteomics 8, 192-205.

Bitgood, M. J. and McMahon, A. P. (1995). Hedgehog and Bmp genes are coexpressed at many diverse sites of cell- cell interaction in the mouse embryo. *Dev Biol* 172, 126-138.

Boskey, A. L., Moore, D. J., Amling, M., Cnalis, E. and Delany, A. M. (2003). Infrared analysis of the mineral and matrix in bones of osteonectin-null mice and their wildtype controls. J Bone Miner Res 18 (6), 1005-1011.

Boskey, A. L., Gadaleta, S., Gundberg, C., Doty, S. B., Ducy, P. And Karsenty, G. (1998). Fourier transform infrared microspectroscopic analysis of bones of osteocalcin-deficient mice provides insight into the function of osteocalcin. Bone 23 (3), 187-196.

Caputo, A., Caci, E., Ferrera, L., Pedemonte, N., Barsanti, C., Sondo, E., Pfeffer, U., Ravazzolo, R., Zegarra-Moran, O and Galietta, L.J.V. (2008). TMEM16A, a membrane protein associated with Calcium-dependent chloride channel activity. Science 322(5901):590-4.

Chen, J. K., Taipale, J., Cooper, M. K. and Beachy, P. A. (2002a). Inhibition of Hedgehog signaling by direct binding of cyclopamine to Smoothened. Genes Dev 10, 2743-2748.

Chen, J. K., Taipale, J., Young, K. E., Maiti, T. and Beachy, P. A. (2002b). Small molecule modulation of Smoothened activity. Proc Natl Acad Sci USA 99, 14071-14076.

Chung, U. I., Schipani, E., McMahon, A. P., Kronenberg, H. M. (2001). Indian hedgehog couples chondrogenesis to osteogenesis in endochondral bone development. J Clin Invest. 107(3):295-304.

Cormack, D. H. (1987). Ham's Histology. Part 3. The tissues of the body. Chapter 12: Bone.

Day, T. F., Guo, X., Garrett-Beal, L., Yang, Y. (2005). Wnt/ß-Catenin signaling in mesenchymal progenitors controls osteoblast and chondrocyte differentiation during vertebrate skeletogenesis. Dev. Cell 8: 739-750

de Crombrugghe, B., Lefebre, V., Nakashima, K. (2001). Regulatory mechanisms in the pathways of cartilage and bone formation. Current opinion in cell biology, 13:721-727.

Desbois, C., Seldin, M. F., Karsenty, G. (1994). Localization of the osteocalcin gene cluster on mouse chromosome 3. Mamm Genome 5(5):321-2.

Ducy, P., Desbois, C., Boyce, B., Pinero, G., Story, B., Dunstan, C., Smith, E., Bonadio, J., Goldstein, S., Gundberg, C., Bradley, A. and Karsenty, G. (1996). Incerased bone formation in osteocalcin-deficient mice. Nature 382 (6590), 448-452.

Ducy, P., Zhang, R., Geoffroy, V., Ridall, A. L. and Karsenty, G. (1997). Osf2/ Cbfa1: a transcriptional activator of osteoblast differentiation. Cell *89*, 747-754.

Ducy, P., Starbuck, M., Priemel, M., Shen, J., Pinero, G., Geoffroy, V., Amling, M., Karsenty, G. (1999). A Cbfa1-dependent genetic pathway controls bone formation beyond embryonic development. Genes Dev. 13(8):1025-36.

Ducy P. (2000). Cbfa1: a molecular switch in osteoblast biology. Dev Dyn 219(4):461-71.

Erlebacher, A., Filvaroff, E. H., Gitelman, S. E. and Derynck, R. (1995). Toward a molecular understanding of skeletal development. Cell 80, 371-8.

Feinberg, A.P. and Vogelstein, B. (1983) A technique for radiolabeling DNA restriction endonuclease fragments to high specific activity. Anal. Biochem. 132(1):6-13.

Feinberg, A.P. and Vogelstein, B. (1984) A technique for radiolabeling DNA restriction endonuclease fragments to high specific activity. Addendum Anal. Biochem., 137, pp.266-267.

Franceschi, R. T, Ge, C., Xiao, G., Roca, H., Jiang, D. (2007). Transcriptional regulation of osteoblasts. Ann N Y Acad Sci. 1116:196-207.

Galindo, B. E., Vacquier, V. D. (2005). Phylogeny of the TMEM16 protein family: some members are overexpressed in cancer. Int J Mol Med. 16(5):919-24.

Ganss B., Kim, R. H. and Sodek, J. (1999). Bone sialoprotein. Crit Rev Oral Biol Med. 10 (1):79-98.

Garimella, R., Bi, X., Camacho, N. P., Joseph B. S. and Anderson, H. C. (2004). Primary culture of rat growth plate chondrocytes: an in vitro model of growth plate histotype, matrix vesicle biogenesis and mineralization. Bone 34, 961-970.

Garimella, R., Bi, X., Anderson, H. C., Camacho, N. P. (2006). Nature of phosphate substrate as a major determinant of mineral type formed in matrix vesicle-mediated in vitro mineralization: An FTIR imaging study. Bone 38, 811-817.

Genge, B. R., Wu, L. N., Wuthier, R. E. (2007). Kinetic analysis of mineral formation dirong in vitro modeling of matrix veicle mineralization: effect of Annexin A5, phosphatidylserine, and type II collagen. Analytical biochemistry 367:159-166.

Genge, B. R., Wu, L. N., Wuthier, R. E. (2008). Mineralization of Annexin-5-containing lipid-calcium-phosphate complexes. Modulation by varying lipid composition and incubation with cartilage collagens. J of Biological chemistry 283 (15): 9737-9748.

Gilbert, S. F. (2003). Developmental Biology. Sunderland: Sinauer Associates, Inc.

Hall, B. K., Miyake, T. (2000) All for one and one for all: condensations and the initiation of skeletal development. BioEssays 22(2):138-47.

Hall, B. K., Miyake, T. (1995) Divide, accumulate, differentiate: cell condensation in skeletal development revisited. Int. J. Dev. Biol. 39(6):881-93.

Harada, S., Rodan, G. A. (2003). Control of osteoblast function and regulation of bone mass. Nature 423(6937):349-355.

Harmey, D., Hessle, L., Narisawa, S., Johnson, A. K., Terkeltaub, R. and Millan, H. L. (2004). Concerted regulation of inorganic pyrophosphate and osteopontin by Akp2, Enpp1, and Ank. An integrated model of the pathogenesis of mineralization disorders. Am. J. of pathology, 164 (4), 1199-1209.

Hasty, P., Rivera-Perez, J., and Bradley, A. (1991). The length of homology required for gene targeting in embryonic stem cells. Mol. Cell. Biol., 11(11):5586-91.

Hasty, P., Abuin, A. and Bradley, A. (2003). Gene targeting, principles, and practice in mammalian cells, in “Gene Targeting. A practical approach”, Oxford University Press, second edition. Edited by Joiner, A.J. pp.1-10.

Helms, J. A. and Schneider, R. A. (2003). Cranial skeletal biology. Nature 423:326-331.

Hill, T. P., Spater, D., Taketo, M. M., Birchmeier, W., Hartmann, C. (2005). Canonical Wnt/ß-Catenin signalling prevents osteoblast from differentiating into chondrocytes. Dev. Cell 8: 727-738.

Hu, H., Hilton, M. J., Tu, X., Yu, K., Ornitz, D. M., Long, F. (2005). Sequential roles of Hedgehog and Wnt signaling in osteoblast development. Development. 132(1):49-60.

Huitema, L. F. A., Vaandrager, A. B. (2007). What triggers cell-mediated mineralization? Frontiers in bioscience 12:2631-2645.

Hunter, G. K. and Goldberg, H. A. (1993). Nucleation of hydroxyapatite by bone sialoprotein. Proc Natl Acad Sci USA, 90(18), 8562-8565.

Inada, M., Yasui, T., Nomura, S., Miyake, S., Deguchi, K., Himeno, M., Sato, M., Yamagiwa, H., Kimura, T., Yasui, N. (1999). Maturational disturbance of chondrocytes in Cbfa1-deficient mice. Dev. Dyn. 214: 279-290.

Invitrogen. (2000-2002). GeneRacer^{tm} Kit. Instruction Manual.

Jacenko, O., LuValle, P., Solum, K. and Olsen, B. R. (1993). A dominant negative mutation in the alpha 1 (X) collagen gene produces spondylometaphyseal defects in mice. *Prog Clin Biol Res* 383B, 427-36.

Kamata, N. (2004). Response to Katoh and Katoh. Am. J. Hum. Genet. 75, 928–929.

Karp, S. J., Schipani, E., St-Jacques, B., Hunzelman, J., Kronenberg, H. McMahon, A. P. (2000). Indian hedgehog coordinates endochondral bone growth and morphogenesis via parathyroid hormone related-protein-dependent and independent pathways. Development 127, 543-8.

Karsenty, G. (2003). The complexities of skeletal biology. Nature, May 15;423 (6937):316-8.

Karsenty, G. and Wagner, E. F. (2002). Reaching a genetic and molecular understanding of skeletal development. Dev. Cell 2, 389-406.

Katoh, M. and Katoh, M. (2004a). Identification and characterization of TMEM16E and TMEM16F genes in silico. Int J Oncol., 24(5):1345-9.

Katoh, M. and Katoh, M. (2004b). GDD1 is identical to TMEM16E, a member of the TMEM16 family, Am. J. Hum. Genet. 75, 927–928.

Kaufmann, M. H. (1992). The atlas of mouse development. San Diego: Academic press.

Kiernan, J. A. (2008). Histologycal and histochemical methods. Theory and Practice. 4th edition.

Kim, I. S., Otto, F., Zabel, B., Mundlos, S. (1999). Regulation of chondrocyte differentiation by Cbfa1. Mech Dev 80: 159-170.

Komori, T., Yagi, H., Nomura, S., Yamaguchi, A., Sasaki, K., Deguchi, K., Shimizu, Y., Bronson, R. T., Gao, Y. H., Inada, M., Sato, M., Okamoto, R., Kitamura, Y., Yoshiki, S., Kishimoto, T. (1997). Targeted disruption of Cbfa1 results in a complete lack of bone formation owing to maturational arrest of osteoblasts. Cell 89(5):755-64.

Krogh, A., Larsson, B., von Heijne, G., Sonnhammer, E. L. (2001). Predicting transmembrane protein topology with a hidden Markov model: application to complete genomes. J Mol Biol. 305(3):567-80.

Kronenberg, H. M. (2003). Developmental regulation of the growth plate. Nature, May 15;423 (6937):332-337.

Kronenberg, H. M. (2007). The role of the perichondrium in fetal bone development. Ann. N.Y. Acad. Sci. 1116:59-64.

Lai, L.P. and Mitchell, J. (2005). Indian hedgehog: its roles and regulation in endochondral bone development. J Cell Biol. 96:1163-1173.

Lanske, B., Karaplis, A. C., Lee, K., Luz, A., Vortkamp, A., Pirro, A., Karperien, M., Defize, L. H. K., Ho, C., Mulligan, R. C., Abou-Samra, A. B., Jüppner, H., Segre, G. V., Kronenberg, H. M. (1996). PTH/PTHrP receptor in early development and Ihh regulated bone growth. Science 273, 663-666.

Liu, W., Toyosawa, S., Furuichi, T., Kanatani, N., Yoshida, C., Liu, Y., Himeno, M., Narai, S., Yamaguchi, A., Komori, T. (2001). Overexpression of Cbfa1 in osteoblasts inhibits osteoblast maturation and causes osteopenia with multiple fractures. J Cell Biol. 155(1):157-66.

Long, F., Zhang, X. M., Karp, S., Yang, Y. and McMahon, A. P. (2001). Genetic manipulation of hedgehog signaling in the endochondral skeleton reveals a direct role in the regulation of chondrocyte proliferation. Development 128: 5099- 5108.

Long, F., Chung, U.I., Ohba, S., McMahon, J., Kronenberg, H. M. and McMahon, A. P. (2004). Ihh signaling is directly required for the osteoblast lineage in the endochondral skeleton. Development 131:1309-1318.

Maruyama, K., and Sugano, S. (1994). Oligo-Cappping: A simple method to replace the Cap structure of eucariotic mRNAs with oligoribonucleotides. Gene 138, 171-174.

Mizuta, K., Tsutsumi, S., Inoue, H., Sakamoto, Y., Miyatake, K., Miyawaki, K., Noji, S., Kamata, N., Itakura, M. (2007). Molecular characterization of GDD1/TMEM16E, the gene product responsible for autosomal dominant gnathodiaphyseal dysplasia. Biochem Biophys Res Commun. 25;357(1):126-32.

Mundlos, S., Otto, F., Mundlos, C., Mulliken, J. B., Aylsworth, A. S., Albright, S., Lindhout, D., Cole, W. G., Henn, W., Knoll, J. H., Owen, M. J., Mertelsmann, R., Zabel, B. U, Olsen B. R. (1997). Mutations involving the transcription factor CBFA1 cause cleidocranial dysplasia. Cell 89(5):773-9.

Nakashima, K., Zhou, X., Kunkel, G., Zhang, Z., Deng, J. M., Behringer, R. R., de Crombrugghe, B. (2002). The novel zinc finger-containing transcription factor osterix is required for osteoblast differentiation and bone formation. Cell 108(1):17-29.

Olsen, B. R., Reginato, A. M. and Wang, W. (2000). Bone development. Annu. Rev.Cell Dev. Biol. 16, 191-220.

Opperman, L. A. (2000). Cranial sutures as intramembranous bone growth sites. Review. Dev Dyn. 219(4):472-85.

Osoegawa K., Tateno M., Woon PY., Frengen E., Mammoser AG., Catanese JJ., Hayashizaki Y., de Jong PJ. (2000). Bacterial artificial chromosome libraries for mouse sequencing and functional analysis. Genome Res. 10 (1):116-28.

Otto, F., Thornell, A. P., Crompton, T., Denzel, A., Gilmour, K. C., Rosewell, I. R., Stamp, G. W., Beddington, R. S., Mundlos, S., Olsen, B. R., Selby, P. B.,

Owen, M. J. (1997). Cbfa1, a candidate gene for cleidocranial dysplasia syndrome, is essential for osteoblast differentiation and bone development. Cell 89(5):765-71.

Riminucci, M., Collins, M. T., Corsi, A., Boyde, A., Murphey, M. D., Wientroub, S., Kuznetsov, S. A., Cherman, N., Robey, P. G., Bianco, P. (2001). Gnathodiaphyseal dysplasia: a syndrome of fibroosseous lesions of jawbones, bone fragility, and long bone bowing. J Bone Miner Res 16:1710–1718.

Roberts, S., Narisawa, S., Harmey, D., Millan, J. L. and Farquharson, C. (2007). Functional involvement of PHOSPHO1 in matrix vesicle-mediated skeletal mineralization. J Bone Miner Res 22:617-627.

Rock, J. R. and Harfe, B. D. (2008). Expression of TMEM16 paralogs during murine embryogenesis. Developmental dynamics 237: 2566-2574.

Rock, J. R., Futtner, C. R. and Harfe, B. D. (2008). The transmembrane protein TMEM16A is required for normal development of the murine trachea. Dev biology 321: 141-149.

Rodda, S. J. and McMahon, A. P. (2006). Distinct roles for Hedgehog and canonical Wnt signaling in specification, differentiation and maintenance of osteoblast progenitors. Development 133, 3231-3244.

Sambrook, J. and Russell, D. W. (2001). Molecular cloning: a laboratory manual. 3rd edition.

Sauer, G. R. and Wuthier, R. E. (1988). Fourier transform infrared characterization of mineral phases formed during induction of mineralization by collagenase-released matrix vesicles in vitro. J Biol Chem 263 (27): 13718-13724.

Schaefer, B.C. (1995). Revolutions in Rapid Amplification of cDNA Ends: new strategies for polimerase chain reaction cloning of full-length cDNA ends. Anal. Biochem. 227, 255-273.

Schroeder, B. C., Cheng, T., Jan, Y. N and Jan, L. Y. (2008). Expression cloning of TMEM16A as a calcium-activated chloride channel subunit. Cell 134, 1019-1029.

Sonnhammer, E. L., von Heijne, G. &Krogh, A. (1998). A hidden Markov model for predicting transmembrane helices in protein sequences. In Proceedings of the Sixth International Conference on Intelligent Systems for Molecular Biology (Glasgow, J., Littlejohn, T., Major, F., Lathrop, R., Sankoff, D. & Sensen, C., eds), pp. 175-182, AAAI Press, Menlo Park, CA.

Southern, E. M. (1975). Detection of specific sequences among DNA fragments separated by gel electrophoresis. J Mol Biol *98*, 503-517.

St-Jacques, B., Hammerschmidt, M., McMahon, A. P. (1999). Indian hedgehog signaling regulates proliferation and differentiation of chondrocytes and is essential for bone formation. Genes Dev.13(16):2072-86.

Stryke, D., Kawamoto, M., Huang, C.C., Johns, S.J., King, L.A., Harper, C.A., Meng, E.S., Lee, R.E., Yee, A., L'Italien, L., Chuang, P.T., Young, S.G., Skarnes, W.C., Babbit, P.C., and Ferrin, T.E. (2003). Nucleic Acids Res. 31, 278-281.

Stevens A., Lowe, J. S. (2005). Human histology.

Stewart, A. J., Roberts, S. J., Seawright, E., Davey, M. G., Fleming, R. H. and Farquharson, C. (2006). The presence of PHOSPHO1 in matrix vesicles and its developmental expression prior to skeletal mineralization. Bone 39: 1000-1007.

Stricker, S., Fundele, R., Vortkamp, A. and Mundlos, S. (2002). Role of Runx genes in chondrocyte differentiation. Developmental biology 245, 95-108.

Taipale, J., Cooper, M. K., Maiti, T. and Beachy, P. A. (2002). Patched acts catalytically to suppress the activity of Smoothened. Nature 418, 892-897.

Takeda, S., Bonnamy, J. P., Owen, M. J., Ducy, P., Karsenty, G. (2001). Continuous expression of Cbfa1 in nonhypertrophic chondrocytes uncovers its ability

to induce hypertrophic chondrocyte differentiation and partially rescues Cbfa1-deficient mice. Genes Dev 15: 467-481.

Thomas, K.R., and Capecchi, M.R. (1987). Site-directed mutagenesis by gene targeting in mouse embryo-derived stem cells. Cell, 51(3):503-12.

te Riele, H., Maandag, E.R., and Berns, A. (1992). Highly efficient gene targeting in embryonic stem cells through homologous recombination with isogenic DNA constructs. Proc. Natl. Acad. Sci. USA, 89, 5128-32.

Tsutsumi, S., Kamata, N., Maruoka, Y., Ando, M., Tezuka, O., Enomoto, S., Omura, K., Nagayama, M., Kudo, E., Moritani, M., Yamaoka, T., Itakura, M. (2003). Autosomal dominant gnathodiaphyseal dysplasia maps to chromosome 11p14.3-15.1. J Bone Miner Res 18:413–418.

Tsutsumi, S., Kamata, N., Vokes, T.J., Maruoka, Y., Nakakuki, K., Enomoto, S., Omura, K., Amagasa, T., Nagayama, M., Saito-Ohara, F., Inazawa, J., Moritani, M., Yamaoka, T., Inoue, H., Itakura, M. (2004) The novel gene encoding a putative transmembrane protein is mutated in gnathodiaphyseal dysplasia (GDD). Am J Hum Genet. Jun;74(6):1255-61.

Tsutsumi, S., Inoue, H., Sakamoto, Y., Mizuta, K., Kamata, N., Itakura, M. (2005) Molecular cloning and characterization of the murine gnathodiaphyseal dysplasia gene GDD1. Biochem Biophys Res Commun. 17;331(4):1099-106.

Ueta, C., Iwamoto, M., Kanatani, N., Yoshida, C., Liu, Y., Enomoto-Iwamoto, M., Ohmori, T., Enomoto, H., Nakata, K., Takada, K., Kurisu, K., Komori, T. (2001). Skeletal malformations caused by overexpression of Cbfa1 or its dominant negative form in chondrocytes. J Cell Biol. 153(1):87-100.

Volloch, V., Schweitzer, B., and Rits, S. (1994). Ligation-mediated amplification of RNA from murine erythroid cells reveales a novel class of beta-globin mRNA with an extended 5'-untranslated region. Nucleic Acids Res.22, 2507-2511.

Vortkamp, A., Lee, K., Lanske, B., Serge, G. V., Kronenberg, H. M. and Tabin, C. J. (1996). Regulation of rate of cartilage differentiation by Indian hedgehog and PTHrP-related protein. Science 273, 613-622.

Vortkamp, A., Pathi, S., Peretti, G. M., Caruso, E. M., Zaleske, D. J., Tabin, C. J. (1998). Recapitulation of signals regulating embryonic bone formation during postnatal growth and in fracture repair. Mech Dev. 71(1-2):65-76.

Weir, E. C., Philbrick, W. M., Amling, M., Neff, L. A., Baron, R. And Broadus, A. E. (1996). Targeted overexpression of parathyroid hormone-related peptide in chondrocytes causes chondrodysplasia and delayed endochondral bone formation. Proc. Natl. Acad. Sci. USA 93, 10240-10245.

Wenzel, H. M. (2003). Identifizierung neuer Zielgene im Indian-Hedgehog Signalweg. Ph.D. thesis, Freie Universitaet, Berlin.

Wu, L. N, Takayuki, Y., Genge, B. R., Sauer, G. R.,` Kirsch, T., Ishikawa, Y. and Wuthier, R. E. (1993). Characterization of the nucleational core complex responsible for mineral induction by growth plate cartilage matrix vesicles. J Biol Chem 268 (33):25084-25094.

Wurst, W., Auerbach, A. B., and Joiner, A. L. (1994). Multiple developmental defects in Engrailed-1 mutant mice: an early mid-hindbrain deletion and patterning defects in forelimbs and sternum. Development,. 120(7):2065-75.

Xiao, Z., Camalier, C. E., Nagashima, K., Chan, K. C., Lucas, D. A., de la Cruz, M. J., Gignac, M., Lockett, S., Issaq, H. J., Veenstra, T. D., Conrads, T. P., Beck, G.R., Jr. (2007). Analysis of the extracellular matrix vesicle proteome in mineralizing osteoblasts. J of cellular physiology 210: 325-335.

Xu, L., Anderson, A. L., Lu, Q. and Wang, J. (2007). Role of fibrillar structure of collagenous carrier in bone sialoprotein-mediated matrix mineralization and osteoblast differentiation. Biomaterials 28: 750-761.

Yamagiwa, H., Tokunaga, K., Hayami, T., Hatano, H., Uchida, M., Endo, N. and

Takahashi, H. E. (1999). Expression of metalloproteinase-13 (Collagenase-3) is induced during fracture healing in mice. Bone 25, 197-203.

Yang X, Matsuda K, Bialek P, Jacquot S, Masuoka HC, Schinke T, Li L, Brancorsini S, Sassone-Corsi P, Townes TM, Hanauer A, Karsenty G. (2004). ATF4 is a substrate of RSK2 and an essential regulator of osteoblast biology; implication for Coffin-Lowry Syndrome. Cell 117(3):387-98.

Yang, Y. D., Cho, H., Koo, J. Y., Tak, M. H., Cho, Y., Shim, W., Park, S. P., Lee, J., Lee, B., Kim, B., Raouf, R., Shin, Y. K. and Oh, U. (2008). TMEM16A confers receptor-activated calcium-dependent chloride conductance. Nature. 455(7217):1210-5

Young, M. F., Ibaraki, K., Kerr, J. M., Lyu, M. S., Kozak, C. A. (1994). Murine bone sialoprotein (BSP): cDNA cloning, mRNA expression, and genetic mapping. Mamm Genome 5(2):108-11.

Xiao G, Jiang D, Ge C, Zhao Z, Lai Y, Boules H, Phimphilai M, Yang X, Karsenty G, Franceschi RT. (2005). Cooperative interactions between activating transcription factor 4 and Runx2/Cbfa1 stimulate osteoblast-specific osteocalcin gene expression. J Biol Chem. 280(35):30689-96.

Zelzer, E., Olsen, B. R. (2003). The genetic basis for skeletal diseases. Nature 423(6937):343-348.

8. Appendix

8.1 Abbreviations

aa amino acids

AMP adenosine monophosphate

AP alkaline phosphatase

AS aminosäuren

ATF adenosine triphosphate

ATF4 activating transcription factor 4

ß-Gal ß-galactosidase

ß-Geo a fusion of ß-galactosidase and neomycin phosphotransferase II

Bsp bone sialoprotein

CaCC calcium-dependent chloride channel

CIP - calf intestinal phosphatase

Col-II/Ihh embryo mouse embryo misexpressing chicken *Ihh* under control of ColII promoter

Col X (**Col10a1**) collagen type X

DNA deoxyribonucleic acid

DAPI- 4',6-Diamino-2'-phenylindole

DEPC diethylpyrocarbonate

DKK1 Dickkopf 1

DNA Desoxyribonucleic acid

DUF590 domain of unknown function 590

E embryonic stage

ECM extracellular matrix

ES embryonic stem

EST(s) - expressed sequence tags

FBS fetal bovine serum

GDD gnathodiaphyseal dysplasia

GFP green fluorescent protein

GSP – gene specific primer

gt gene trap

h hour(s)

HE Hematoxylin and Eosin (staining)

het heterozygous

Ihh Indian hedgehog

kb kilo base pairs

ko knockout

lacZ beta galactosidase gene

min minute(s)

ml milliliters

µl microliters

MMP matrix metalloproteases

MVs matrix vesicles

neo^r neomycine phosphotransferase-encoding gene

NGSP nested gene specific primer

NPP1 nucleotide triphosphate pyrophosphatase phosphodiesterase

On osteonectin

ORF open reading frame

Osc osteocalcin

Osp osteopontin

Osx osterix

PAC- P1-derived Artificial Chromosome

PBS phosphate-buffered saline

PCR polymerase chain reaction

P_i inorganic phosphate

PPi pyrophosphate

PPR PTH/PTHrP receptor

PS phosphatidylserine

PTH parathyroid hormone

PTHrP Parathyroid related peptide (Parathyroid hormone-related protein)

5'RACE rapid amplification of cDNA ends

RNA ribonucleic acid

RNAse ribonuclease

RT reverse transcriptase

RT-PCR reverse transcription PCR

SA splice acceptor

Shh Sonic hedgehog

sec seconds

TAP tobacco acid pyrophosphatase

TM transmembrane domain

TMEM16A transmembrane protein A

TMEM16E transmembrane protein E

TMEM16F transmembrane protein F

TNAP tissue nonspecific alkaline phosphatase

TRAP Tartrate Resistant Alkaline Phosphatase

wt wild type

X-gal bromo-chloro-indolyl-galactopyranoside

8.2 Table of figures

8.3 Index of tables

9. Acknowledgements

I would like to thank my supervisor Professor Dr. Andrea Vortkamp for letting me work on this exciting project, for her excellent supervision, personal attention, encouragement and support.

I am very grateful to Dr. Manuela Wülling for constructive discussions, critics, advises and personal support.

I am thankful to Dr. Andreas Ratzka for his readiness to help, advises and critical discussions.

I thank Dr. Markus Moser of Max Planck Institute of Biochemistry, Martinsried for teaching me to work with ES cells and creating the chimeric mice.

I would also like to thank my colleagues in the OWL lab in Max-Planck-Institute in Berlin and in Developmental biology lab in Essen: Laetitia Buelens, Dr. Lydia Didt-Koziel, Marianne Gillner, Conny Kreschel, Melanie Kunath, Dr. Eleonora Minina, Insa Nölle, Virginia Piombo, Sabine Schneider, Dr. Markus Wenzel.

I also want to acknowledge my first molecular biology teachers Prof. Dr. Valentina A. Kratasyuk and Prof. Dr. Nikolai I. Matvienko for their support.

I am very grateful to my friends and family for their encouragement and help.

10. Curriculum Vitae

Milana Chinenkova

Tel.: +1-631-675-1252

e-mail: milana.chinenkova@uni-due.de

Education

09/1986-05/1988	High School N249, Tashkent, Uzbekistan
09/1988-06/1996	High School N20, Krasnoyarsk, Russia
09/1996-07/2001	Krasnoyarsk State University, Krasnoyarsk, Russia
09/1999- 05/2001	B.S., *with honors*, Molecular Biology Educational Center, Institute of Protein Research, Pushchino, Russia. Diploma thesis: *Production of superproducents of the DNA-polymerase, RNA-ligase, polynucleotide kinase of T4 phage and Tth DNA-polymerase from Thermus thermophilus HB 8*

Professional experience

09/1997-06/1998	Student in the laboratory of photobiology, Institute of Biophysics, Krasnoyarsk, Russia
09/1999-05/2001	Undergraduate student in the laboratory of Prof. Matvienko, Institute of Protein Research, Pushchino, Russia
09/2001-12/2001	Practical course as postgraduate student in the laboratory of Andrea Vortkamp, Max-Planck-Institute for Molecular Genetics, Berlin, Germany
02/2002-12/2004	Ph.D. student in the laboratory of Dr. Andrea Vortkamp, Max-Planck-Institute for Molecular Genetics, Berlin, Germany
12/2004-04/2007	Ph.D. student / teaching assistant in the Developmental Biology laboratory of Professor Dr. Andrea Vortkamp, University of Duisburg-Essen, Essen, Germany

Meetings:

The 5th Conference of the young scientists, April 16-20, 2001, Pushchino, Russia

1st Wittgenstein Conference: Genetics and Molecular Biology of skeletal Development, 12-14 October 2002, Lucca, Italy

The 5th EMBL Mouse Molecular Genetics Meeting, 03-07 September 2003, EMBL Heidelberg, Germany

Society for Developmental Biology, 63rd Annual Meeting, 24-28 July 2004, University of Calgary, Alberta, Canada

16th Scientific Meeting of the Society of Developmental Biology (GfE Meeting), 6-9 April, Westfaelische Wilhelms-Universitaet Muenster, Muenster, Germany

Gordon Research Conference Bones & Teeth, 10-15 July 2005, University of New England, Biddeford, ME, USA

3rd International PhD Student Symposium Horizons in Molecular Biology 14-16 September 2006, Goettingen, Germany

1st International Students' Symposium Crossroads in Biology 22-23 March 2007, Cologne, Germany

Gordon Research Conference Bones & Teeth, 15-20 July 2007, University of New England, Biddeford, ME, USA

Publications

Kudinova,I., Chinenkova, M., Shtarkova, M., Gerzic, Y. (1998). Working out the methods of ecological education in the scientific-research laboratory. Reconstruction of homeostasis: material of IX International symposium, V. 3, p. 14

Kudinova,I., Chinenkova, M., Shtarkova, M., Kratasyuk, V. (1998). Popular enzymology in high school. Journal of Bioluminescence and Chemiluminescence, V. 13, N 4, p.212,

M. Chinenkova, D. E. Kainov, N. I. Matvienko. (2001). Using the type II-S restriction endonucleases for cloning PCR DNA fragments. Collected theses 'Biology- the science of the XXI century', the 5th Conference of the young scientists, Pushchino, Apr. 16-20,

Essen, February 2nd, 2010

(Milana Chinenkova)

11. Erklärungen

Erklärung:
Hiermit erkläre ich, gem. § 6 Abs. 2, Nr. 6 der Promotionsordnung der Math.-Nat.-Fachbereiche zur Erlangung des Dr. rer. nat., dass ich die vorliegende Dissertation selbständig verfasst und mich keiner anderen als der angegebenen Hilfsmittel bedient habe.

Essen, den 2.02.2010

(Milana Chinenkova)

Erklärung:
Hiermit erkläre ich, gem. § 6 Abs. 2, Nr. 7 der Promotionsordnung der Math.-Nat.-Fachbereiche zur Erlangung der Dr. rer. nat., dass ich das Arbeitgebiet, dem das Thema „Isolation and functional characterization of the osteoblast specific gene, Tmem16f“ zuzuordnen ist, in Forschung und Lehre vertrete und den Antrag von Frau Milana Chinenkova befürworte.

Essen, den 2.02.2010

(Prof. Dr. Andrea Vortkamp)

Erklärung:
Hiermit erkläre ich, gem. § 6 Abs. 2, Nr. 8 der Promotionsordnung der Math.-Nat.-Fachbereiche zur Erlangung des Dr. rer. nat., dass ich keine anderen Promotionen bzw. Promotionsversuche in der Vergangenheit durchgeführt habe und dass diese Arbeit von keiner andern Fakultät abgelehnt worden ist.

Essen, den 2.02.2010

(Milana Chinenkova)